POLITECNICO DI TORINO
Collegio di Ingegneria Chimica e dei Materiali

Corso di Laurea Magistrale
in Ingegneria Chimica e dei Processi Sostenibili

Tesi di Laurea Magistrale

Analysis of the crystallization behaviour of plant-based mixtures of triglycerides for the formulation of vegan chocolate products

Relatore
prof. Elena Simone
Correlatore
dott. Cecilia Fiore
firma del relatore (dei relatori)

Candidato
Irene Giovando
firma del candidato

Dicembre 2023

Abstract

Cocoa butter (CB) products, especially chocolate, occupy a relevant position in the food industry. Addition of Milk Fat (MF) to chocolate is required to enhance sensory and physical properties of finished products (S. Metin et al., 2012). At the same time, attention to environmental issues has become a crucial factor to take into consideration as well. For this reason, together with intolerance problems customers are demanding milk free chocolate products. Hence, plant based fats step in as an alternative to animal ones (H. Ewens et al., 2021). In order to be a suitable option for this purpose the replacement fats need to satisfy specific physical and chemical requirements equally to milk fat that is used because of its ability to create a product that has unique organoleptic properties.

The aim of this thesis work is to analyse two plant based fat mixtures crystallization process when mixed with cocoa butter compared to MF. Cocoa butter is a mixture of triglycerides (TAGs) and because of its variable composition its crystallization behaviour is a very complex subject (S. Marty-Terrade et al., 2012). CB can form six different polymorphs named from Form I to Form VI from the least to the most stable, characterised by different subcell geometry, TAGs conformation and physical properties (B.J.D. Le Révérend et al., 2009). Milk Fat constituents are dominated by TAGs as well, although the composition is more heterogeneous than that of CB and its variability is very high. Plant based fats are made of triglycerides and show a polymorphic behaviour too (M. Lipp et al., 2001). When mixed together with cocoa butter they alter its crystallization process seeming a good candidate in MF replacement (M. El Hadri et al., 2022).

Samples of CB, MF and plant based fats and their mixtures were studied via multiple analytical techniques.

Polarized Light Microscopy was used to obtain crystallization and melting temperatures and their variations when changing cooling rates. Additionally, it was used to visualize crystal growth and some perceptible changes in crystal morphology during crystallization. Moreover, thanks to Matlab software it was possible to create a qualitative trend of the crystal number in time during cooling crystallization. This allowed to identify the presence of multiple phases crystallizing at different instants and possible polymorphic transitions.

Raman spectroscopy analysis of room temperature stored, molten and recrystallized samples were compared to evaluate the presence of multiple recrystallized phases. At the same time, it was useful to study the differences in the spectrum of pure compounds and cocoa butter mixtures.

Differential Scanning Calorimetry, by monitoring the heat flow from the sample, allowed to detect polymorphic changes and phase transitions and the temperature related to these facts.

Finally, X-Ray Powder Diffraction was used to determine the number and nature of the crystal forms obtained at room temperature storage; while Small Angle X-ray Scattering analyses consented to have a detailed understanding of polymorphism during dynamic experiments. These were performed with multiple cooling and heating ramps to have a clearer view of the crystallization process leading to more stable polymorphs.

In the end crystal phases have been associated to the TAGs present in the sample that more likely were responsible for their formation. This was achieved comparing the crystallographic results to the chemical composition of the studied samples, which ultimately led to a better

comprehension of how different TAGs from different fat mixtures can interact during crystallization processes.

Table of contents

Aim and structure of the thesis

The aim of this thesis is to study the crystallization behaviour of two plant-based fat mixtures, one is a fat of non lauric origin from palm and shea and the other one is a vegan milk fat replacer. The work focuses on determining the chemical composition, physical properties and in particular the crystallization behaviour of the two mixtures. Multiple analyses through different analytical techniques were performed on pure samples of the investigated fats and repeated on the mixtures of cocoa butter with different percentage of milk fat replacers and milk fat. Finally, the results obtained from plant-based fats were compared to those achieved by animal milk fat.

Chapter 1 describes the background of this thesis work.

Chapter 2 provides a general view of the subject from literature. Triglycerides mixtures characteristics are displayed, followed by a description of cocoa butter and milk fat properties. A brief overview on the usage of plant-based fats as substituents in cocoa industry is given. Analytical techniques applied in this work are also displayed as well as their main applications in the field of interest.

Chapter 3 proposes a detailed report on the materials used for this study, the methodology used in experiments and the specifications on the equipment.

Chapter 4 covers the totality of the experiments focusing on those who brought to the most significant results.

Finally, *Chapter 5* is a summary of the main aspects of this work wrap-up in conclusions.

Chapter 1: Introduction

The study of cocoa butter crystallization is an important subject in chocolate manufacturing because it influences physical and consequently sensory properties of the finished product. Indeed, chocolate tempering is a fundamental process to obtain the required chocolate characteristics that depend on the crystalline form of cocoa butter molecules (H.R. Pirouzian et al., 2020). Moreover, because of the limitation of geographic areas where cocoa is grown and the economic situation in many of these countries that is often very unstable, cocoa price and availability are very variable, causing some problems in its supply to food industries (M.H.A. Jahurul et al., 2012).

Milk fat is added to chocolate products to enhance their organoleptic properties and reach the right mouthfeel. Milk chocolate is produced using multiple milk derived ingredients, milk fat being one of them. Even dark chocolate can be improved with milk fat to avoid fat blooming and to reduce hardness (S. Metin et al., 2012). However, even if milk fat advantages are undoubted and its usage is very well consolidated, it brings to the table some important negative issues as well. Particularly, it cannot be eaten by some categories of consumers, in particular vegan or lactose intolerant people. In addition, milk fat is a product of the dairy industry that is based on animal farming. This field is one of the most significant causes of air pollution, making milk fat production an obstacle to sustainability (H. Ewens et al., 2021).

Plant based fats become more and more important as they can be a suitable substitute for milk fat and their role as CB replacers can be more exploited as well. Those fats can be artificially formulated to maximise positive aspects of milk fat while reducing bad ones. According to the European law it is possible to replace up to 5% of cocoa butter in chocolate with fats from different origins listed as Cocoa Butter Equivalents (CBE) (S. Verstringe et al., 2012). In addition, the possibility to develop fat mixtures whose properties can be modelled to satisfy particular requests can give an answer to common problems. For example, the usage of chocolate in tropical countries is held back by its scarce resistance to hot temperatures. It is possible to formulate cocoa butter with plant based fats coming from other sources that are able to increase chocolate melting point in order to obtain a product that can coexist with tropical weather to satisfy consumers living in such areas (H. Ewens et al., 2021).

Crystallographic studies of cocoa butter are then essential in understanding the interactions between cocoa butter and other fats. Cocoa butter can occur in six different polymorphs numbered from I to IV from the least to the most stable, form V being the desired one in chocolate because of its melting temperature (B.J.D. Le Révérend et al., 2009). Cocoa butter polymorphs are very well known and their physical properties and crystallization kinetics are object of numerous studies. This gives a solid starting point to better understand how extraneous fat addition can alter the usual crystallization process.

Chapter 2: Literature review

In this chapter fats structure and main traits are displayed. An overview of Cocoa Butter composition and properties is provided, along with a detailed analysis of its polymorphic behaviour. Milk Fat characteristics are also described followed by a general description of plant fats. The analytical techniques used during the experiments are finally described.

2.1 Fats

The most abundant component of natural fats used in the food industry are Triglycerides (TAGs). These molecules are constituted of three fatty acids (FA) chains linked to a glycerol molecule as in Fig. 2.1. Even if the key structure remains constant, molecules belonging to this group show different properties. Characteristics of the FA, such as chain length or the presence of unsaturated bonds and their position along the chain, determine the behaviour of the TAG.

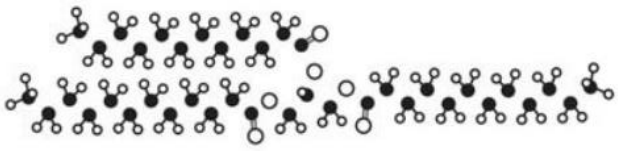

Fig. 2.1 Example of TAG molecule where glycerol is found in the middle and FA chains extend from it (M. Sasaki et al., 2012).

Some fatty acids play an important role in natural fats, specifically in cocoa butter and other plant-based fats such as shea or palm. Stearic acid (S) represented in Fig. 2.2 (C. Himawan et al., 2006) is a fatty acid formed by a chain of 18 carbon atoms, which belongs to saturated FA. Generally, saturated TAGs show a higher melting point thanks to their linear structure. Indeed, stearin or tristearin (SSS) is the main example of unsaturated TAG as it is formed by three stearic chains. Its melting point ranges from 55°C when in the less stable α form to 73°C when in the stable β form.

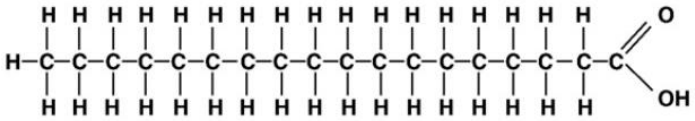

Fig. 2.2 Stearic acid. (C. Himawan et al., 2006)

Palmitic acid belongs to saturated FAs as well but its chain is shorter as it is formed by 16 carbon atoms. It is commonly found in cocoa butter and its behaviour is similar to stearic acid. Oleic acid is the most common unsaturated fatty acid. It is formed by 18 carbon atoms and shows one unsaturated bond. Contrarily to stearin, olein molecules show a very low melting point that is below zero. Fats containing a large amount of unsaturated TAGs, particularly triunsaturated and diunsaturated ones are often in the form of liquid oils. It is important to

notice that olein is not able to form ordered crystal structures but when it reaches its solid state it creates an amorphous solid.

Fatty acid chains in the TAG molecule can occur in two different conformations affecting TAG mixing ability. They can occur in chair conformation or tuning fork conformation as in Fig. 2.3 (M. Sasaki et al., 2012).

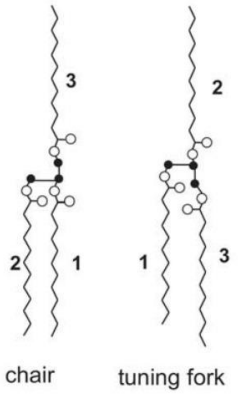

Fig. 2.3 Chair and tuning fork conformations of TAGs. Black dots represent glycerol carbon atoms, white dots oxygen atoms and zigzag lines numerated from 1 to 3 are the FA chains. (M. Sasaki et al., 2012)

Polymorphism is defined as the "ability" of a compound to crystallize in different forms, distinguished by the different crystallographic structures and characterised by different physical properties. CB properties are hugely influenced by this phenomenon, as its crystallization behaviour is very complex and it can form six different polymorphs.

The main crystal forms of TAGs are α, β' and β forms. The first one has a hexagonal cell, the second one an orthorhombic-perpendicular cell while the last one has a triclinic-parallel cell. Crystals can also differ in the way they stack, particularly they can arrange as a double layer or triple layer as represented in Fig. 2.4 (M. Sasaki et al., 2012).

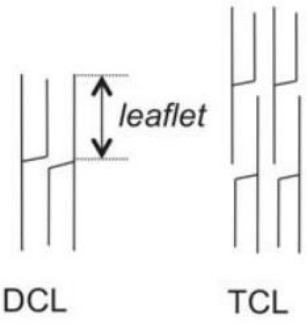

Fig. 2.4 Double and triple layer chain structure. (M. Sasaki et al., 2012)

2.2 Cocoa butter

Cocoa butter is mainly composed by triglycerides where the fatty acids are primarily palmitic (P), oleic (O) and stearic (S), respectively weigth percentages of ~25%, ~35% and ~35%. Oleic

acid contains a double bond and usually occupies the second position in monosaturated TAG molecules, while P and S are saturated FAs (S.D. MacMillan et al., 2002). Indeed, up to 80/90% of CB is constituted by POP, POS and SOS giving cocoa butter a less heterogeneous composition than MF.

Given its importance in cocoa butter, SOS molecule is taken as an example to understand differences in polymorphic structures. This TAG is constituted by two stearic acid chains placed on R1 and R3 and an unsaturated oleic acid chain in the middle, hence being a symmetrical molecule. It is usually found in tuning fork conformation and can create different polymorphs as shown in Fig. 2.5 (M. Sasaki et al., 2012).

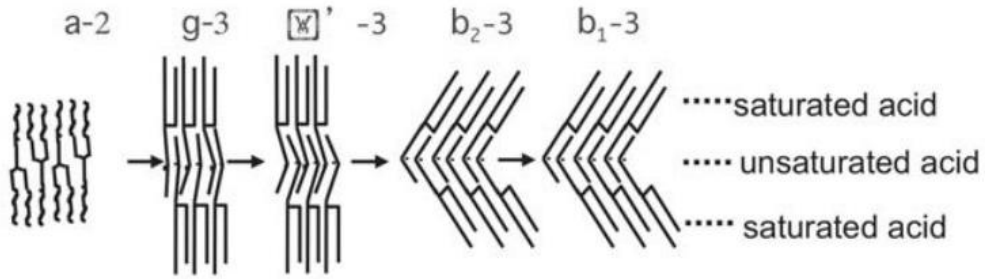

Fig. 2.5 Polymorphism of SOS. (M. Sasaki et al., 2012)

Another symmetrical molecule is OPO, where the lateral chains are unsaturated oleic acid and palmitic acid is in R2. Its behaviour is similar to that of SOS due to the fact that they both are symmetrical molecules in tuning fork conformation. Fig. 2.6 (M. Sasaki et al., 2012) shows possible structures of OPO crystals.

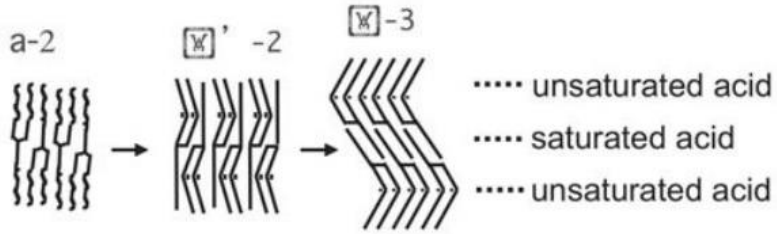

Fig. 2.6 Polymorphism of OPO. (M. Sasaki et al., 2012)

Asymmetric molecules behave differently as they are usually arranged in chair conformation. Common asymmetric TAGs in Cocoa Butter are SSO and PPO and their crystal structures are represented in Fig. 2.7 (M. Sasaki et al., 2012).

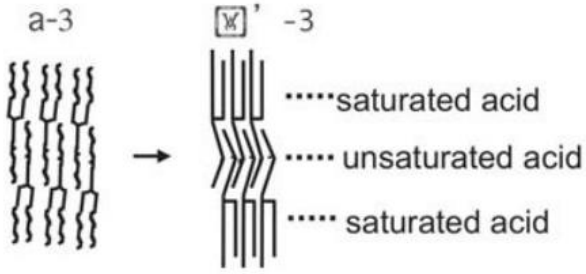

Fig. 2.7 Asymmetric TAG (SSO or PPO) polymorphism. (M. Sasaki et al., 2012)

SOS polymorphism was hence studied as its behaviour can influence the crystallization process of its mixtures. It occurs in five different polymorphic forms displayed in Tab. 2.1, while a sixth form was detected but not fully characterized (M. Sasaki et al., 2012).

Tab. 2.1 SOS polymorphs.

Form	Chain length	Long spacing [Å]	Melting point [°C]
A	2L	48.3	23.5
γ	3L	70.5	35.4
β'	3L	70.0	36.5
β_2	3L	67.5	41
β_1	3L	66.0	43
sub- α	2L	-	Low temperature

POP shows numerous polymorphs as well. It can occur in α form, similar to SOS as well as in γ form. This TAG can form two different β'(2L) polymorphs and one δ(3L) form. It also can occur in two β forms, similarly to SOS. The stable β_2 and β_1 polymorphs are comparable to cocoa butter form V and form VI respectively. The sub-α form is instead analogous to CB form I (M. Sasaki et al., 2012).

Tab. 2.2 POP polymorphs.

Form	Chain length	Long spacing [Å]	Melting point [°C]
α	2L	46.5	15.2
γ	3L	65.4	27.0
δ	3L	62.5	29.2
β'_2	2L	42.4	30.3
β'_1	2L	42.4	33.5
β_2	3L	61.0	35.1
β_1	3L	61.0	36.7

Cocoa butter can form six different polymorphs that are widely described in literature. Their specific temperatures of crystallization are well known even if slight variations can still be found from one study to the other. Tab. 2.3 collects information about CB polymorphs from multiple sources in order to have a clearer overview on their characteristics.

Tab. 2.3 CB polymorphs melting points.

Form	Cell	Chain length	Melting point [°C] (M.Sasaki et al.)	Melting point [°C] (H.R. Pirouzian et al.)
I	γ	2L	17.3	16-18
II	α	2L	23.3	21-22
III	β'	2L	25.5	25.5
IV	β'	2L	27.5	27-29
V	β	3L	33.8	32-34
VI	β	3L	36.3	34-36

In Fig. 2.8 (Redrawn from H.R. Pirouzian et al.) all the possible ways of formation of all six cocoa butter polymorphs are depicted.The most stable form does indeed transition from the less stable one and is not able to directly nucleate from the liquid bulk.

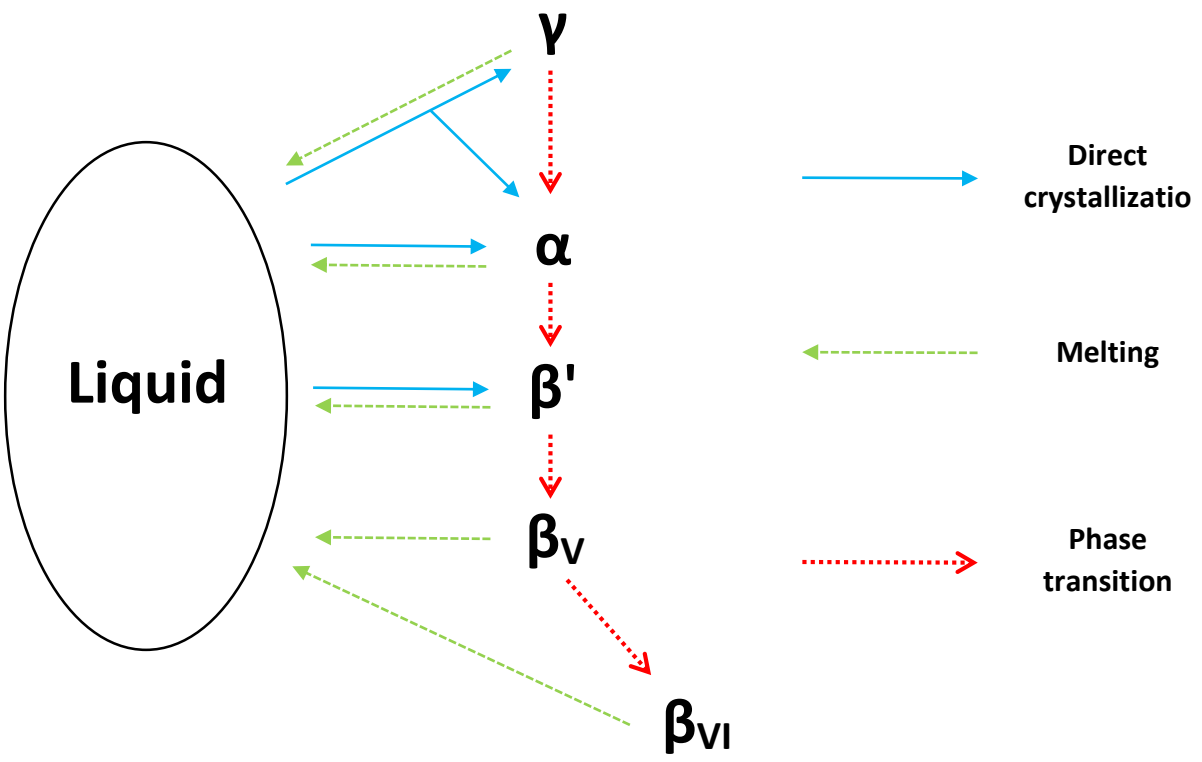

Fig. 2.8 CB polymorphs formation and polymorphic transitions. (Redrawn from H.R. Pirouzian et al.)

2.3 Milk fat

Milk Fat (MF) is a mixture of fats with very complex composition depending on a number of factors such as feeding, living conditions or age of the animal it derives from. It contains a wide range of fatty acids where chain length and unsaturation scheme play a major role in its properties, together with more specific chain characteristics such as spatial conformation or

aromatic rings presence (S. Metin et al., 2012). Due to this high variability MF includes more than 400 different FA that can rearrange in thousands of different TAGs (A. Lambert et al., 2018).

TAGs in MF are classified as high-melting, middle melting and low-melting. Tab. 2.4 resumes the main properties of each category.

Tab. 2.4 TAGs classification in milk fat (recreated from S. Metin et al., 2012).

	High-melting	Middle-melting	Low-melting
Concentration (%)	5	25	70
Melting temperature (°C)	>50	35-40	<15

The high-melting fraction is constituted by long-chain trisaturated TAGs, middle-melting one by TAGs with two long-chain saturated FA and one short-chain or unsaturated FA, while TAGs belonging to the low-melting class contain a single long-chain saturated and two short-chain or unsaturated FA. Milk fat commonly presents a considerable amount of short chain FA, more precisely C4 and C6 chains, usually on R3 position of glycerol.

This extremely variable composition explains the wide melting temperature (Tm) range and the difficulty encountered when studying MF crystallization process. Tm can vary from down to -40°C up to +40°C and in between these boundaries a liquid-solid mixture where higher melting crystals are surrounded by molten lower melting components is found.

As studied by S. Metin et al. in 2012, given this complexity MF is rarely found in the most stable β form, while it is more common for it to exist in β' form. MF crystallization is slower than that of CB because it requires higher activation energies to form a compact crystal matrix because of the presence of a multitude of different TAGs that can form mixed crystals. However, crystallization begins earlier because much different TAGs can form mixed crystal better than TAGs quite similar to each other as in CB. Mixed crystals are mostly found in the α phase and will secondly transform into purer ones reaching a more stable state (M. Bayard et al., 2022). If the cooling phase is followed by a temperature holding crystallization proceeds including more TAG species, crystals rearrange in purer forms and polymorphic transitions happen. Solid fat content (SFC) will then arise.

It is important to notice differences in crystals shape according to the cooling rate applied. Firstly, small crystal with a needle shape appear, followed by an aggregation process into spherulites. Very slow cooling rate is associated with larger crystals formation allowing diffusion within the liquid fraction (S. Metin et al., 2012).

2.4 Fat mixtures

Mixing different TAGs can lead to three possible solid structures: solid solution, eutectic phase or molecular compound (Fig. 2.9).

- A solid solution (Fig. 2.9 (a)) occurs when similar compounds mix easily at any percentage and the physical properties of the solution (i.e. melting temperature)

depend on those of pure components according to their respective percentages. A solid solution is formed when SOS and POS are put together.

- A eutectic phase (Fig. 2.9 (b)) is typical of fats that perfectly mix in liquid solution but are not miscible when solid. Examples of fats that behave this way is PPP with SSS, both trisaturated TAGs, or in the case of PPP and POP, one trisaturated and one monounsaturated, or POP and OOP or SOS and OOS, couples of monounsaturated and biunsaturated TAGs containing the same saturated fatty acid.
- Molecular compounds (Fig. 2.9 (c)) develop when two TAGs can arrange in a specific compact structure due to their conformation, such as SOS with OSO or with SSO or POP with OPO or with PPO. Those fats are able to reach a high regularity because molecule conformation match together because of specific molecular interactions coming from their FA chains.

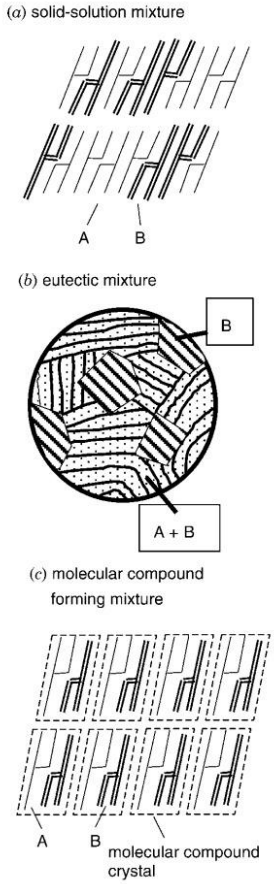

Fig. 2.9 Solid structures of TAGs mixtures: solid-solution mixture (a), eutectic mixture (b) and molecular compound forming mixture (c). (K. Sato et al., 2005).

It is reported that a mixture of SOS, POP and POS can behave as a solid solution or eutectic in relation to the relative concentration of the components and in the case of CB they mix together forming a solid solution.

2.5 Plant-based fats

CB cost has increased in the last few years due to the intense usage of chocolate products, paving the way to studies about vegetable fats mixtures created to duplicate CB properties with a reduced cost. These are denominated CBAs (Cocoa Butter Alternatives), mixtures of fats especially triglycerides, resembling natural CB that classify as CBEs (Cocoa Butter Equivalents) or CBSs (Cocoa Butter Substitutes). The main difference between these two categories is found in their ability to mix with CB: CBEs able to blend with it, unlike CBSs which contain lauric acid and other FAs absent in CB and can only replicate CB's properties when CB is fully replaced (H. Ewens et al., 2021).

CBEs are plant-based fats mixtures prepared to recreate the physical and organoleptic properties of CB. The most used plant-based fats in CBEs production are palm oil, shea and illipé. Usually CBEs are constituted by a larger POP fraction and lower POS one compared to CB, coming from the fact that POS is less present in palm and shea oils (M. Lipp et al., 2001).

2.6 Analytical Techniques for fats crystal characterization

Numerous techniques can be used to study crystalline compounds, more specifically to understand crystal morphology and behaviour, as well as polymorphism.

2.6.1 Polarized Light Microscopy

Polarized Light Microscopy (PLM) is an optical microscopy technique that enhances contrast to obtain a more detailed image of the analysed material. Usually, light waves are not characterized by a specific planar oscillation of the electric field but it can happen in all directions. Polarized light is defined as a light wave that is filtered to obtain a plane-polarized light beam where there is a single vibration direction. It is obtained thanks to a polarizer that filters the incoming light allowing passing to a single planed light. Light comes from the bottom of the microscope and the sample is placed over an empty window where polarized light can pass through the material and reach the analyser. It is commonly used to perform qualitative analysis on the samples, but because of its high contrast it is possible to do a quantitative study as well. Thanks to image processing software it is possible to separate the background from the contrasting forefront. For example, in the case of crystals it is possible to process the image with filters to obtain the number of crystals in a frame or to focus on specific aspects such as crystals size.

2.6.2 Raman spectroscopy

Raman spectroscopy is a vibrational spectroscopy technique. It exploits the interaction between chemical bonds and light wave represented by a high intensity laser. Raman spectroscopy is based on the fraction of the light wave that is scattered by the chemical bonds at different wavelengths from the original source. Specific regions of the Raman spectra are linked to specific chemical bonds such as C=C or C-C bonds or to entire groups such as benzene (S. Bresson et al., 2011). Each molecule creates a particular spectrum and for this reason this

technique is very useful for multiple purposes. It can be easily used to identify a certain material or even to detect impurities in a sample.

Raman microscope can also be added to a Raman spectrometer to obtain clear images of the analysed sample in the range of μm (Fig. 2.10).

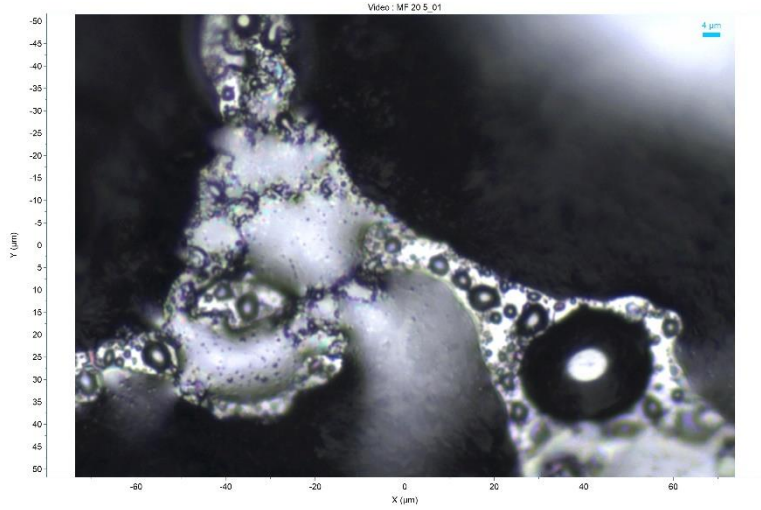

Fig. 2.10 Example of Raman microscopy from MF2 20% sample.

Raman spectroscopy is also useful in identifying different CB polymorphs thanks to relevant regions of the spectrum, listed in Tab. 2.5 (Y. Yao et al., 2016). Fig. 2.11 shows a TAG example where Raman active groups are highlighted (S. Bresson et al., 2011).

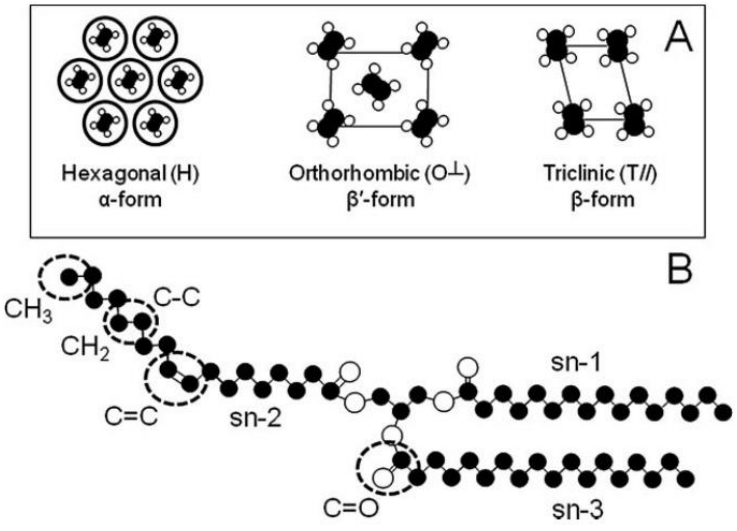

Fig. 2.11 a) TAG cells arrangement, b) Raman-active groups in a POS molecule where black is carbon and white is oxygen (S. Bresson et al., 2011).

Tab. 2.5 Raman active bonds and groups.

Raman shift (cm^{-1})	Y. Yao et al. (2016)	
	Origin	**Structures**
525	-	S-S stretching vibrations (gauche-gauche-trans)
726	-	C-S (protein) / CH_2 rocking / adenine
860	Phospholipid	-
957	-	Hydroxyapatite/carotenoid/cholesterol
1010	Carotenoids	Ring compounds
1063-1083	Fatty acid	ν(C-C) stretching
1125	Saturated fatty acid	φ(C-C)
1160	Carotenoids	ν(C-C)
1270	PC, PI, PS	C=C cis unsaturated C-H in-plane bending of ethylene groups
1303	PC, PI, PS	$\delta(CH_2)$ twisting unsaturation
1443	Cholesterol PC, PI, PS	Saturated fatty acid $\delta(CH_2)$ scissoring
1530	Carotenoids	ν(C=C)
1658	PC, PI, PS	ν(C=C) cis unsaturation
1742	Triacylglycerol	Ester ν(C=O)
2850	Cholesterol	CH_2 symmetric stretching
2885 ± 5	Acyl chains in crystalline state	Fermi resonance CH_2 stretching CH_2 anti-symmetric stretching

C-H stretching region in Fig. 2.12 (S. Bresson et al., 2011) is the most relevant portion of the Raman spectra in order to distinguish CB forms through this technique. In 3050-2700 cm^{-1} region two overlapped peaks relate to symmetric and antisymmetric stretching of the CH2 group, respectively around 2845 and 2882 cm^{-1}. In the liquid phase the symmetric stretching is playing the major role in the overall Raman signal because lateral chains are less packed and thus there are limited interactions; whereas when in solid state the influence of adjacent methylene groups is stronger causing important antisymmetric stretching peak to grow. In the liquid phase a band at 2935 cm^{-1} shows the stretch of the terminal CH_3 group.

Stretching region of the carbonyl group C=O (Fig. 2.13) (S. Bresson et al., 2011) consents to determine stable forms of CB and it is situated between 1800 and 1700 cm^{-1}. The liquid phase, together with the less stable forms I and II, are characterized by a single wide peak at 1745 and 1742 cm^{-1} respectively. Forms III and IV have a similar spectrum with two overlapped peaks at 1732 and 1744 cm^{-1} forming a doublet. The more stable form V shows a triplet with peaks at 1732, 1737 and 1745 cm^{-1} while form VI differs because the middle peak is less defined and moved to 1740 cm^{-1}.

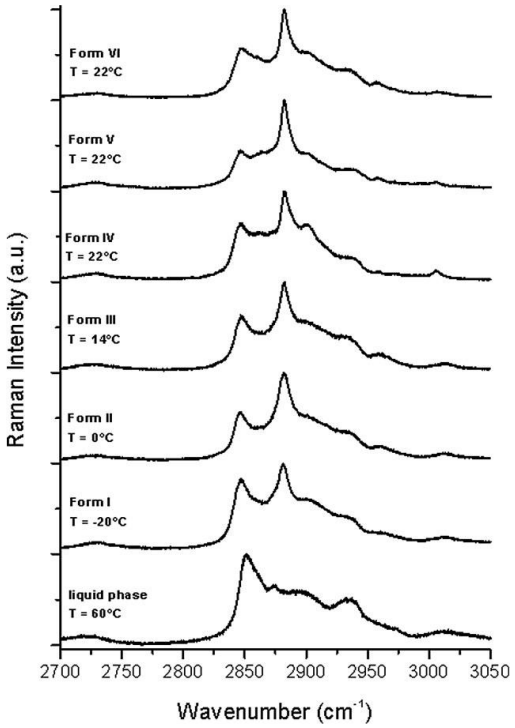

Fig. 2.12 CH stretching region of Raman spectra of CB (S. Bresson et al., 2011).

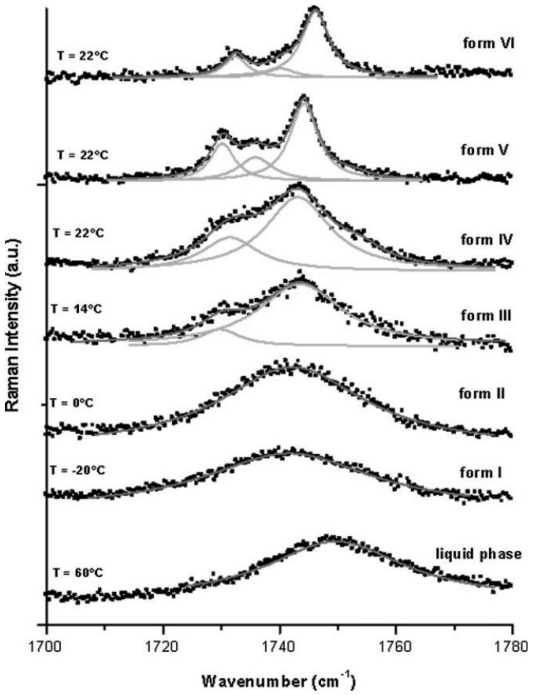

Fig. 2.13 Carbonyl group stretching region of Raman spectra of CB (S. Bresson et al., 2011).

Olefinic bond C=C is characteristic of the oleic acid, thus the corresponding band (Fig. 2.14 from S. Bresson et al., 2011) at ~1660 cm^{-1} is useful to distinguish the 2L from the 3L layering. The intensity of this band is higher in liquid state and forms from I to IV while is weaker in the

two most stable forms V and VI. This is coherent with the reduced molecular mobility in 3L arrangement typical of the stable forms.

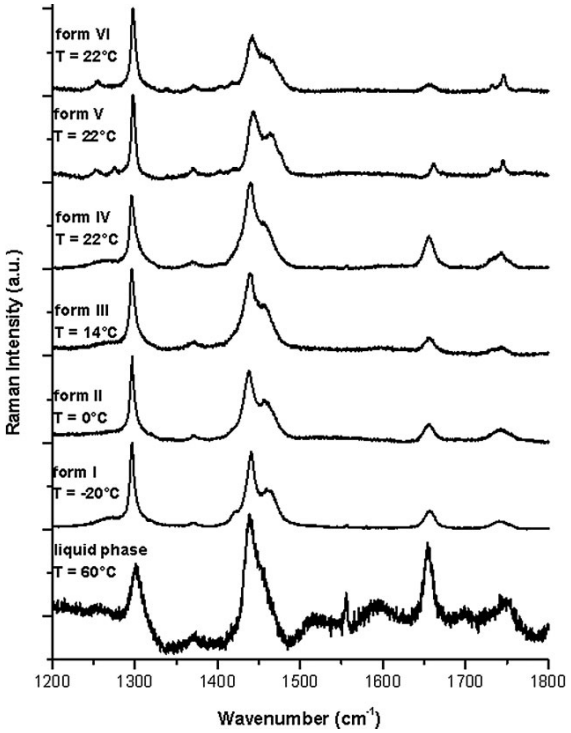

Fig. 2.14 Olefinic bond C=C corresponding region of Raman spectra of CB (S. Bresson et al., 2011).

The 1200-1000 cm^{-1} region related to C-H skeletal modes shown in Fig. 2.15 (S. Bresson et al., 2011) does not change after the first solidification process suggesting that the alkyl chains structure is the same in all the polymorphs.

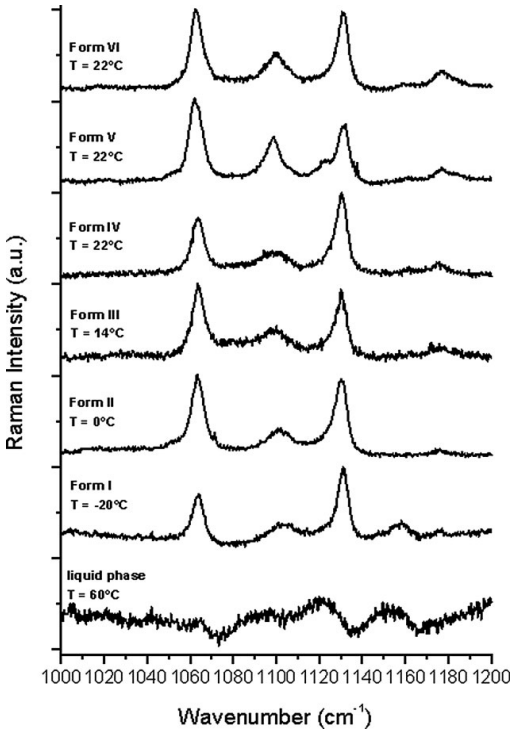

Fig. 2.15 C-H skeletal modes region of Raman spectra of CB (S. Bresson et al., 2011).

2.6.3 Differential Scannig Calorimetry

Differential Scanning Calorimetry (DSC) is a valuable tool to detect polymorphic transitions and more in general to understand crystallization behaviour of a sample. This technique is classified as thermal analysis as it monitors the heat capacity of the sample. The analysis needs the presence of a reference sample whose properties are defined. The analysis is performed by monitoring the heat flux transferred to the sample when applying cooling and heating, according to the desired thermal protocol. The results are obtained as a curve representing the heat flux as a function of the temperature. It is possible to represent the results both with exothermic or endothermic peaks in the positive direction. Endothermic peaks are caused by energy consuming transformations, in particular crystal melting, while exothermic peaks can be associated to polymorphic transitions from less to more stable forms or crystallization steps. Both these processes free certain energy and so the heat flux to the sample is reduced.

2.6.4 X-ray Powder Diffraction

X-ray diffraction is a valid technique to obtain a good view on crystal structure because it allows to distinguish crystal forms based on their X-ray pattern. Indeed, each polymorph shows a characteristic pattern that differs from the others. In order to achieve this result, monochromatic X-rays are created and then oriented onto a crystalline structure or a single crystal and a detector collects the reflected rays. These reflected rays can even be generated when the angle of incidence is very low. This is possible because parallel crystalline planes constituted by the crystal atoms cause X-ray scattering. More precisely each atom behaves like a secondary source of electromagnetic waves reflecting X-rays.
This technique allows to obtain reflected radiation intensity in relation to 2Θ, where Θ is the angle of incidence. The d-spacing value can be derived through Bragg's Law (Eq. 1):

$$\lambda = 2d\ sin\ \theta \qquad \textit{(Eq. 1)}$$

where λ is the wavelength of the X-ray beam and d is the d-spacing characteristic of the measured crystal structure. Peaks are generated when crystalline planes are distanced in a proper way to diffract X-rays with that specific incidence angle (D.A. Tzompa-Sosa et al., 2016). In the case of TAGs crystals, short spacing refers to the distance between crystal planes, hence it is linked to the subcell geometry while long spacing describes chain length structures and depend on the lamellae size and TAGs layering.
While it is quite difficult to obtain clear XRD results from a chocolate sample because of sugar interference, cocoa butter polymorphic behaviour during XRD analyses is very well visible (H.R. Pirouzian et al., 2020). Each polymorph is associated to typical peak values related to short spacing and long spacing measures, depending on their specific subcell geometry. Tab. 2.6 lists the characteristic XRD peaks of all six CB polymorphs.

Tab. 2.6 CB polymorphs typical d-spacings (S. Bresson et al., 2011).

	Subcell	Layering	Short spacing peaks [Å]	Long spacing peaks [Å]
Form I	orthorhombic	2L	4.22 3.85	50.80
Form II	hexagonal	2L	4.24	49.30
Form III	orthorhombic	2L	4.28 3.90	45/48.5
Form IV	orthorhombic	2L	4.38 4.19	44.80
Form V	triclinic	3L	4.60 4.00 3.88 3.79 3.70	63
Form VI	triclinic	3L	4.60 3.90 3.71	63.4

Given the importance of the stable form V of cocoa butter, typical values of its peaks from different works have been compared in Tab. 2.7.

Tab. 2.7 Short spacing values of CB form V.

Ghazani and Marangoni (2021) – form V (3L) β_2		**Sasaki, Ueno and Sato (2012) – form V**		**Podchong, Aumpai, Sonwai and Rousseau (2022) – form V**	
Short spacing [Å]	Intensity	Short spacing [Å]	Intensity	Short spacing [Å]	Intensity
5,4	(m)	-			
5,15	(w)	-			
4,58	(vs)	4,58	(vs)	4,58	(vs)
4,23	(vvw)	-			
3,98	(s)	3,98	(m)	4,01	(m)
3,87	(m)	-		3,88	(m)
3,75	(m)	-		3,78	(m)
3,67	(w)	3,67	(m)	3,68	(m)
3,39	(vw)	-			

Tab. 2.8 collects short spacing values from literature works on Milk Fat samples.

Tab. 2.8 MF typical short spacing values.

Ramel and Marangoni (2017)			**Lambert et al. (2018)**
Short spacing [Å] – forma α	Short spacing [Å] – forma β'	Short spacing [Å] – forma β	Short spacing [Å] – forma 2Lβ' (T=22°C)
-	-	4,6	-
-	-	-	4,25
-	4,2	-	-
4,15	-	-	-
-	3,8	3,8	3,81
-	3,7	3,7	-

MF influence on a CB-MF mixture crystallization is significant when the MF percentage exceeds 2%. However, if the MF percentage is less than 30% it does not affect CB polymorphism, but it lowers Tm compared to pure CB (S. Metin et al., 2012). For this reason, XPRD diffractograms of mixtures containing less of 30% of MF would be qualitative equivalent to pure CB ones.

2.6.5 Small Angle X-ray Scattering

Small Angle X-ray Scattering measurements exploit a point or line focused beam that is directed on the sample and then a detector that collects the scattered radiation. The scattering vector modulus (q) is defined as

$$q = 4\pi/\lambda \sin(\Theta) \qquad \textit{(Eq. 2)}$$

where λ is the wavelength of the X-ray radiation and Θ is half of the scattering angle. It is performed at very small angles meaning larger structures are detected, in the range of nanometres. Those instruments work in a very similar way to XRD ones, but SAXS instruments exploit a higher distance between the radiation source, the sample holder and the detector in order to achieve the needed resolution at small scattering angles. Indeed, long spacing values listed in the previous paragraph in relation to CB polymorphs are applied to SAXS as well.
Peaks from the SAXS diffractogram that belong to the same phase can be recognised thanks to their relation to Miller indexes (h). Indeed, centres of peaks originated from the same lamellar phase can be perfectly aligned on a straight line in a q vs h chart.
Miller indexes are used to identify the different directions and planes in a crystalline structure. In the previous described application, the h index refers to the order of the same crystal phase, thus to different parallel planes of the structure.

Chapter 3: Materials and Methods

This chapter gathers the information about the samples analysed through this work and the equipment used for the analysis, together with the methodology employed.

3.1 Materials

Cocoa butter (CB) and milk fat (MF) samples as well as plant based fat mixtures, named Milk Fat 2 (MF2) and Milk Fat 4 (MF4), were supplied by Nestlé Product Technology Centre Confectionery. MF2 is a compound of oils and fats from palm and shea while MF4 is a vegan milk fat replacer.
In order to study the behaviour of the milk fat replacers in the presence of CB, mixtures of 20% and 5% in weight of MF, MF2 and MF4 in CB were prepared as summarised in Tab. 3.1.

Tab. 3.1 Mixture samples used in experiments.

Weight percentage in CB	20 wt%	5 wt%
MF	MF 20	MF 5
MF2	MF2 20	MF2 5
MF4	MF4 20	MF4 5

3.2 Analytical characterizaiton procedures

Crystallization behaviour of samples was studied using different techniques in order to recognise multiple crystal forms and so to determine their suitability to be used as MF replacers in chocolate products. Samples were considered completely molten at 70°C therefore samples were heated to such temperature before each cooling process.

The chemical composition of Milk fat was kindly studied by Dr. Yoga Pratama from the University of Leeds. The chemical composition of the plant based samples was studied by liquid chromatography and high resolution mass spectrometry following the MP-80053 method. This analysis was performed by an external laboratory as well, in particular Nestlé Research group based in Switzerland shared these results to improve this work accuracy. The list of triacylglycerol (TAG) regioisomers contained in each compound allowed to characterize the behaviour as a result of the different saturation of the fatty acids.

A laboratory oven was used to heat the samples until they were fully molten, and the melting was obtained setting temperature to 50°C while the duration of this process varied in relation to the time necessary for the samples to appear visibly as a homogeneous liquid.

Hot-stage Polarized Light Microscopy (PLM) analysis was intended to determine melting points and crystallization temperatures at different heating and cooling rates in addition to particularly noticeable polymorphic transformations temperatures. Samples of CB, MF, MF2, MF4 and mixtures at 20 wt% of the milk fat replacers were observed. A Linkam

PE120 temperature-controlling microscope stage was used to apply the selected thermal protocol while the structure of the sample was observed through a Zeiss Axiolab 5 microscope with a x50 zoom. After melting the samples at 50°C in the oven, a drop was placed on the hot plate on a microscope slide. Temperature was first raised to 70°C at 10°C/min rate. Then a faster cooling ramp with a cooling rate of -1 or -2°C/min to 5 or 0°C was performed. Samples were then heated again to 70°C with a heating rate of 0.5°C/min. At the end they were cooled down to 5°C with a slower rate of -0.5°C/min (Tab. 3.2).

Tab. 3.2 heating and cooling ramps used in hot-stage PLM analyses.

	Reached temperature [°C]	**Temperature changing rate [°C/min]**
Ramp 1: melting	70	+10
Ramp 2: fast cooling	5 or 0	-1 or -2
Ramp 3: heating	70	+0.5
Ramp 4: slow cooling	5	-0.5

Videos of the process were taken using a mobile phone camera. Images obtained from video frames were processed through Matlab R2022b software. Frames were filtered and binarized in order to represent crystals with white pixels and the background with black pixels. Counting white pixels allowed to highlight crystals arising during the temperature decreasing ramp.

Differential Scanning Calorimetry (DSC) analyses were conducted using DSC 1 by Mettler Toledo equipment. The DSC analysis was performed using the same thermal protocol illustrated in Tab. 3.3 on each sample. Samples were molten increasing temperature to 70°C at 10°C/min, then a fast cooling was performed to -10°C at a rate of -5°C/min. Finally, samples were heated to 70°C at 2°C/min and then cooled to -10°C at -2°C/min.

Tab. 3.3 Heating and cooling ramps used in DSC analyses.

	Reached temperature [°C]	**Temperature changing rate [°C/min]**
Ramp 1: melting	70	+10
Ramp 2: fast cooling	-10	-5
Ramp 3: heating	70	+2
Ramp 4: slow cooling	-10	-2

Spectroscopy analyses were performed using LabRAM HR Evolution Raman spectrometer with a Synapse Plus detector by Horiba Scientific and laser wavelength of 532nm. Raman hot stage studies were also carried out using Linkam PE120 microscope stage as before. The Raman spectroscopy hot-stage protocol (Tab. 3.4) consisted of a heating ramp to 70°C at 10°C/min followed by a cooling ramp to -5°C or to 5°C at -2°C/min rate.

Tab. 3.4 Heating and cooling ramps used in Raman spectroscopy.

	Reached temperature [°C]	Temperature changing rate [°C/min]
Ramp 1: melting	70	+10
Ramp 2: cooling	-5 or 5	-2

X-Ray Powder Diffraction (XRPD) was also used to determine the presence of different crystal polymorphs in samples stored at room temperature without any previous manipulation. The diffractograms were obtained through Empyrean instrument by Malvern Panalytical. XRPD diffractograms were taken at room temperature without any previous treatment.

Small Angle X-ray Scattering (SAXS) technique was useful to determine the formation of different polymorphs according to temperature and cooling rate. This was performed at Elettra Synchrotron in Basovizza (Trieste, Italy). SAXS spectra were acquired with an exposure period of 60 seconds and an exposure time of 20s.

Thermal protocol for MF2 sample started with a first heating process to 70°C through two ramps, first one to 50°C at 2°C/min and second one to 70°C at 10°C/min. The sample was then maintained at 70°C for 5min, then cooled to 45°C at -10°C/min, followed by a 5min temperature holding. First crystallization occurred during slow cooling to 5°C at -0.5°C/min. Then MF2 was hold at 5°C for 90 min. MF2 was heated to 50°C at 0.5°C/min rate, then cooled at -5°C/min to 0°C and kept at 0°C for 30min. Finally, it was heated to 20°C at 2°C/min and removed from the sample holder.

The thermal protocol for MF4 was slightly different from the one above. The first heating process to 70°C was performed through a single ramp to 70°C at 10°C/min rate. MF4 analysis was then interrupted after a short temperature holding at 5°C and the sample was kept at 5°C in a refrigerator without being monitored. It was then studied for 50 min at 5°C, heated to 50°C at 0.5°C/min rate, cooled at -5°C/min to 5°C. Temperature was held constant at 5°C for 25 min then the sample was reheated to 40°C at 1°C/min.

Mixtures of MF2 and MF4 at 20% in CB underwent the same thermal protocol as well as pure CB. The compound was firstly heated to 50°C at 2°C/min, then the heating process was completed through a second ramp to 70°C at 20°C/min. Following a 5 min temperature holding, the sample was cooled to 45°C at -20°C/min and then cooled to 5°C at a slow rate of -0.5°C/min. Temperature was then kept constant for 20 min and finally increased to 45°C at 1°C/min rate and held for 5 min. At the end of the analysis the sample was cooled to 5°C at a faster -5°C/min rate.

MF 20 sample was heated from 20 to 40°C at 2°C/min, then temperature was further increased to 70°C at 20°C/min and held for 5 min. MF 20 sample was then cooled to 40°C at -20°C/min and kept at this temperature for 2 min. It was then cooled to 5°C at -0.5°C/min, held for 20 min, and heated again to 40°C at 1°C/min rate.

All applied protocols are summarized in Tab. 3.5. It is important to draw attention to the fact that even if thermal ramps used in experiments were not exactly the same from one sample to the other the major scheme was preserved in all the tests. Specifically, the slower cooling process is most relevant for the results because time is given to the sample to form the more stable and pure crystal structures.

Tab. 3.5 Heating and cooling ramps used in SAXS analyses.

	Phase	**Reached temperature [°C]**	**Temperature changing rate [°C/min] or duration [min]**
MF2	melting	50 then 70	+2 then +20
	slow cooling	5	-0.5
	holding	5	90 min
	heating	50	+0.5
	fast cooling	0	-5
	holding	0	30 min
	heating	20	+2
MF4	melting	70	+10
	slow cooling	5	-0.5
	holding	5	50 min
	heating	50	+0.5
	fast cooling	5	-5
	holding	5	25 min
	heating	40	1
CB **MF2 20** **MF4 20**	melting	50 then 70	+2 then +20
	slow cooling	5	-0.5
	holding	5	20 min
	heating	45	+1
	fast cooling	5	-5
MF 20	melting	40 then 70	+2 then +20
	slow cooling	5	-0.5
	holding	5	20 min
	heating	40	+1

Matlab R2022b, Origin 2023b and Microsoft Excel 2016 were used for data processing.

Chapter 4: Results

This chapter describes the main outcomes obtained from the work performed. In particular results from each analytical technique are exposed in detail and further deductions are displayed. In the first place the chemical composition of the samples was investigated, following by less sophisticated techniques results that allowed to found the general melting behaviour and major morphology aspects. Finally, more specific techniques consented to clearly depict crystal structures and lay the foundations to additional studies of these fats mixtures.

4.1 Samples chemical composition

The study of fats samples firstly concentrated on understanding their chemical composition, in order to identify the most abundant TAGs and to determine the overall complexity of the TAGs mixtures studied. Physical and chemical properties of the compounds are strongly linked to the fatty acids composition, but most importantly to the TAG distribution.

Samples were studied by liquid chromatography and liquid spectrometry. Tab. 4.1 lists TAGs contained in the two samples.

Analysing in detail the composition of TAGs it is possible to notice some important features. MF2 is mainly composed by monounsaturated TAGs, mostly in the form of saturated-unsaturated-saturated FA, such as SOS, POP or POS that make respectively 28%, 24% and 8% (rounded to the nearest unit) of the sample. Thus, 60% of this compound is formed by the same major components of CB. Tri-saturated TAGs appear in lower concentrations of 1.25% and 1.01% in form of PPP and SSS. However, this type of TAGs can crystallize in very stable structures whose melting point is very high. The third place is occupied by OOP, which is part of di-unsaturated TAGs. Tab. 4.2 shows the fatty acids composition of MF2 where the total amount of saturated FA exceeds 50% and monounsaturated percentage is higher than 35%. This is consistent with TAGs composition described before and highlights that the amount of di-unsaturated FA is lower than 8%.

On the other hand, MF4 composition is very different. The major components are OOO and OOP, tri-unsaturated and di-unsaturated TAGs. It is necessary to highlight that tri-oleic TAG does not form crystalline structures but creates an amorphous solid. Thus, it is not detected by the analytical techniques used in this work, such as SAXS and XPRD where it creates an amorphous band. SSO, SOS and POS are the most abundant monounsaturated TAGs in MF4 and collectively they constitute almost 15% of the mixture. Tab. 4.3 Shows FA composition where it is clear the high relevance of unsaturated fats in this sample. Concerning the high melting fraction of MF4 the only trisaturated TAG above 1% is SSS at 1.76%.

Tab. 4.4 and Tab. 4.5 collect information about MF4 and MF2 solid fat content (SFC). MF4 has a lower SFC and at room temperature (20°C) only 25% of the mixture is solid, while at 35°C it is almost molten and the remaining solid fraction is just 3%. MF2 solid fat content is generally higher and at room temperature is around 50%, meaning half of the mixture is solid. This reflects the appearance of the samples, where MF2 appears as a soft solid while MF4 has a creamy consistence.

Tab. 4.1 TAG composition of MF2 and MF4 samples.

MF2		MF4	
TAG	**%wt**	**TAG**	**%wt**
18:0 - 18:1 - 18:0	28.24	18:1 - 18:1 - 18:1	12.08
16:0 - 18:1 - 16:0	23.51	18:1 - 18:1 - 18:0	11.48
18:1 - 18:1 - 16:0	8.68	18:0 - 18:0 - 18:1	9.23
16:0 - 18:1 - 18:0	8.33	18:1 - 18:0 - 18:1	6.17
16:0 - 18:2 - 16:0	4.29	18:0 - 18:1 - 18:0	5.11
16:0 - 16:0 - 18:1	2.91	16:0 - 18:1 - 18:0	5.03
18:1 - 18:1 - 18:0	2.38	18:1 - 18:1 -18:2	4.90
18:0 - 18:2 - 18:0	2.16	16:0 - 18:0 - 18:1	4.62
16:0 - 18:2 - 18:1	2.15	18:1 - 18:1 - 16:0	4.22
18:0 - 18:1 - 20:0	1.53	18:0 - 16:0 - 18:1	4.04
18:1 - 18:1 - 18:1	1.52	16:0 - 16:0 - 18:1	4.02
16:0 - 16:0 - 16:0	1.25	18:1 - 18:0 - 18:2	2.52
16:0 - 18:2 - 18:0	1.03	16:0 - 18:1 -16:0	1.87
18:0 - 18:0 - 18:0	1.01	18:0 - 18:2 - 18:1	1.78
16:0 - 18:1 - 18:2	0.91	18:0 -18:0 -18:0	1.76
14:0 - 18:1 - 16:0	0.66	18:1 -16:0 - 18:1	1.65
18:1 - 16:0 - 18:2	0.65	18:0 - 18:1 -18:2	1.57
16:0 - 16:0 - 18:2	0.61	18:0 - 18:0 - 18:2	1.19
18:2 - 18:2 - 16:0	0.43	18:1 - 18:2 - 18:1	1.10
18:1 - 18:2 - 18:1	0.36	18:0 - 18:0 - 16:0	0.87
18:1 - 18:1 - 18:2	0.31	16:0 - 18:2 - 18:0	0.81
16:0 - 18:0 - 18:1	0.31	18:1 - 16:0 - 18:2	0.78
18:0 - 18:0 - 18:1	0.29	18:0 - 18:2 - 18:0	0.77
16:0 - 16:0 - 18:0	0.28	16:0 - 18:0 - 18:2	0.76
18:0 - 18:2 - 18:1	0.23	16:0 - 18:2 - 18:1	0.76
		18:0 - 16:0 - 18:2	0.70
		16:0 - 16:0 - 18:0	0.61
		16:0 - 16:0 - 18:2	0.55
		18:2 - 18:1 - 18:2	0.47
		16:0 - 16:0 - 16:0	0.43
		18:0 - 20:0 - 18:1	0.41

		18:1 - 18:1 - 20:0	0.41
		18:0 - 18:1 - 20:0	0.34
		16:0 - 18:1 - 18:2	0.31
		16:0 - 18:2 - 16:0	0.26
		18:2 - 18:2 - 18:1	0.24
		18:0 - 16:0 - 18:0	0.24
		2:0 - 18:0 - 18:1 &isomers	0.21
		18:1 - 18:1 - 20:1	0.20
		18:1 - 20:0 - 18:1	0.20
Total	94.04	**Total**	94.66

Tab. 4.2 FA composition of MF2 sample.

MF2	
Fatty Acid	**%**
C16:0	29.3 ± 0.6
C18:0	27.4 ± 0.4
C18:1	35.6 ± 0.5
C18:2	5.1 ± 0.2
Others	2.50

Tab. 4.3 FA composition of MF4 sample.

MF4	
Fatty Acid	**%**
Saturated	38
Monounsaturated	49
Polyunsaturated	8

Tab. 4.4 Solid fat content of MF2 sample.

MF2	
Temperature	**Solid fat content (%)**
20°C	42 - 51
25°C	35 - 45
30°C	23 - 30
35°C	Max 6

Tab. 4.5 Solid fat content of MF4 sample.

MF4	
Temperature	**Solid fat content (%)**
20°C	25
25°C	17
30°C	7
35°C	3

The same analysis was performed on the MF sample. As reported in the literature, this compound has a very complex composition and the amount of different FAs that form various TAGs is very high. In particular, it can be noticed that many short chain FAs, such as Butyric acid that is the saturated 4:0, appear very frequently.

Tab. 4.6 (a) TAG composition of MF sample.

MF			
TAG	**%wt**	**TAG**	**%wt**
Bu-P-O	7.71918	S-P-O	1.826725
Bu-P-S	5.749005	P-P-C	1.681575
Bu-M-O	5.247485	La-P-P	1.596075
Bu-P-P	5.10211	M-P-P	1.573025
Bu-M-P	4.870255	Bu-La-P	1.50599
Co-S-P	3.93958	P-Cy-O	1.49438
Bu-O-O	3.637615	P-P-Cy	1.386685
Co-P-P	3.42184	P-P-P	1.37553
Bu-S-O	3.37531	C-O-O	1.342135
O-P-P	3.105605	O-P-L	1.283085

n/i	3.08187	O-O-O	1.216095
P-O-O	2.738725	O-O-S	1.082555
P-M-O	2.64449	P-M-L	1.07687
Co-M-P	2.467125	Bu-Co-P	1.06032
Bu-P-L	2.11293	P-P-S	0.860555
P-La-O	2.10469	Bu-C-M	0.82692
P-C-O	2.100165	Bu-La-O	0.774455
Bu-C-P	1.91997	S-P-S	0.56809
O-M-O	1.84122		
Total		89.71024	

Tab. 4.6 (b) Fatty acids from composition of MF sample.

MF fatty acids		
Abbreviation	**Fatty acid**	**Chain length and unsaturated bonds**
Bu	Butyric acid	4:0
Co	Caproic acid	6:0
Cy	Caprylic acid	8:0
C	Capric acid	10:0
La	Lauric acid	12:0
M	Myristic acid	14:0
P	Palmitic acid	16:0
S	Stearic acid	18:0
O	Oleic acid	18:1
L	Linoleic acid	18:2

4.2 Polarized Light Microscopy

Analysis under Polarized Light Microscopy (PLM) had the aim of highlighting the temperature of crystallization and melting point of the samples at different cooling rates. For each sample significant frames have been extracted from the video of the slow cooling process with a cooling rate of -0.5°C/min and qualitatively compared. Corresponding binarized images are also shown. The Matlab software was used to binarize video frames and quantify crystal formation as the number of white pixels in binarized frames as a function of time. Temperature profile is also shown.

PLM images of CB sample (Fig. 4.1) did not show a visible variation of crystal appearance, while the quantity increase was clear.

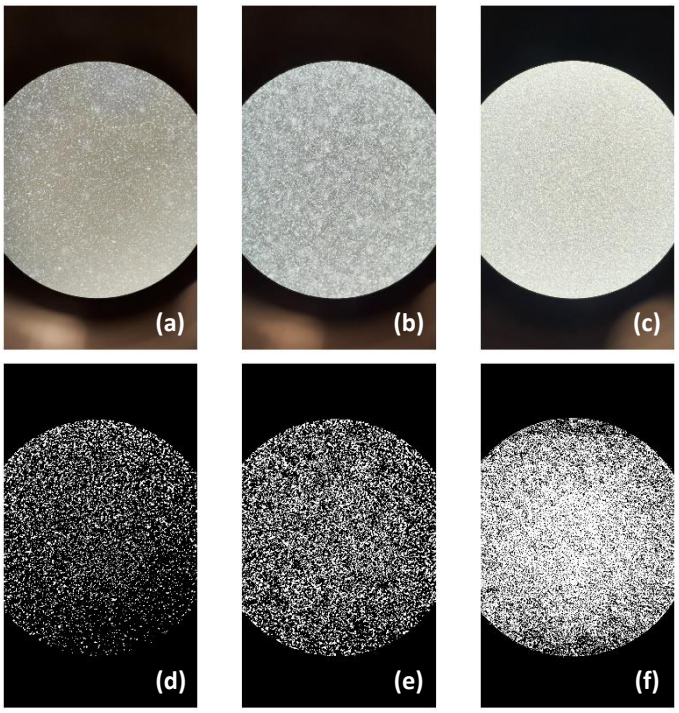

Fig. 4.1 PLM images of CB sample (a), (b) and (c) and their binarized version (d), (e), (f).

MF frames showed evidence of different crystal shapes recognisable even at this first stage of analysis. Fig. 4.2 (a) represented a first polymorph with smaller and more regularly shaped crystals, while at lower temperature new crystals presented a different morphology as indicated in Fig. 4.2 (b) and (c). This result confirms that MF firstly crystallized in smaller needle shaped crystals that than aggregated in spherical structures that grew in size and finally connected in a more compact network as the crystallization process was almost complete with the remaining fraction, with a lower melting point, crystallized as well.

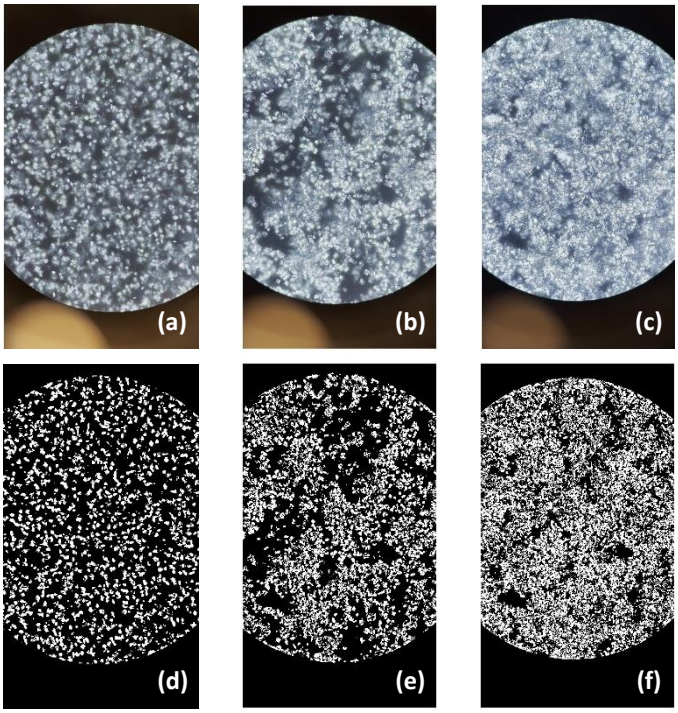

Fig. 4.2 PLM images of MF sample (a), (b) and (c) and their binarized version (d), (e), (f).

MF2 frames are reported in Fig. 4.3. Its appearance clearly changed from Fig. 4.3 (c) to Fig. 4.3 (d), thus it likely underwent a polymorphic transition. Similarly to MF, it firstly showed few spherical agglomerates (Fig. 4.3 (a)), increasing in number and in size until Fig. 4.3 (c). Finally, in frame (d) crystal form was drastically different as spherulites were no further seen and the crystal matrix seemed more regular and compact.

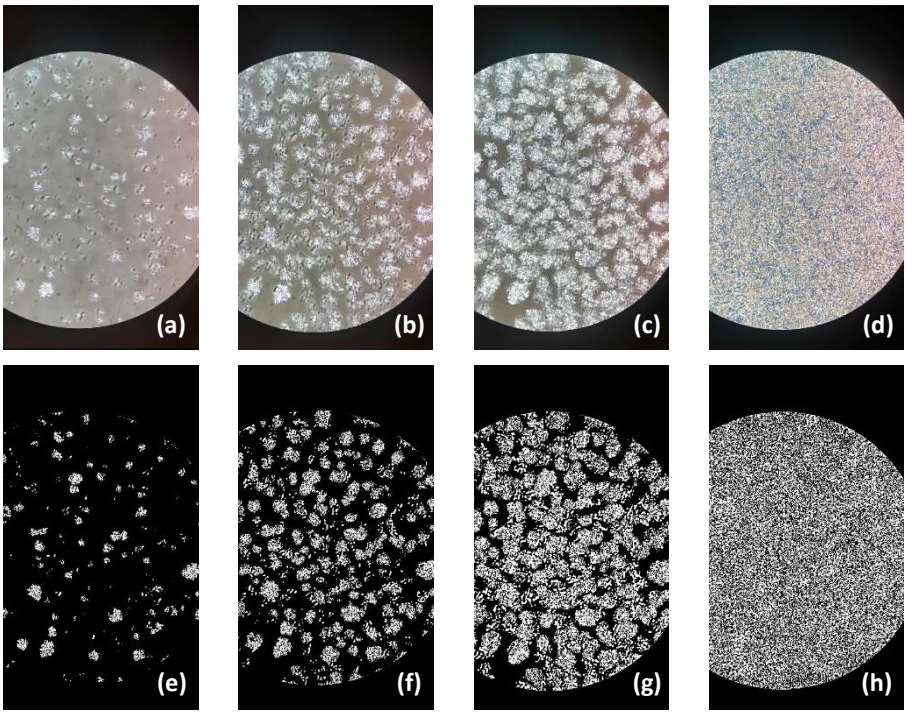

Fig. 4.3 PLM images of MF2 sample (a), (b), (c) and (d) and their binarized version (e), (f), (g) and (h).

MF4 sample appeared slightly different from the previous ones. Needle shaped crystals formed and grew without any spherical structure formation. Simultaneously, it was possible to see wider clear spots in the background growing with the needles.

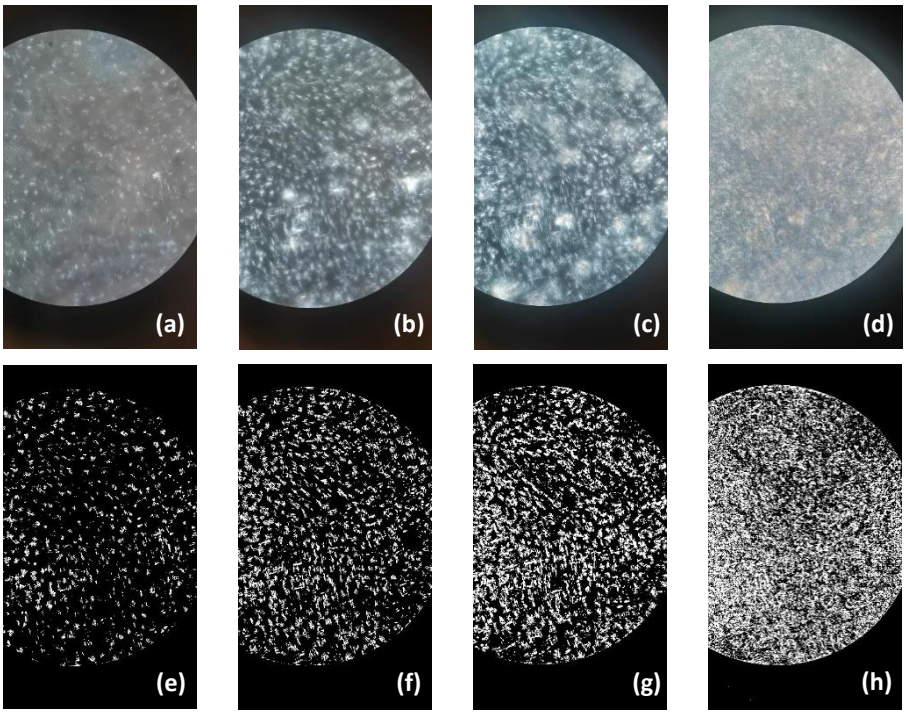

Fig. 4.4 PLM images of MF4 sample (a), (b), (c) and (d) and their binarized version (e), (f), (g) and (h).

Setting the microscope focus on a different level bigger crystals were then highlighted (Fig. 4.5), suggesting that two different crystal phases that are unable to mix and co-crystallize coexist in MF4.

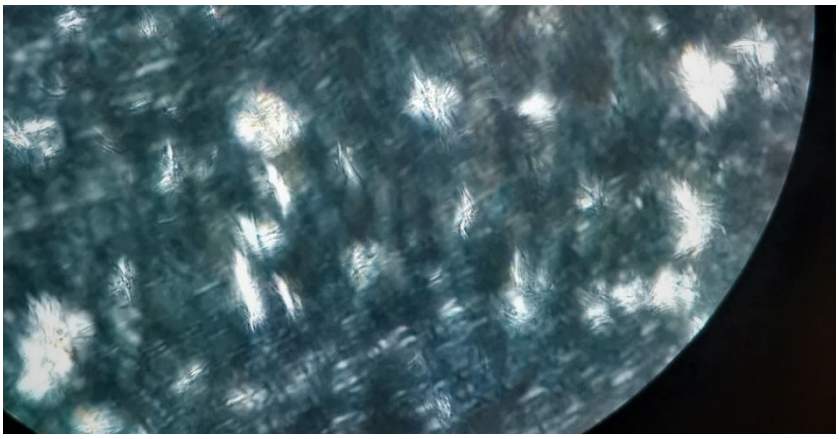

Fig. 4.5 PLM images of MF4 second crystal phase.

In the MF 20% mixture it was possible to recognize small crystals as in pure CB but the crystal matrix was less regular.

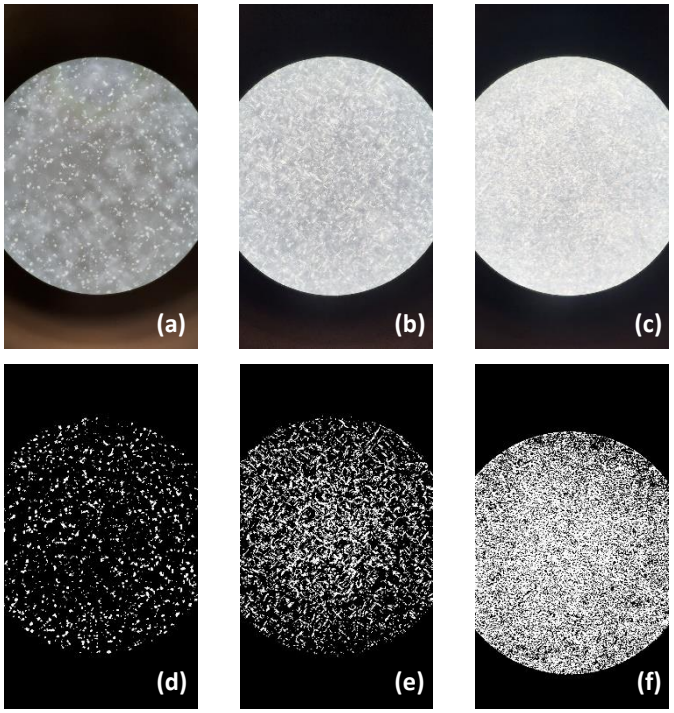

Fig. 4.6 PLM images of MF 20% sample (a), (b) and (c) and their binarized version (d), (e), (f).

In MF2 20% mixture small crystals from CB and aggregates typical of MF2 coexisted. As in pure MF2 the appearance became visually homogeneous when crystallization was complete.

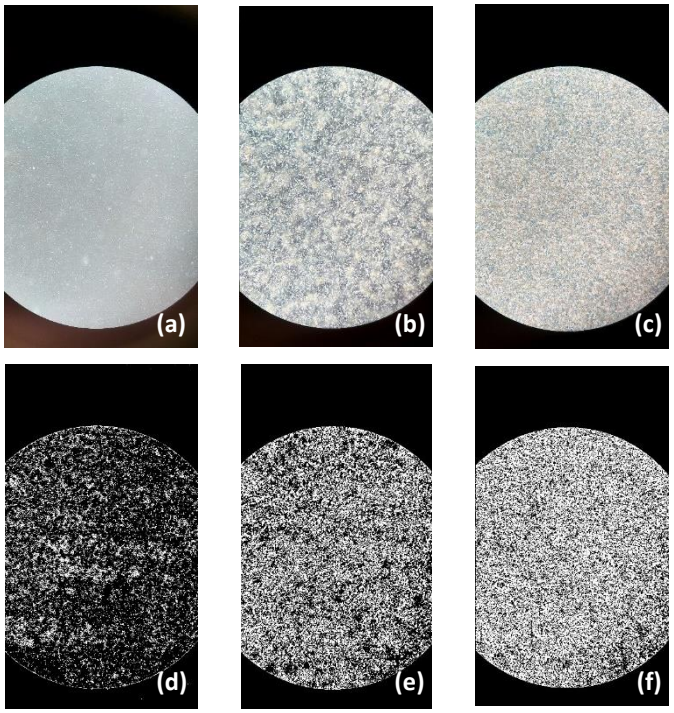

Fig. 4.7 PLM images of MF2 20% sample at (a), (b) and (c) and their binarized version (d), (e), (f).

MF4 20% mixture sample showed a similar behaviour to the previous case as characteristics of CB and pure MF4 both were clear.

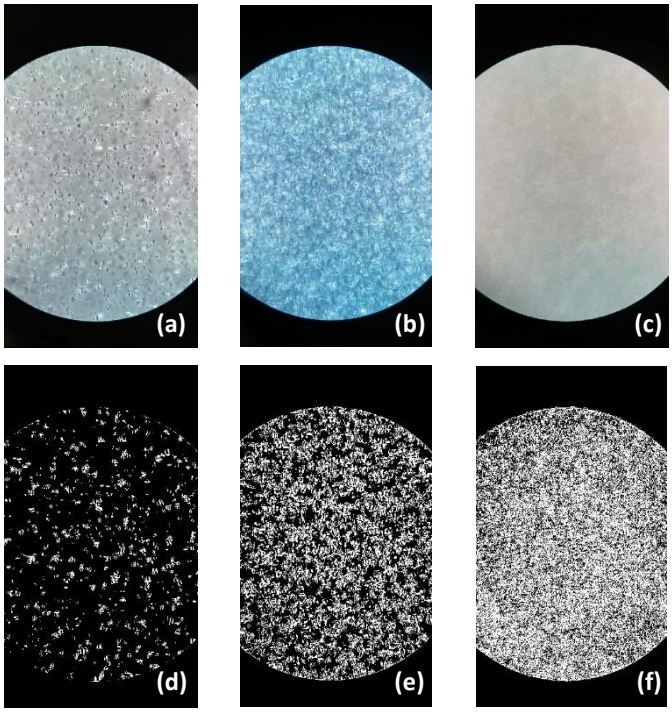

Fig. 4.8 PLM images of MF4 20% sample at (a), (b) and (c) and their binarized version (d), (e), (f).

The crystal growth profile obtained from the counting the white pixels of binarized video frames through Matlab software allowed to highlight changes in the growing rate as well as possible polymorphic transitions. Each one of the following profiles shows a first step where the number of pixels was increasing, then a quite stationary phase, which was more important in some of the samples, while in others it was just represented by a variation in growth rate and finally a secondary increase leading in the number of white pixels to complete crystallization.

In CB profile (Fig. 4.9 (a)) the three steps are well defined, as well as in MF (Fig. 4.9 (b)). It is possible to notice that MF sample reached a stability at around 0°C, while CB crystallization process was already stable at higher temperature, particularly at ~5°C. In both samples the first crystals started to form between 20 and 25°C. However, in CB the second steep increase in crystallization took place at ~13.5°C, while in MF it occurred around 5°C meaning that a fraction of this sample is molten until low temperatures are reached.

Plant based fats MF2 (Fig. 4.9 (c)) and MF4 (Fig. 4.9 (d)) exhibit a different crystallization profile. MF2 sample underwent two sharp crystallization steps at ~22.5°C and ~12°C. In between those, the number of white pixels barely changed. This behaviour suggests the presence of two phases that crystallize at very different temperatures. This is consistent with the formation of spherical agglomerates that lately are seen transitioning into the more compact crystal structure seen in the PLM images. On the other hand, MF4 profile indicates a more constant growth even though the major three step scheme was still recognizable. It is

interesting to highlight that MF4 started crystallizing above 25°C differing from all the previous samples and underwent a further higher rate crystallization from ~13°C to ~7°C.

Mixtures behaviour (Fig. 4.9 (e), (f) and (g)) clearly changes although all of them are composed by CB at 80%. It is hence highlighted the important role that MF or plant based fats can play in food products containing cocoa butter, chocolate in particular.

MF 20% profile showed a first crystallization step from ~22°C followed by a slow increasing of the white pixels count until the signal stabilized and finally a very sharp increase took place from ~14 to ~9°C, with the sample being completely crystallized at 5°C. Temperature range of the crystallization start was comparable to that of pure CB and pure MF and the second crystallization phase is consistent with CB second step. However, the second step played a major role in terms of quantity of crystals in the mixture compared to the amount of crystals formed in the first phase of the cooling process than in the pure components.

MF2 20% exhibited an unusual linear growth from 21°C to 15°C where growth rate suddenly became higher reaching a plateau around 10°C. Under this temperature few further crystals formed keeping the curve almost constant from around 5°C.

MF4 20% started crystallizing around 23°C with a high rate growth up to ~21°C. Then it increased almost linearly from 15°C to around 5°C where it reached stability. The constant rate growth under 15°C is coherent to MF4 pure sample behaviour which was alike.

Tab. 4.7 resumes first crystallization temperatures from cooling profiles in Fig. 4.9 together with complete melting temperatures extracted from melting videos.

Tab. 4.7 Start of crystallization at -0.5°C/min and complete melting temperatures extracted from PLM hotstage videos.

	First crystallization (Cooling rate -0.5 °C/min)	**Complete melting**
CB	22.5	37
MF	21.1	37.6
MF 20%	22	28
MF2	24	39
MF2 20%	23.5	29.9
MF4	25	39.5
MF4 20%	23	37.5

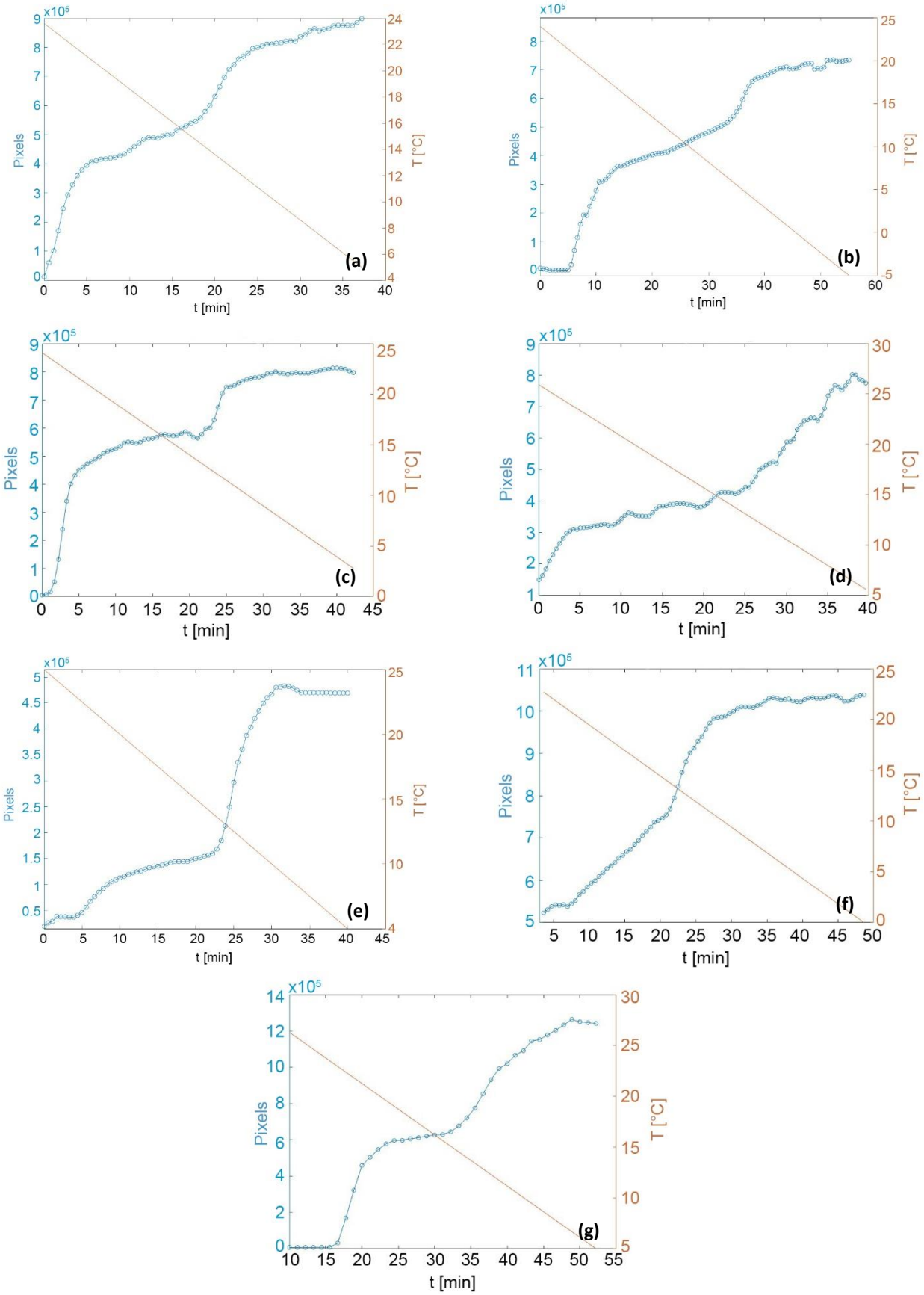

Fig. 4.9 Number of white pixels (representing crystals) and temperature evolution in time from PLM videos of CB (a), MF (b), MF2 (c), MF4 (d), MF 20% (e), MF2 20% (f) and MF4 20% (g) samples.

4.3 Differential Scanning Calorimetry results

Differential Scanning Calorimetry analysis is important to understand temperatures associated to melting and crystallization, but most importantly to polymorphic transitions. The variation of the heat flux to the sample is indeed a clear indication of an energy release linked to the transformation from one polymorph to a most stable one.

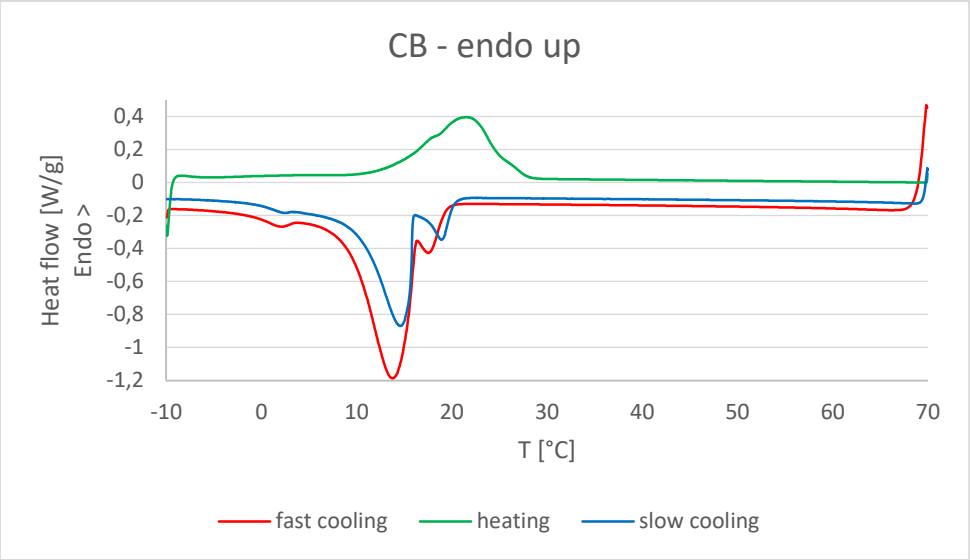

Fig. 4.10 DSC analysis of CB sample.

DSC analysis performed on the CB sample during the slower cooling phase (Fig. 4.10) showed a first weaker negative peak, corresponding to an exothermic phenomenon, from ~21.5°C. This temperature range corresponds to the first step of the crystallization process as seen by PLM. Also the secondary crystallization temperature is collocated from 16.8°C with an intense peak, as demonstrated by the corresponding steep increase in PLM crystal growth profile. This two crystallization steps represent the first and second α forms detected during the SAXS analysis. It was also noticed that the melting process occured in a single step from ~11°C to ~28.5°C. This final temperature is coherent to the melting temperature given from SAXS analysis regarding the most stable α form. Even if during SAXS ramps the complete melting point was higher, the faster cooling ramp did not allow the formation of the higher melting β' phase, hence the final melting temperature is lower. The fast cooling profile shows the same energy variations as also confirmed by X-ray scattering analysis but the intensity is higher because a faster crystallization requires to compensate the limited time given to molecules to arrange in crystal structures.

MF profiles show a more complex trend compared to CB, caused by the numerous crystal forms that originated during cooling crystallization. Slow cooling is characterised by two peaks, the first between 20 and 16°C and the second starting from ~12°C. This second exothermic phenomenon lasted until the end of the cooling ramp, meaning fractions of MF are still crystallizing at very low temperatures. This confirms again the wide crystallization

range of MF caused by the complexity of its composition and the variety of TAGs in it, especially short chained ones and so very low melting ones.

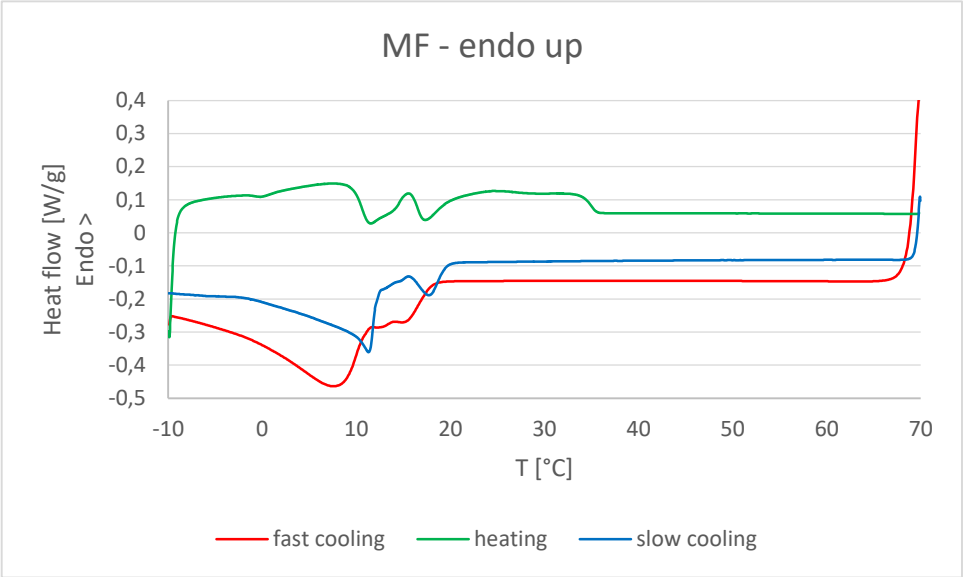

Fig. 4.11 DSC analysis of MF sample.

MF2 sample DSC curves reflected its behaviour from PLM and SAXS analysis as well. The first crystallization occurred from 23°C while secondary crystallization began at around 14°C. The melting is characterised by a very broad peak indicating a wide crystal compostion. As confirmed in PLM analysis the two peaks are well separated, meaning crystal structure remains almost constant in this range. The two peaks are associated to α phases from SAXS diffractograms.

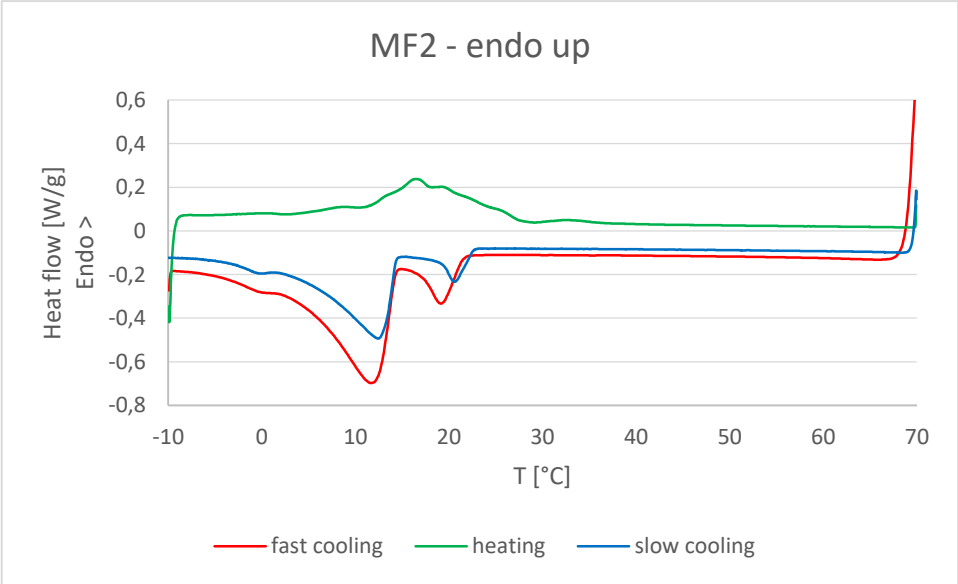

Fig. 4.12 DSC analysis of MF2 sample.

MF4 sample created a similar DSC profile to the one from milk fat. This is because both of them have a low melting fraction that remains molten in the temperature range of the analysis. However, the first step of crystallization showed in PLM studies is clear from 24°C, while secondary crystallization occurs from 15°C. The heating profile shows an endothermic peak from 27 to 42°C that corresponds to the high melting fraction of the mixture.

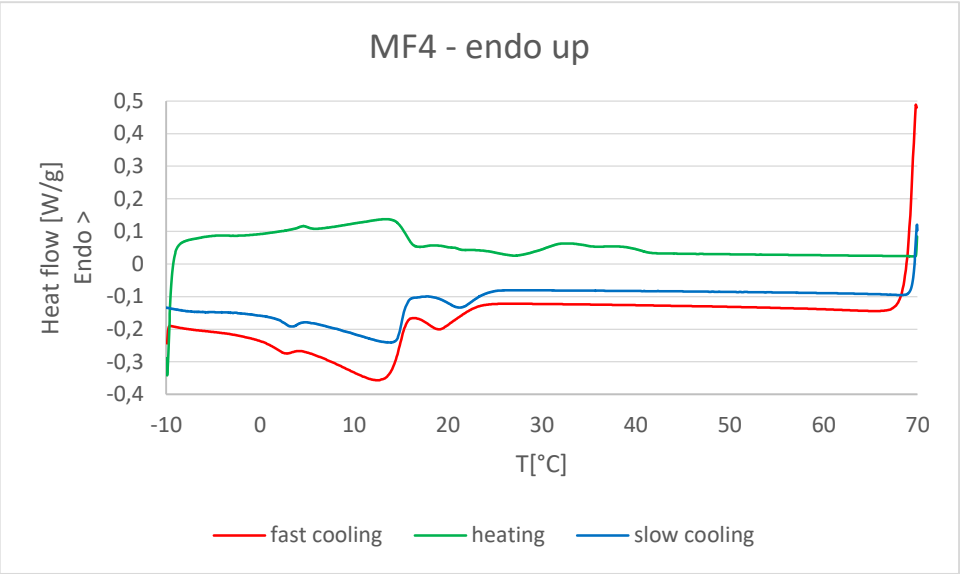

Fig. 4.13 DSC analysis of MF4 sample.

DSC analysis of mixture samples at 20% in CB are all characterized by the same trend. They all show a crystallization process in two steps, confirming again the results from the PLM study. However, it is clear the influence of the added fats. Particularly, MF4 20% has a less defined profile caused again by the olefinic fraction of this fat mixture. It is important to remember that the first component of this sample is OOO, whose melting point is below 0°C. For this reason, the exothermic curve is further from the zero line even at very low temperatures.

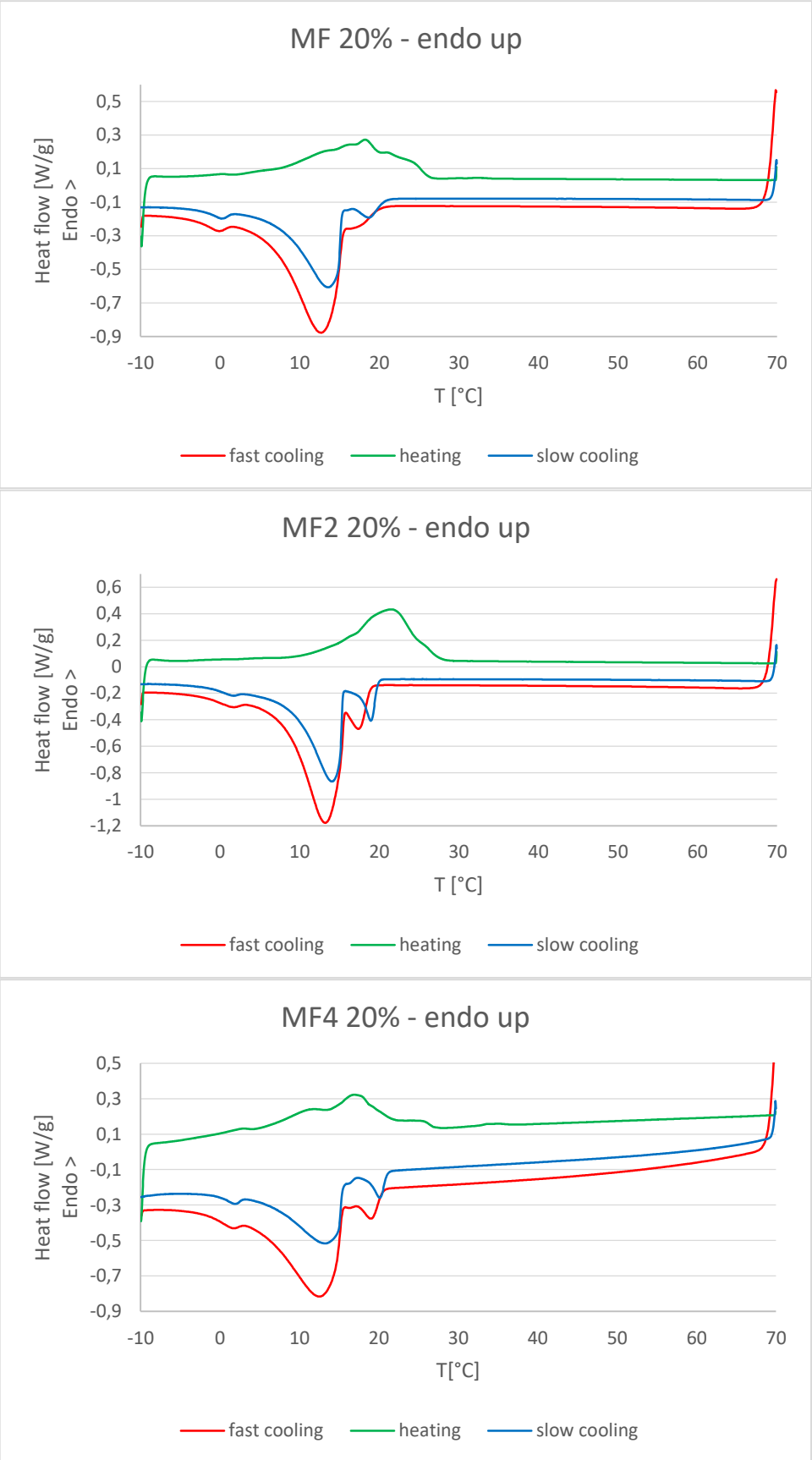

Fig. 4.14 DSC analysis of MF 20%, MF2 20% and MF4 20% samples.

4.4 Raman spectroscopy

Raman spectra could be used to distinguish different crystal forms using relevant regions of Raman shift.

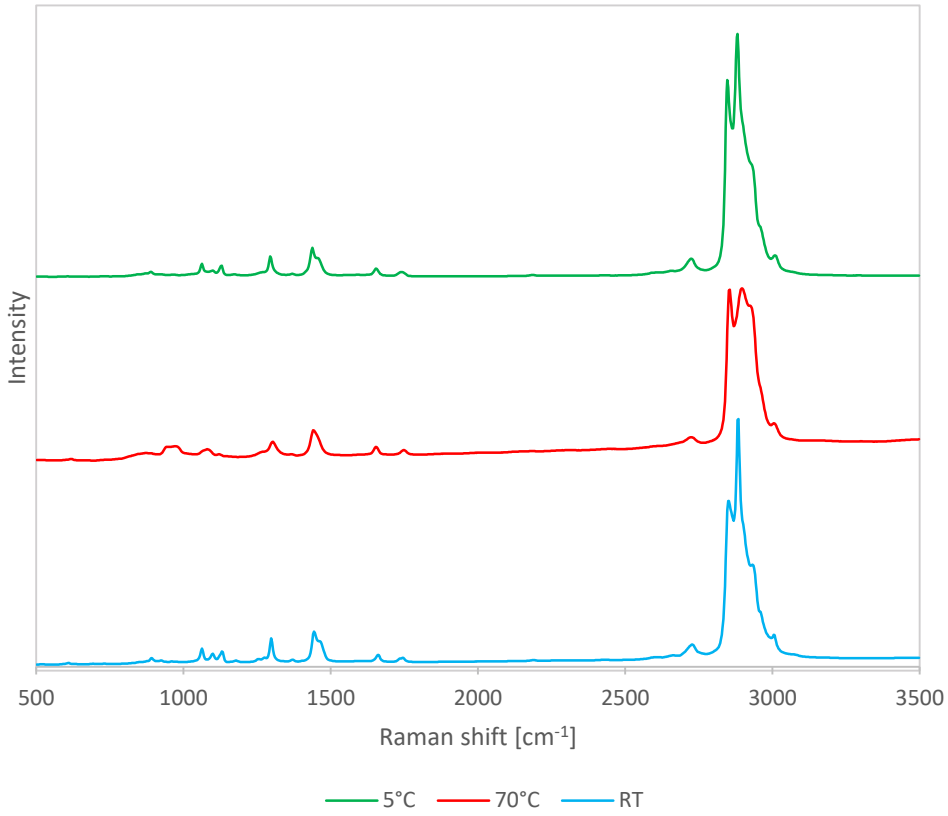

Fig. 4.15 CB Raman spectra at room temperature, molten (70°C) and recrystallized (5°C).

CB spectra was taken in the 500-3500 cm^{-1} range where relevant TAGs bonds vibrational modes can be detected (Fig. 4.15).

CB spectra in 1000-1200 cm^{-1} region (Fig. 4.16) referring to C-C bond stretching are comparable to those shown in Chapter 2 (S. Bresson et al., 2011). Room Temperature (RT) spectrum is typical of stable polymorphs while after the melting phase at 70°C it recrystallizes in less stable forms, as seen in the 5°C spectrum resembling form III proposed in literature (S. Bresson et al., 2011).

In Fig. 4.17 referring to the 1200-1800 cm^{-1} region, C=C double bond stretching characteristic of olefinic chains in TAGs can be analysed. In accordance to the C-C bond region spectra, at RT and 5°C form V and form III spectra proposed in literature can be recognised, respectively.

Fig. 4.18 related to CH groups is very noteworthy. The liquid spectrum only shows CH_3 group stretching band around 2935 cm^{-1}, becoming weaker in both solid spectra because of reduced chain terminations movements, as stated in literature (S. Bresson et al., 2011). At RT a sharp peak at 2882 cm^{-1} appears stronger than that at ~2850 cm^{-1}, meaning that antisymmetric stretching of this bond is more intense that symmetric one as chains are in a compact solid structure as of form V, as previous regions suggested.

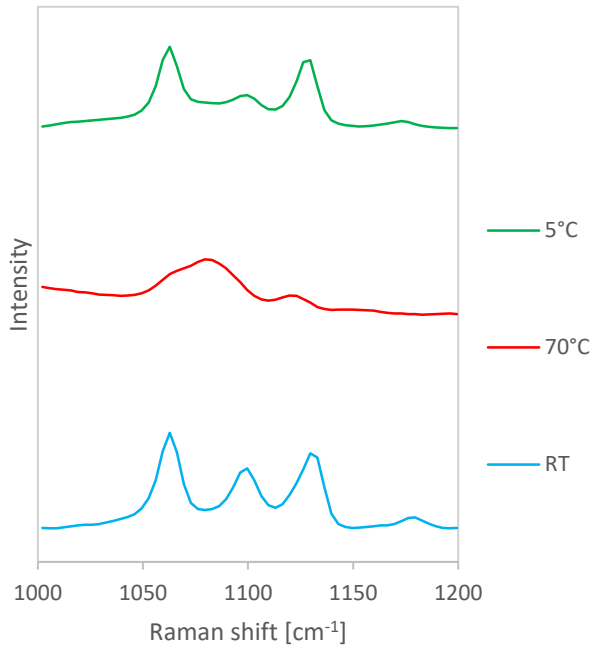

Fig. 4.16 CB Raman spectra of 1000-1200 cm^{-1} region related to C-C bond stretching at room temperature, molten (70°C) and recrystallized (5°C).

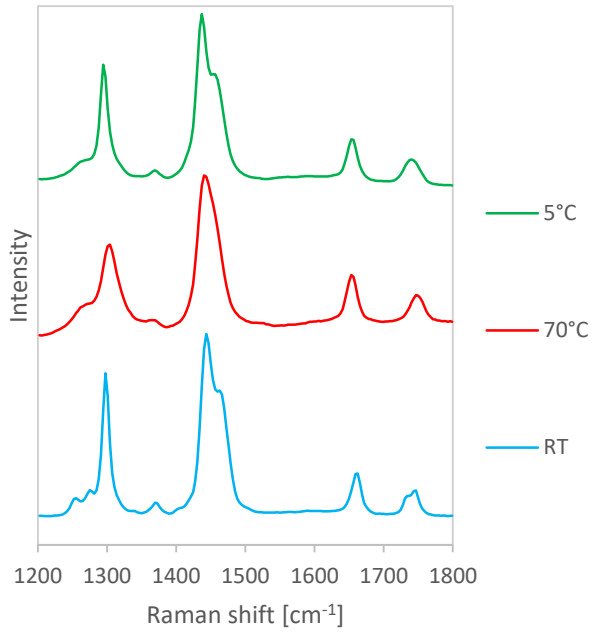

Fig. 4.17 CB Raman spectra of 1200-1800 cm^{-1} region related to C=C olefinic double bond at room temperature, molten (70°C) and recrystallized (5°C).

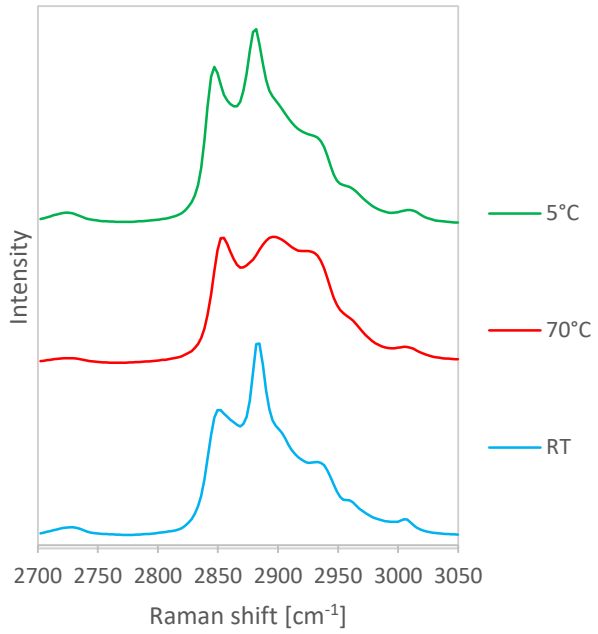

Fig. 4.18 CB Raman spectra of 2700-3050 cm^{-1} region related to C-H bond stretching at room temperature, molten (70°C) and recrystallized (5°C)

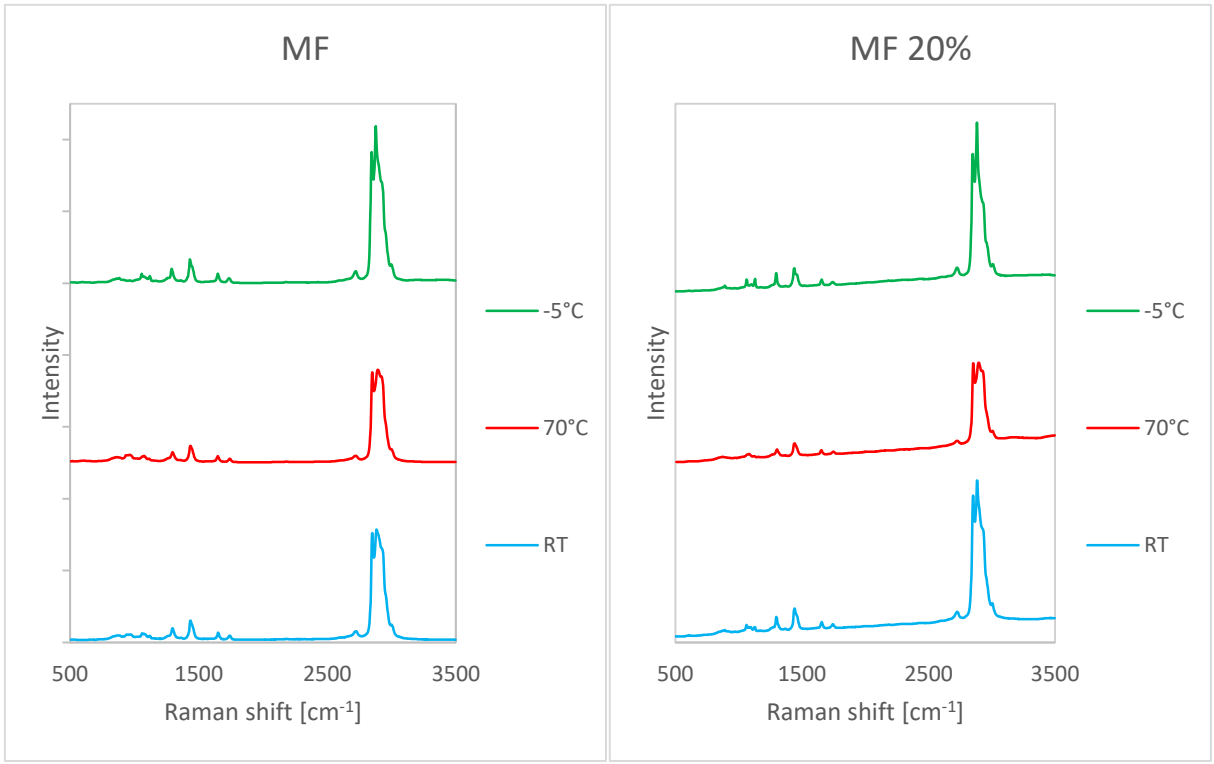

Fig. 4.19 MF and MF 20% Raman spectra at room temperature, molten (70°C) and recrystallized (-5°C).

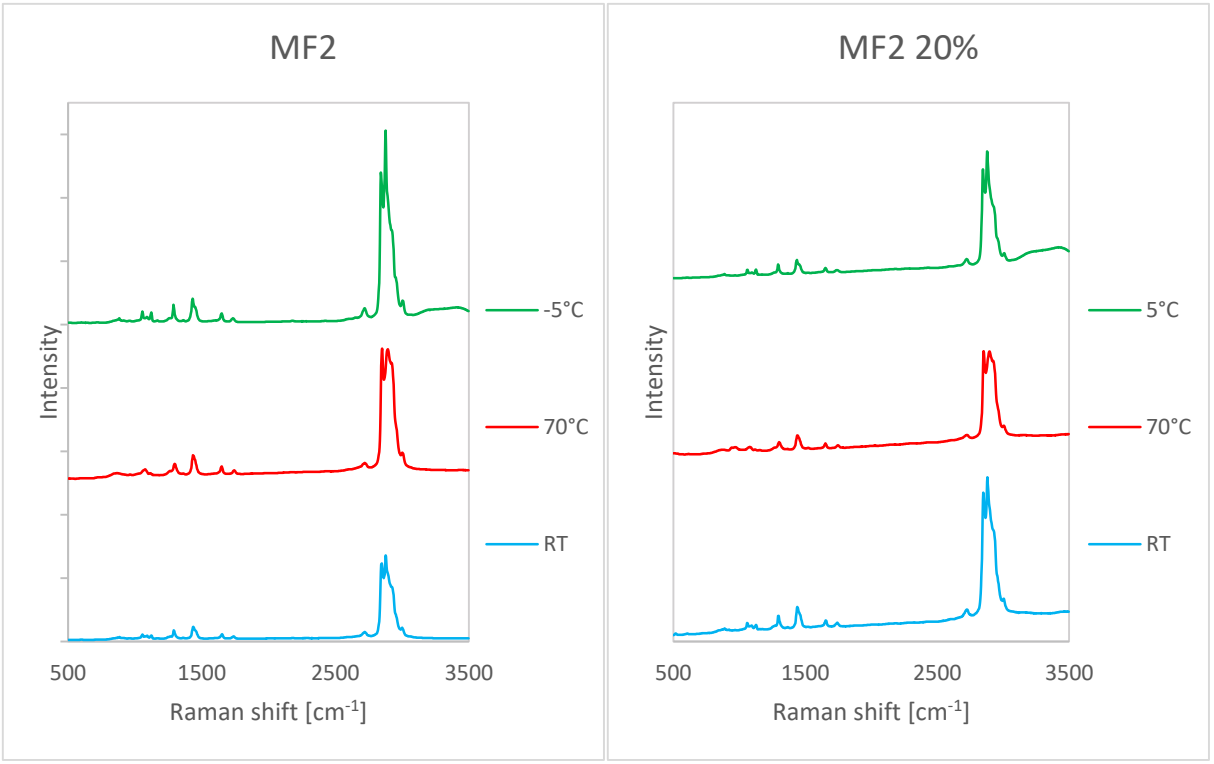

Fig. 4.20 MF2 and MF2 20% Raman spectra at room temperature, molten (70°C) and recrystallized (-5°C and 5°C, respectively).

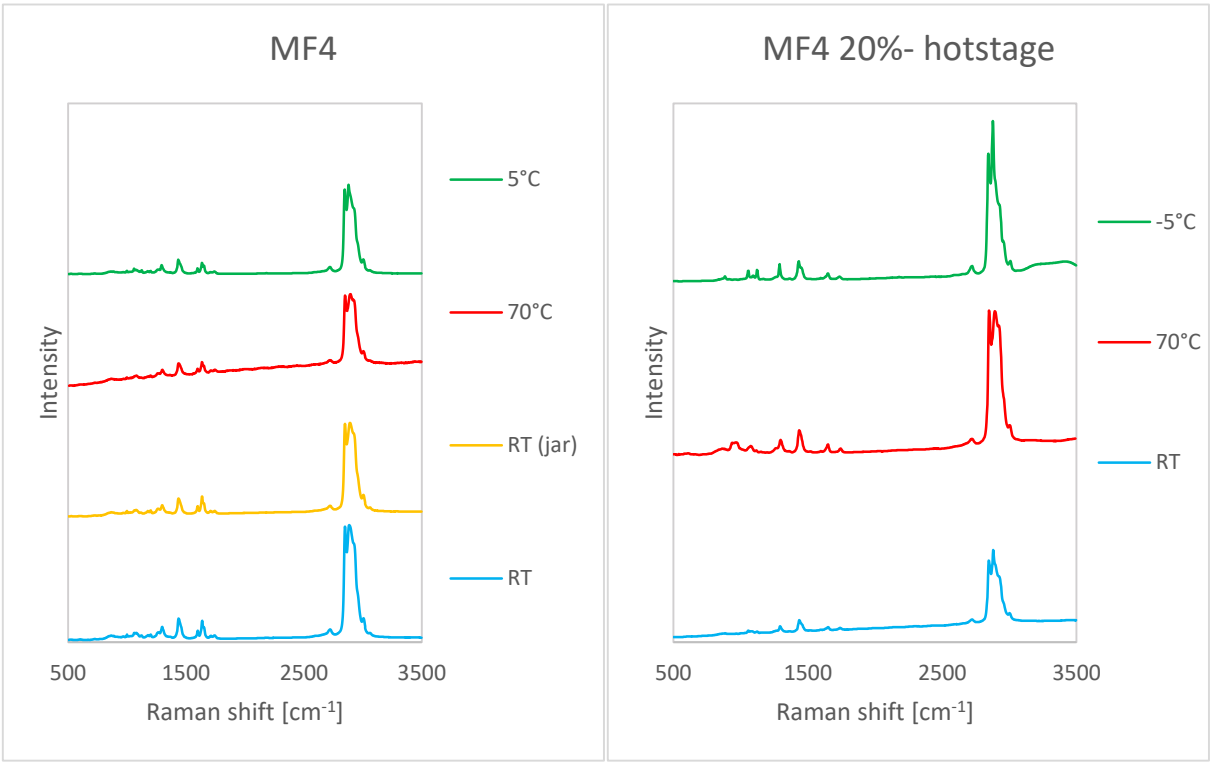

Fig. 4.21 MF4 and MF4 20% Raman spectra at room temperature, molten (70°C) and recrystallized (5°C and -5°C, respectively). MF4 sample was also analysed from the original jar: this sample had been kept at room temperature for about 2 months.

Raman spectra from MF, MF2, MF4 and their mixtures have been acquired as CB ones. All the samples showed a similar behaviour where the sample was found in a more stable form before the melting ramp and in a metastable form after the recrystallization took place.

However, while MF2 sample exhibits a sharper peak in the spectrum corresponding to the recrystallized sample compared to the molten phase, in MF4 analysis this difference was less evident. This again shows the molten nature of a major fraction of the MF4 sample because the sharp peak is caused by the presence of the stable β polymorph that is absent in MF4. A similar consideration can be made regarding MF sample.

4.5 XRPD results

XPRD diffractograms taken at RT without any melting or cooling process involved, can be very useful to determine the stable form which the sample tends to when left without any controlled parameter after a certain time span.

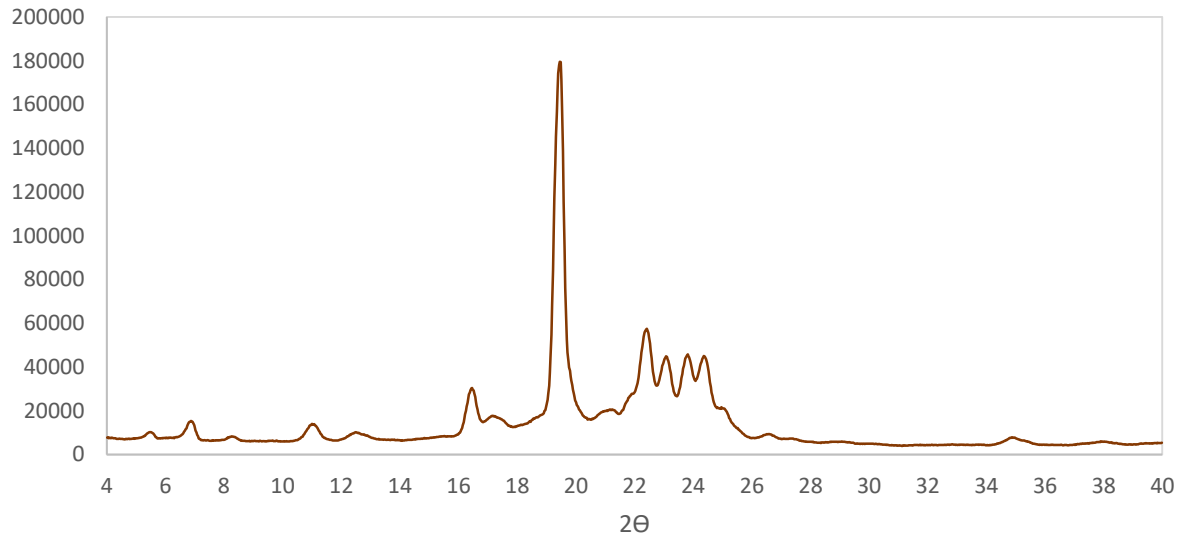

Fig. 4.22 XPRD of CB sample taken at room temperature (~20°C).

CB polymorphism has been extensively described in Chapter 2 as well as the main XPRD peaks related to each crystal form. Fig. 4.22 shows the CB diffractogram and the major peaks angles and intensity are listed in Tab. 4.8, where q and short spacing values were also calculated. As described in literature, CB diffractogram when in form V is clearly defined by five sharp peaks, one very intense peak at 4.6 Å short spacing and four of medium intensity at 4.0 Å, 3.9 Å, 3.8 Å e 3.7 Å. The current sample exhibits the peaks at 4.56 Å, 3.96 Å, 3.85 Å, 3.73 Å e 3.65 Å, respectively consistent with short spacing values found in literature. Hence, crystal form of this sample is identified as form V.

Tab. 4.8 XPRD peaks of CB sample taken at room temperature (~20°C). Intensity of the peaks is classified as very weak (vw), weak (w), medium (m), strong (s) and very strong (vs).

2Θ	Intensity	q [Å^{-1}]	Short spacing [Å]
16.46	30398 (m)	1.168	5.38
17.14	17661 (w)	1.216	5.17
19.45	179466 (vs)	1.378	4.56
21.06	20150 (vw)	1.490	4.22
22.42	57398 (s)	1.586	3.96
23.08	44897 (m)	1.632	3.85
23.81	45742 (m)	1.683	3.73
24.37	45075 (m)	1.721	3.65
26.57	9375 (vw)	1.875	3.35

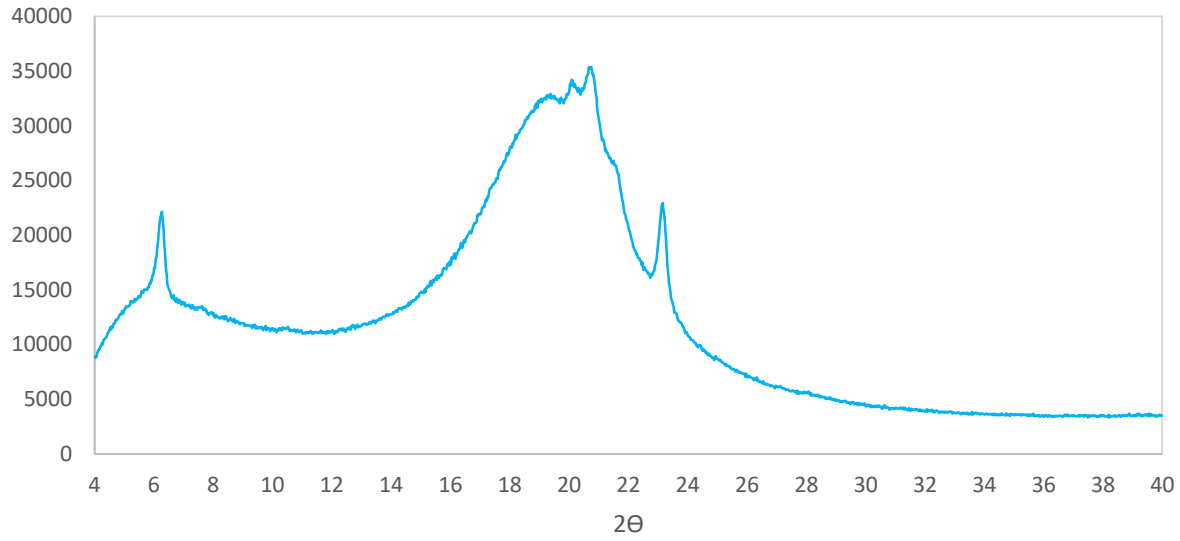

Fig. 4.23 XPRD of MF sample taken at room temperature (~20°C)

A significant MF fraction at RT is over its melting point and hence is in liquid phase. This was clearly revealed in the diffractogram in Fig. 4.23, where an amorphous band is evident. For this same reason peaks analysis was challenging since these are covered by the broad band of the liquid phase and only intense peaks can be seen. Tab. 4.9 summarizes all information showing all peaks and their comparison to literature (P.R. Ramel et al., 2017) (A. Lambert et al., 2018). Peak at 3.8 Å is linked to both β' and β forms, however the absence of a peak at 4.6 Å typical of the most stable form leads to the conclusion that β' crystals exist. Peaks around 4.2 Å are related to β' form as well, while peak at 4.16 Å can be associated to α form.

Tab. 4.9 XPRD peaks of MF sample taken at room temperature (~20°C).

2Θ	Intensity	q [Å^{-1}]	Short spacing [Å]
6.27	22152	0.446	14.08
20.08	34218	1.422	4.42
20.74	35393	1.468	4.28
21.34	27056	1.511	4.16
23.16	22939	1.637	3.84

Fig. 4.24 shows MF2 diffractogram and its similarity to CB is clear. A sharp peak at 4.6 Å, and peaks of medium intensity at 3.9 Å, 3.8 Å and 3.7 Å suggest the presence of a fraction that crystallized in β form, as well as the medium peak at 5.4 Å (Tab. 4.10). At the same time the poorly defined band demonstrates that part of the components of this sample are still in liquid form at room temperature as testified by the amorphous band.

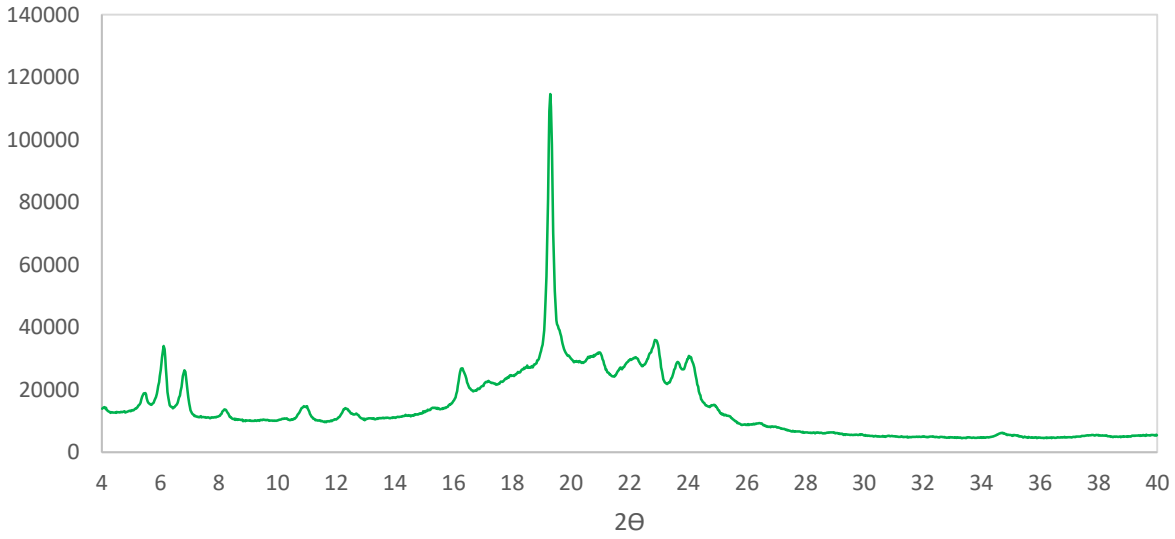

Fig. 4.24 XPRD of MF2 sample taken at room temperature (~20°C).

Tab. 4.10 XPRD peaks of MF2 sample taken at room temperature (~20°C).

2Θ	Intensity	q [Å^{-1}]	Short spacing [Å]
6.11	33988	0.435	14.44
6.82	26188	0.485	12.94
16.28	26873	1.155	5.44
19.30	114677	1.367	4.60
22.87	35956	1.617	3.89
23.63	28901	1.670	3.76
24.02	30809	1.698	3.70

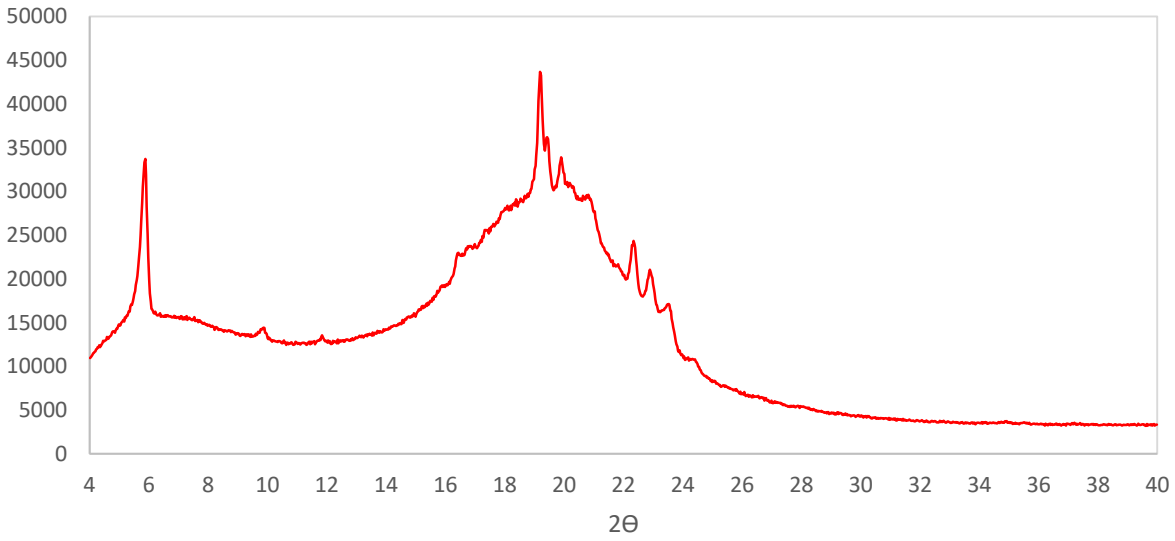

Fig. 4.25 XPRD of MF4 sample taken at room temperature (~20°C).

Tab. 4.11 XPRD peaks of MF4 sample taken at room temperature (~20°C).

2Θ	Intensity	q [Å^{-1}]	Short spacing [Å]
5.88	33717	0.418	15.02
1919	43663	1.360	4.62
19.43	36198	1.376	4.57
19.90	33881	1.409	4.46
22.34	24341	1.580	3.98
22.89	21036	1.619	3.88
23.52	17127	1.663	3.78

MF4 sample (Fig. 4.25) diffractogram was mainly characterised by an amorphous band due to an important fraction of the compound being in liquid form at room temperature, alike milk fat. Even though this band covers weaker peaks, higher ones are still seen. Two neat peaks around 4.6 Å (Tab. 4.11) indicate two β form phases that do not mix together, confirmed by medium intensity peaks typical of more stable polymorphic forms.

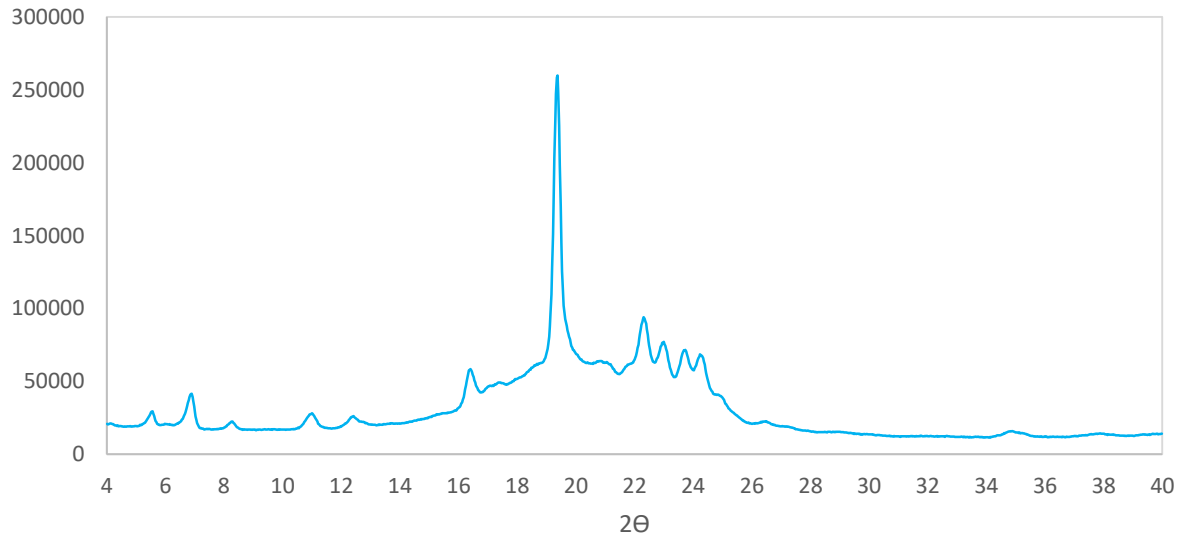

Fig. 4.26 XPRD of MF 20% mixture in CB taken at room temperature (~20°C).

XPRD analyses of pure samples created a starting point to understand diffractograms of MF, MF2 and MF4 mixtures in CB. Diffraction peaks of MF mixture at 20% in CB shown in Fig. 4.26 are mostly typical peaks of β form crystallized fats. Indeed, CB is the main component of this sample and the sharp peak at 4.6 Å undoubtedly indicates β form presence, in addition to 4.0, 3.9, 3.8 and 3.7 Å peaks. Indefinite region corresponding to the amorphous band values from MF diffractogram proves the liquid state of this fraction coming from the MF percentage in the sample.

Tab. 4.12 XPRD peaks of MF 20% mixture in CB taken at room temperature (~20°C).

2Θ	Intensity	q [Å^{-1}]	Short spacing [Å]
6.90	41644	0.491	12.80
16.41	58487	1.164	5.40
19.38	259726	1.373	4.58
22.32	94116	1.579	3.98
23.00	77162	1.626	3.86
23.68	71341	1.674	3.75
24.23	68502	1.712	3.67

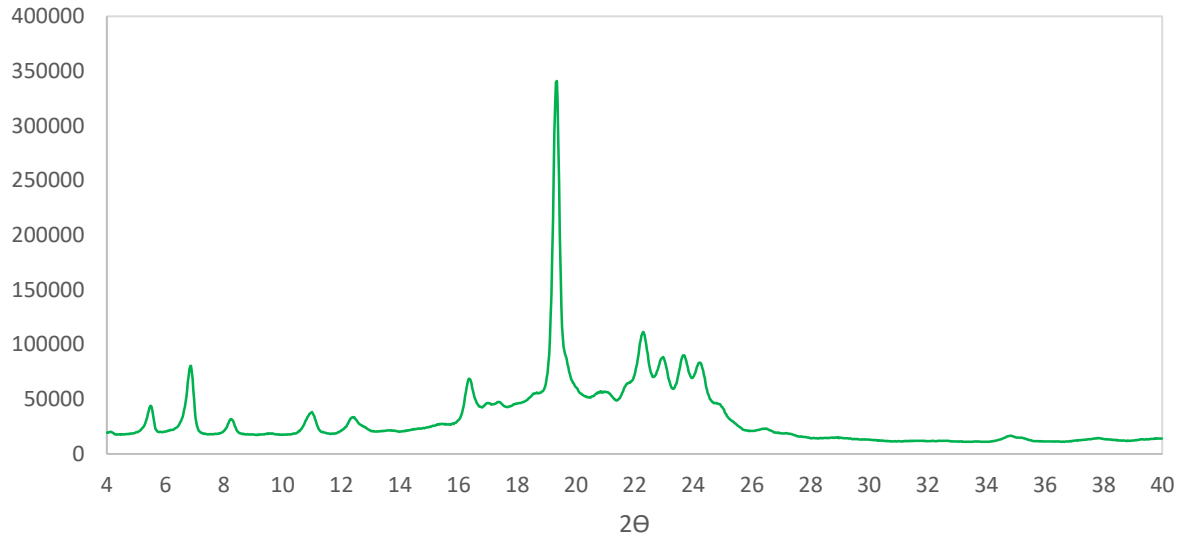

Fig. 4.27 XPRD of MF2 20% mixture in CB taken at room temperature (~20°C).

MF2 20% sample diffractogram (Fig. 4.27) exhibits β form peaks listed in Tab. 4.13. Actually, this result was expected because both the components of this mixture, CB and MF2, formed the same crystal structure when analysed as pure samples.

Tab. 4.13 XPRD peaks of MF2 20% mixture in CB taken at room temperature (~20°C).

2Θ	Intensity	q [Å^{-1}]	Short spacing [Å]
6.88	80379	0.489	12.85
16.36	68579	1.160	5.42
19.35	341046	1.371	4.58
22.29	111458	1.577	3.99
22.95	87673	1.623	3.87
23.68	90130	1.674	3.75
24.21	83412	1.710	3.67

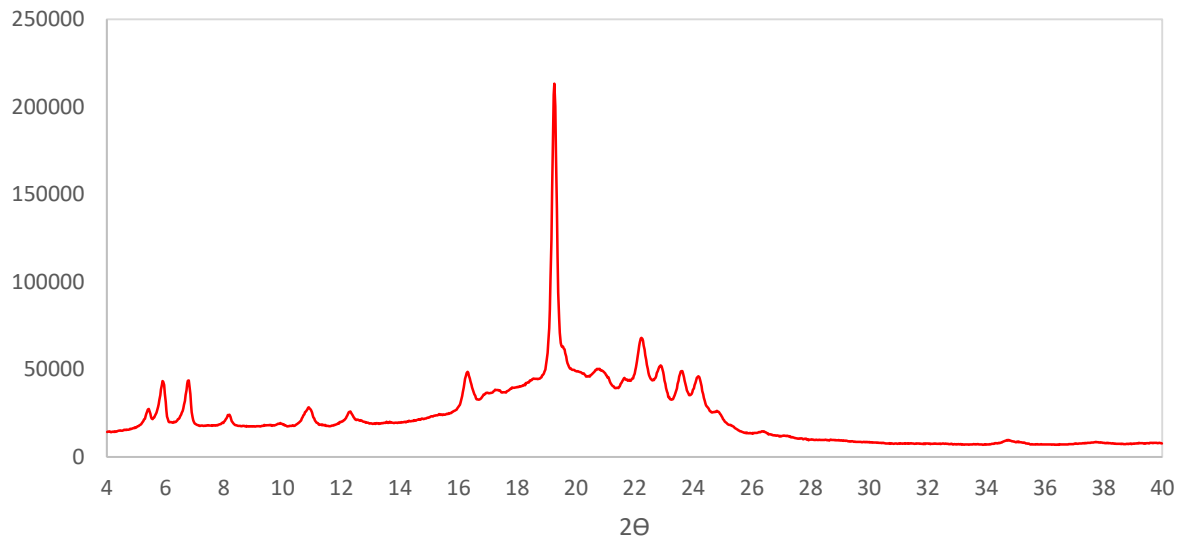

Fig. 4.28 XPRD of MF4 20% mixture in CB taken at room temperature (~20°C).

MF4 20% mixture diffractogram (Fig. 4.28) shows as well the distinctive plot of the most stable form as confirmed by peaks at 4.60, 3.99, 3.88, 3.76 and 3.68 Å (Tab. 4.14). However, it is still distinguishable the amorphous undefined band corresponding to the molten fraction of MF4.

Tab. 4.14 XPRD peaks of MF4 20% mixture in CB taken at room temperature (~20°C).

2Θ	Intensity	q [$Å^{-1}$]	Short spacing [Å]
16.30	48655	1.157	5.43
19.27	213279	1.365	4.60
22.24	68133	1.573	3.99
22.89	52271	1.619	3.88
23.63	49014	1.670	3.76
24.18	46095	1.709	3.68

XPRD analysis were also performed on samples with a smaller amount of MF, MF2 and MF4. Mixtures at 5% in weight of the three fats in CB diffractograms showed a typical β form pattern with almost no difference between them. Fig. 4.29 (a), (b) and (c) show the respective diffractograms whose peaks are recapped in Tab. 4.15 (a), (b) and (c). In Fig. 4.30 the diffractograms of mixtures at 5% have been overlapped to CB one to highlight how this small percentage of extraneous fats barely alters CB crystallization.

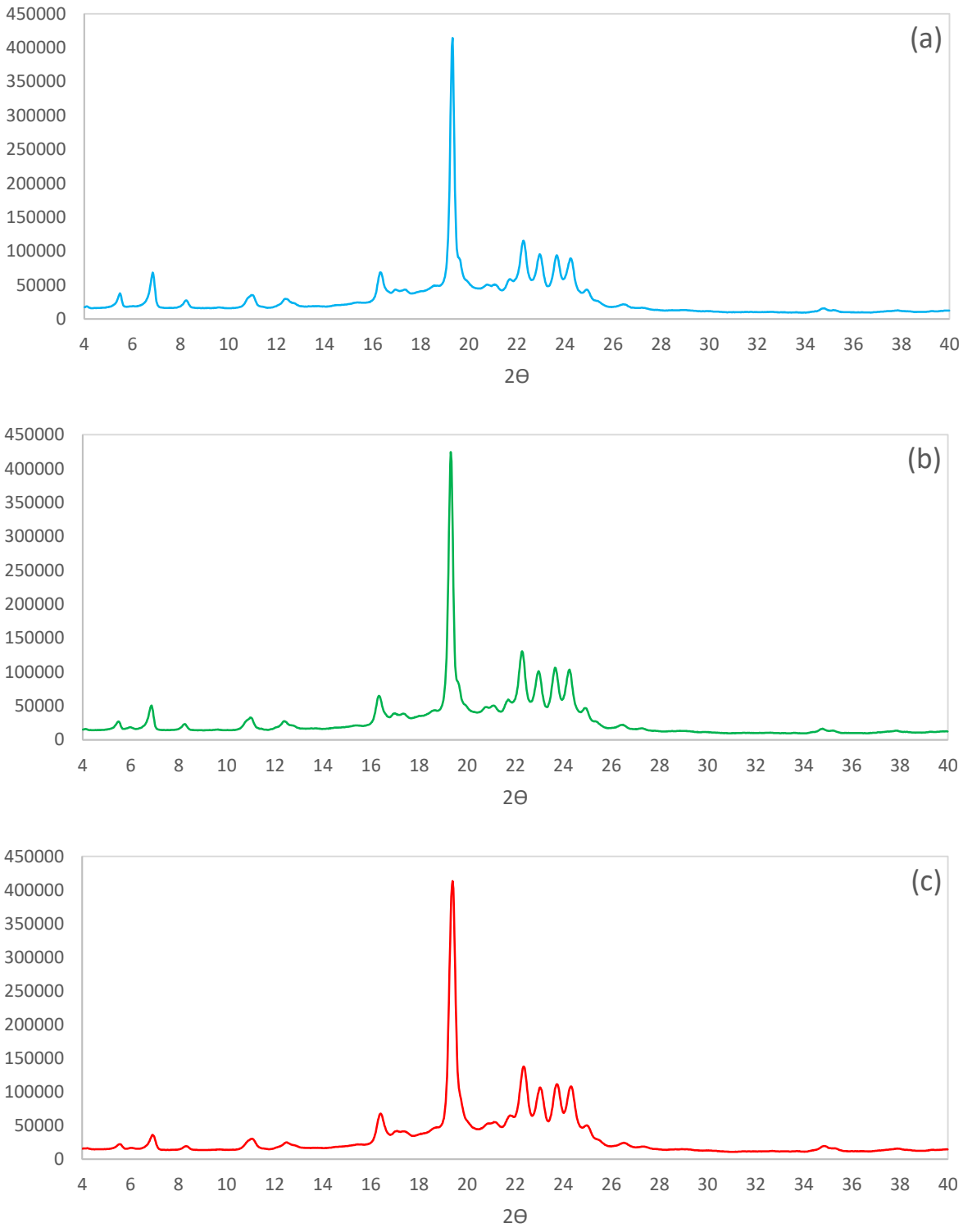

Fig. 4.29 XPRD of MF 5% (a), MF2 5% (b) and MF4 5% (c) mixture in CB taken at room temperature (~20°C).

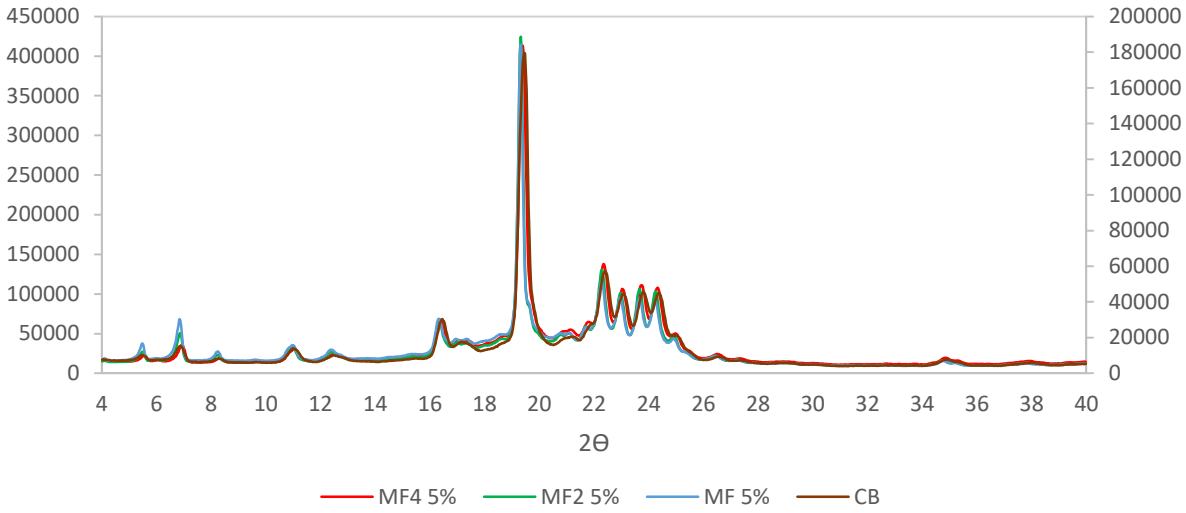

Fig. 4.30 Overlapped XPRD of mixtures at 5% of MF, MF2 and MF4 in CB and pure CB taken at room temperature (~20°C).

Tab. 4.15 XPRD peaks of MF 5% (a), MF2 5% (b) and MF4 5% (c) mixtures in CB taken at room temperature (~20°C).

a)

2Θ	Intensity	q [Å^{-1}]	Short spacing [Å]
16.33	68794	1.158	5.42
19.32	414455	1.369	4.59
22.26	115440	1.575	3.99
22.95	95618	1.623	3.87
23.66	94099	1.672	3.76
24.23	89218	1.712	3.67

b)

2Θ	Intensity	q [Å^{-1}]	Short spacing [Å]
16.33	65024	1.158	5.42
19.32	424591	1.369	4.59
22.29	130633	1.577	3.99
22.97	101459	1.624	3.87
23.66	106497	1.672	3.76
24.26	103606	1.714	3.67

c)

2Θ	Intensity	q [Å^{-1}]	Short spacing [Å]
16.41	67727	1.164	5.40
19.40	413292	1.374	4.57
22.34	137671	1.580	3.98
23.05	106378	1.630	3.86
23.73	111233	1.677	3.75
24.34	107939	1.719	3.65

4.6 SAXS

SAXS analyses allowed to understand in detail the crystal structure of the samples and different polymorphic phases and their significant temperatures.

4.6.1 MF2

Each sample diffractogram was firstly acquired without any temperature control in order to study crystal phases after the compound was given a longer period at room temperature to transform into more stable forms. MF2 static diffractogram (Fig. 4.31) exhibits a complex peak scheme indicating the presence of multiple phases.

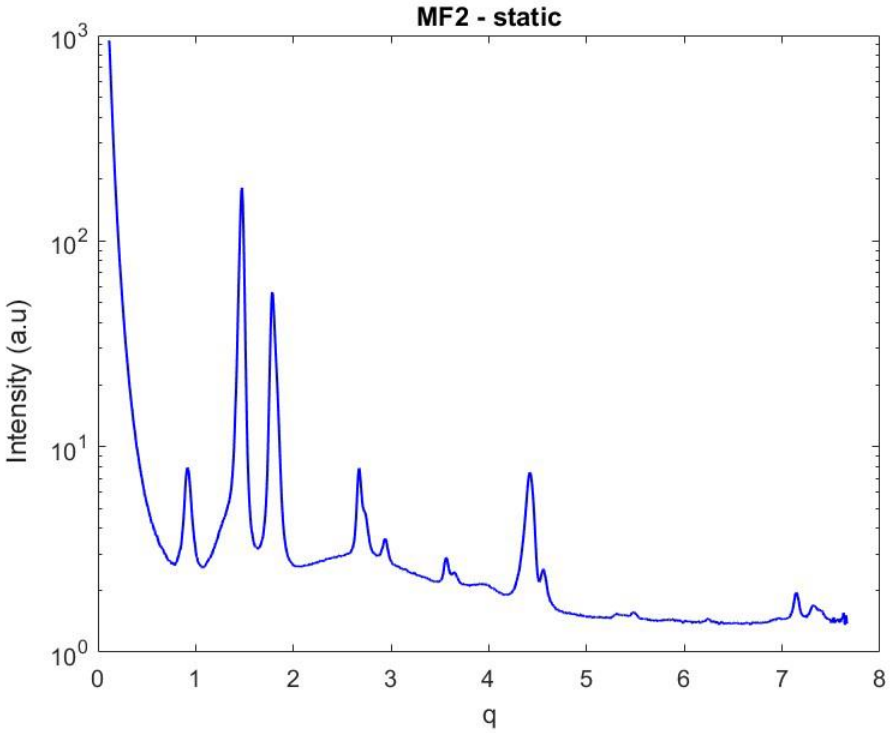

Fig. 4.31 Static SAXS diffractogram of MF2 taken at room temperature (~20°C).

The peaks have been associated to different crystal phases thanks to miller indexes. Indeed, q values of peaks of the same lamellar phase can be aligned on a straight line (Fig. 4.32) in relation to the corresponding miller index, given that they represent different orders of the same crystal structure. Tab. 4.16 summarizes all the peaks sorted depending on the crystal phase they come from. The first peak with the lowest q value corresponds to the typical d-spacing of a 1st order of a trilayered β form whose 3rd, 4th and 5th orders also visible (Tab. 4.16 (a)). These peaks are already disappeared at 36.5°C meaning that this phase melts under this temperature. A second 3L-β form seems to be represented by its 2nd, 4th and 8th order peaks (Tab. 4.16 (b)) as the d-spacing of the first of these peaks is 35.26 Å that when doubled corresponds to a first order d-spacing of 70.51 Å, which can be related to a trilayered structure different from the one above. These peaks are still partly seen at 36.5°C but completely missing at 38.5°C meaning that its melting temperature is around 37/38°C. The presence of two different trilayered structures can be explained by the sample composition. It is known

from literature that mixtures of SOS and POP in a similar proportion to the one in MF2 sample form a eutectic, meaning they do not mix when in solid phase. Regarding β-2L forms the presence of two of them appears clear. One of them (Tab. 4.16 (c)) generates three peaks corresponding to the 1st, 2nd and 3rd orders and it is fully molten at 42.5°C (it still shows peaks at at 38.5°C suggesting a melting temperature around 40.5°C). Lastly, another phase whose d-spacings are characteristic of a bilayered crystal causes the formation of a shoulder (1st order) and a minor peak (2nd order) still observable at 42.5°C (Tab. 4.16 (d)). This polymorph is attributed to a tristaurated TAG because its melting point is higher and compatible to this kind of molecules. Those two bilayered forms have been described as β-2L structures because of their melting temperatures. Indeed, their d-spacing could have been caused by β' crystals as well, but being a less stable polymorph they could not reach a higher melting temperature than trilayered β phases.

Tab. 4.16 Crystal phases from SAXS static analysis of MF2.

a)

β (3L)			
q	**h**	**d-spacing [Å]**	**Melting temperature [°C]**
0.91721	1	68.5	~36
2.73064	3	23.0	
3.64444	4	17.2	
4.55469	5	13.8	

b)

β (3L)			
q	**h**	**d-spacing [Å]**	**Melting temperature [°C]**
1.78212	2	35.3	~37/38
3.56074	4	17.6	
7.1459	8	8.8	

c)

β (2L)			
q	**h**	**d-spacing [Å]**	**Melting temperature [°C]**
1.47522	1	42.6	~40/41
2.93997	2	21.4	
4.41867	3	14.2	

d)

β (2L)			
q	**h**	**d-spacing [Å]**	**Melting temperature [°C]**
1.34269	1	46.8	> 42.5
2.66097	2	23.6	

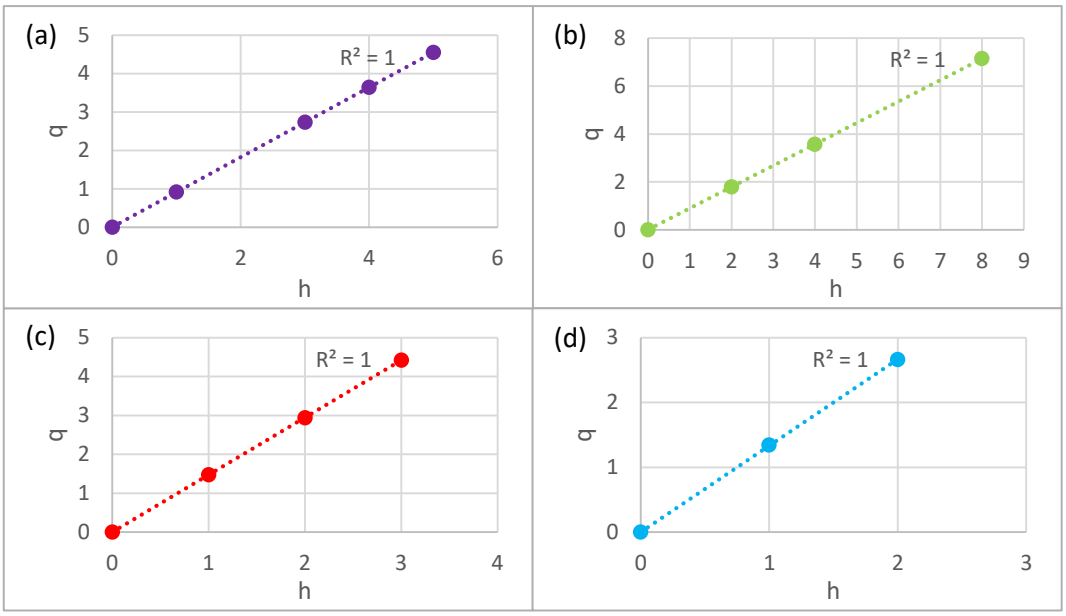

Fig. 4.32 Peaks of crystal phases from static SAXS diffractogram of MF2 in relation to Miller indexes.

Fig. 4.33 shows the melting process of the sample where it is possible to notice how peaks disappear at variable temperatures as described before.

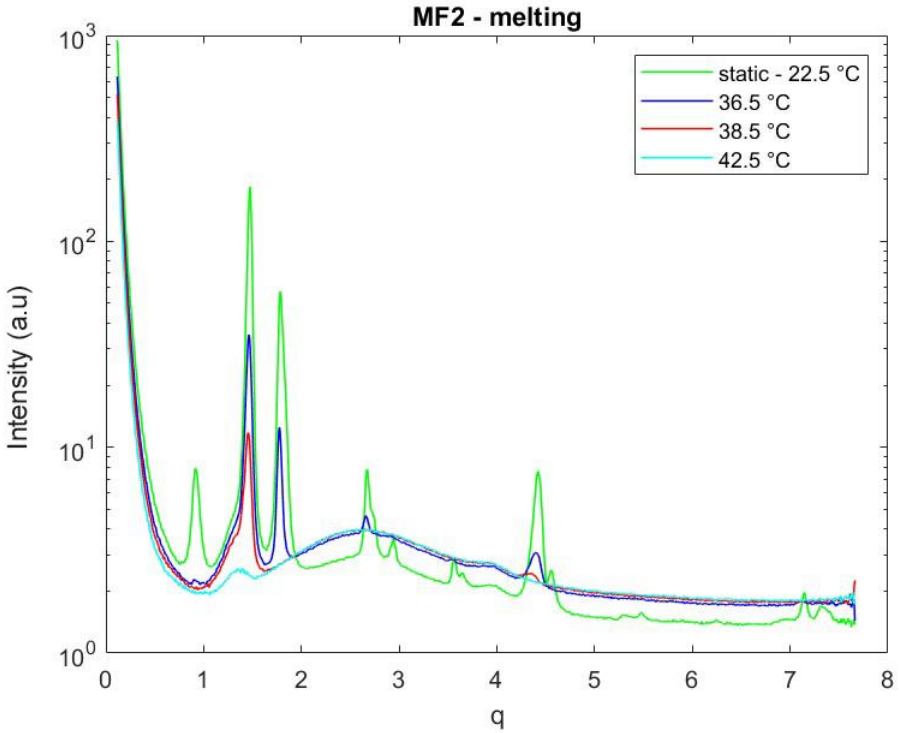

Fig. 4.33 SAXS diffractogram of the melting phase of MF2 sample.

The sample was then recrystallized at a slow cooling rate of -0.5°C/min as explained in Chapter 3 and this process is shown in Fig. 4.34. The first peak began to show at 23.1°C and grew together with the 2nd and 3rd order reflections of this same crystal phase (Tab. 4.17 (a)), which was identified as α form because of its early appearance. As the sample is cooled another phase (Tab. 4.17 (b)) crystallized between 13 and 12°C, which was classified as a second α form that is found at lower temperatures. It is important to notice that starting from the 5.2°C peaks related to the second α form began to shrink. In the last part of the cooling process before reaching the target temperature of 5°C α phases peaks continue to develop while shoulders from a more stable form started to appear. Indeed, during the following holding process where temperature is kept constant at 5°C this third phase shoulders develop into peaks (Tab. 4.17 (c)) indicating that when the sample is given enough time for molecules to rearrange it transitions to a more compact crystal matrix. This third phase was associated to β' form as suggested from literature (S. Bresson et al., 2011). Tab. 4.17 lists those three crystal phases with associated peak values while Fig. 4.36 proves the connection between peaks of the same phase as they are perfectly aligned in relation to their Miller index.

Tab. 4.17 Crystal phases from SAXS slow cooling analysis of MF2.

a)

α_1				
q	**h**	**d-spacing [Å]**	**Crystallization temperature [°C]**	**Melting temperature [°C]**
1.29386	1	48.6	~23	~24
2.56332	2	24.5		
3.86764	3	16.2		
6.46223	5	9.7		

b)

α_2				
q	**h**	**d-spacing [Å]**	**Crystallization temperature [°C]**	**Melting temperature [°C]**
1.17529	1	53.5	~13	5 (during holding)
2.34709	2	26.8		
4.68372	4	13.4		

c)

β' (2L)				
q	**h**	**d-spacing [Å]**	**Crystallization temperature [°C]**	**Melting temperature [°C]**
1.38223	1	45.5	~5	~41
2.77257	2	22.7		
4.19709	3	15.0		

Fig. 4.35 represents four different instants during the temperature holding at 5°C that followed the slow cooling process. It is interesting to highlight that the second α phase is almost molten after 27 minutes, hence it is reasonable to assume it is gone after ~30min. This indicates that this phase is really unstable and forms at low temperatures but quickly

transitions into another one, likely the growing β'. After 90 minutes of holding the first phase starts to retrocede as well, while β' peaks are still growing at a sustained rate.

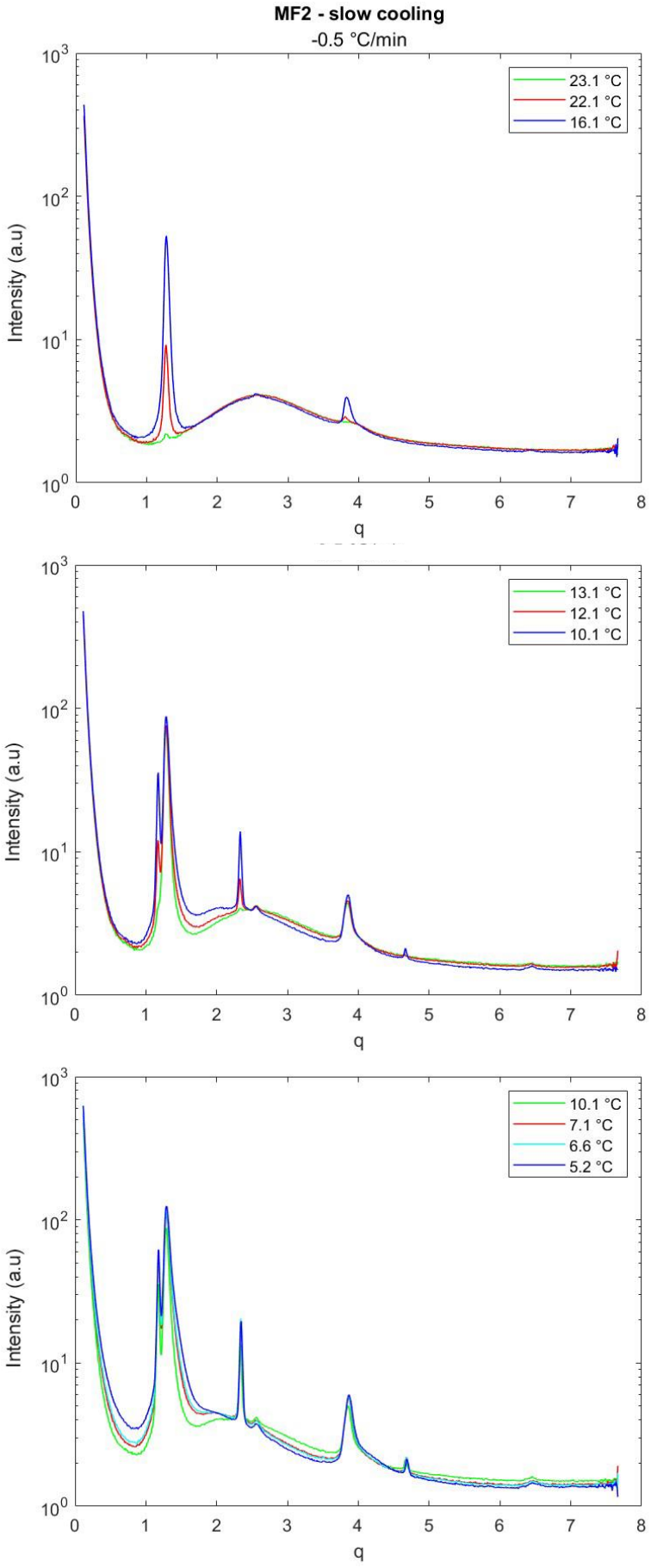

Fig. 4.34 SAXS diffractogram of the slow cooling phase at -0.5°C/min of MF2 sample.

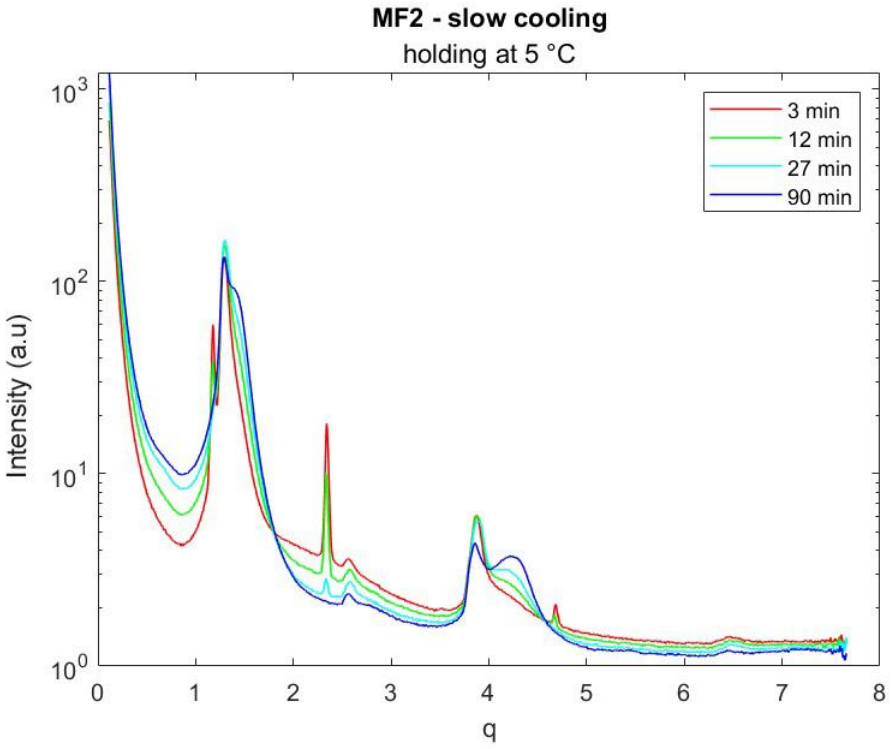

Fig. 4.35 SAXS diffractogram of the temperature holding at 5°C after slow cooling phase of MF2 sample.

Peaks that belong to the same polymorph are again aligned perfectly on a straight line when plotted against the respective Miller indexes. Fig. 4.36(a) shows trendlines of all the polymorphs that appeared during cooling process that are visible at 5.2°C, meaning both α phases. Fig. 4.36(b) represents the peaks after 90 minutes of temperature holding.

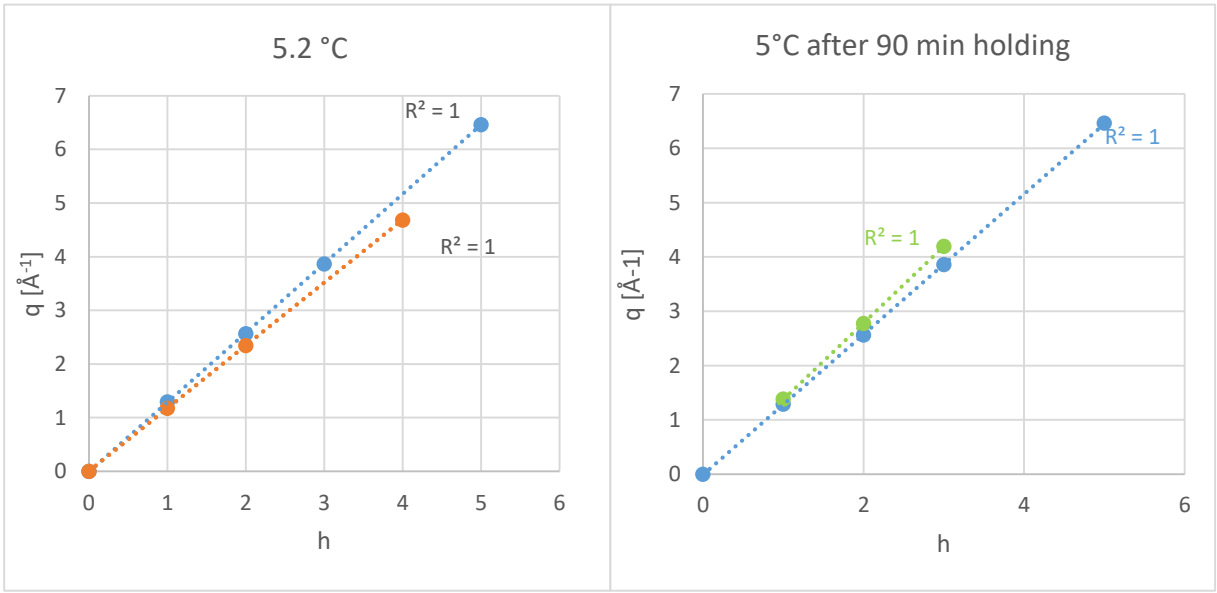

Fig. 4.36 Peaks of crystal phases from SAXS diffractogram of MF2 sample in relation to Miller indexes after slow cooling. Blue phase represents peaks of first formed α polymorph, orange those of the second α polymorph and green those of β' polymorph.

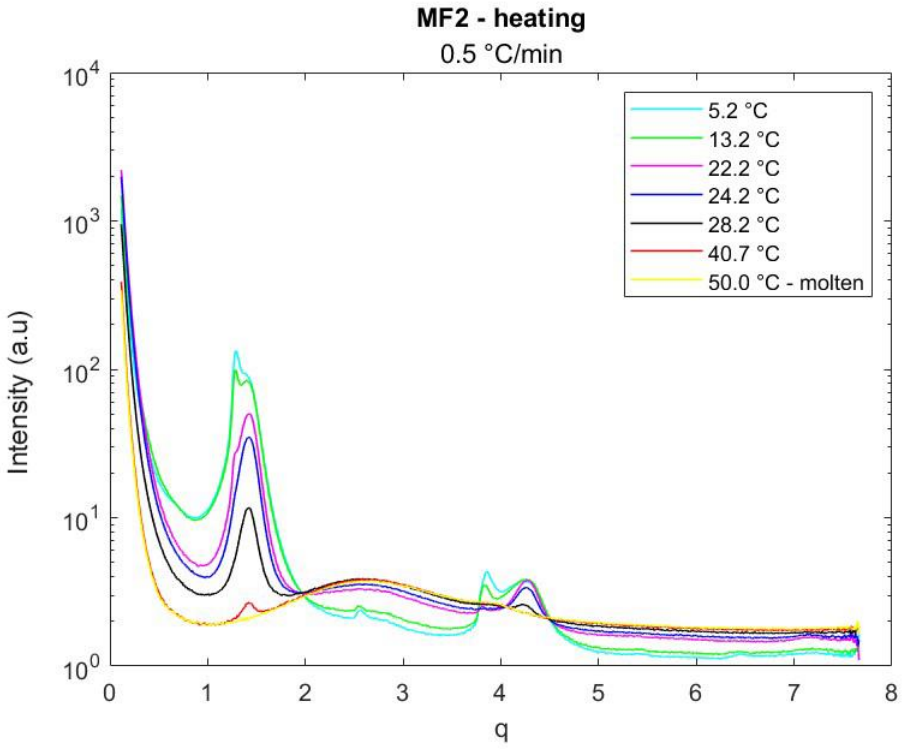

Fig. 4.37 SAXS diffractogram of the heating phase at +0.5°C/min of MF2 sample.

Heating phase (Fig. 4.37) is an important step to better understand the stability level of each polymorph as it allows to know precisely their melting point. The first α-phase melts around 25°C due to the unstable nature of this form; the β' polymorph peaks disappear at higher temperatures and are still partly visible above 40°C. Diffractogram captured when the sample has reached 50°C shows typical trend of completely molten compound.

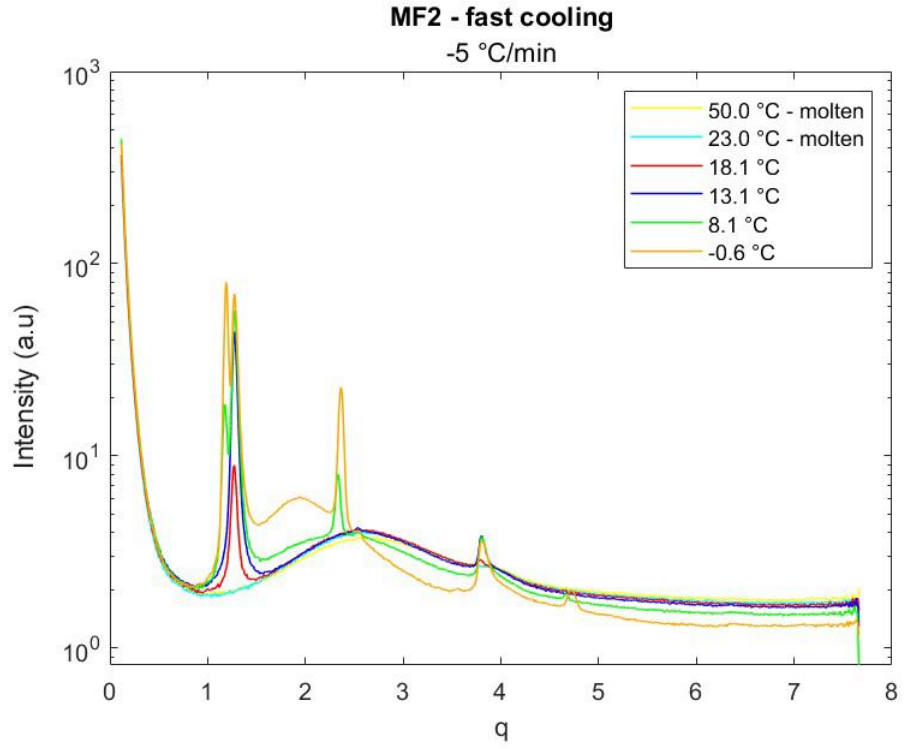

Fig. 4.38 SAXS diffractogram of the fast cooling phase at -5°C/min of MF2 sample.

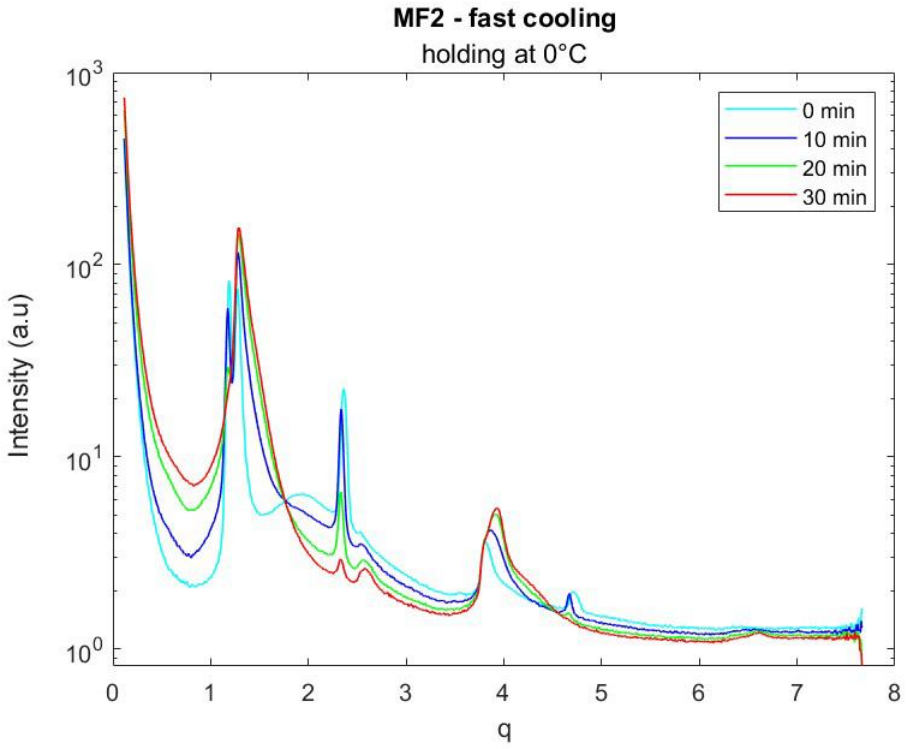

Fig. 4.39 SAXS diffractogram of the temperature holding at 0°C after fast cooling phase of MF2 sample.

The sample then underwent another cooling crystallization process where temperature was decreased with a faster rate, therefore crystals ability to rearrange in regular structures was limited. Looking at Fig. 4.38 it is immediately clear that the crystallization scheme reflects the one of the slower cooling process; however, some major points need to be paid attention to. Firstly, the diffractogram at 23°C is still representing a molten sample, meaning that the crystallization temperature is lowered. This was expected because molecules did not have enough time to organise in crystalline structures as before. As the sample reached 18.1°C peaks characteristic of the first α form (Tab. 4.18 (a)) began to show while a second α phase (Tab. 4.18 (b)) formed again at lower temperatures, being visible at 8.1°C. When the sample reached 0°C both α forms were still present and a third form (Tab. 4.18 (d)) started to show. Due to the d-spacings values it can be associated to a 3L-γ one because it is very unstable as demonstrated by the fact that it disappears quickly (Fig. 4.40) and is completely molten before 20°C. During the holding phase peaks related to the β' polymorph (Tab. 4.18 (c)) appeared as before. By the end of the holding at 0°C, the most unstable α form disappears repeating the same behaviour it had during the previous slow cooling crystallization. In the same way, peaks associated to the first α polymorph start decreasing during the raising of the temperature while taking the sample back to room temperature, even if they are still strong at the end of the experiment at 20°C. The late formed β' polymorph kept growing during the heating to room temperature. This behaviour is coherent to what happened in the first cycle where it melted above 40°C.

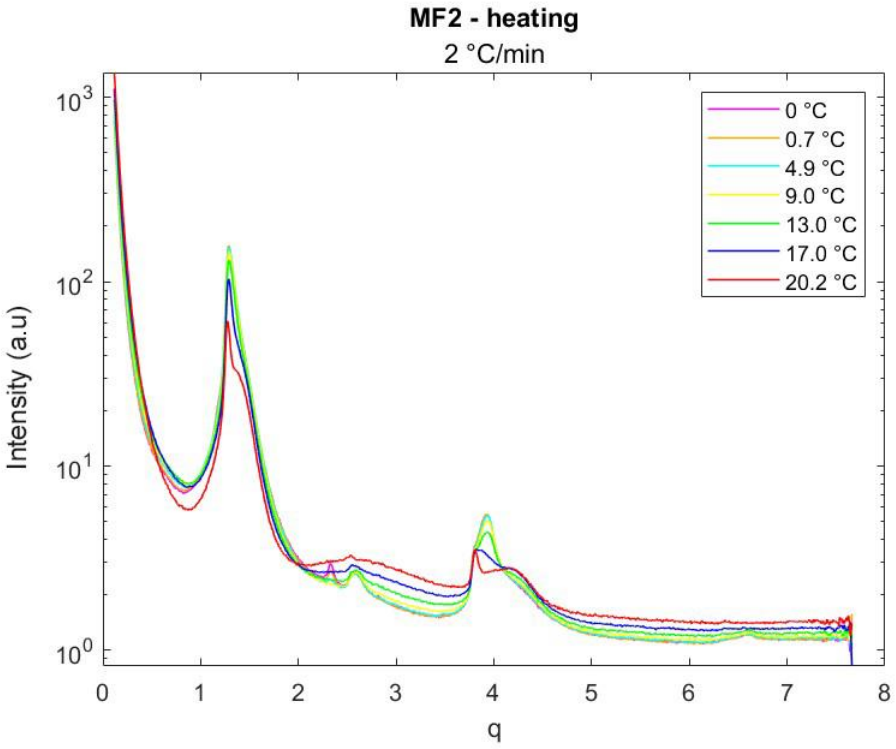

Fig. 4.40 SAXS diffractogram of the ending phase of MF2 sample analysis (return to RT).

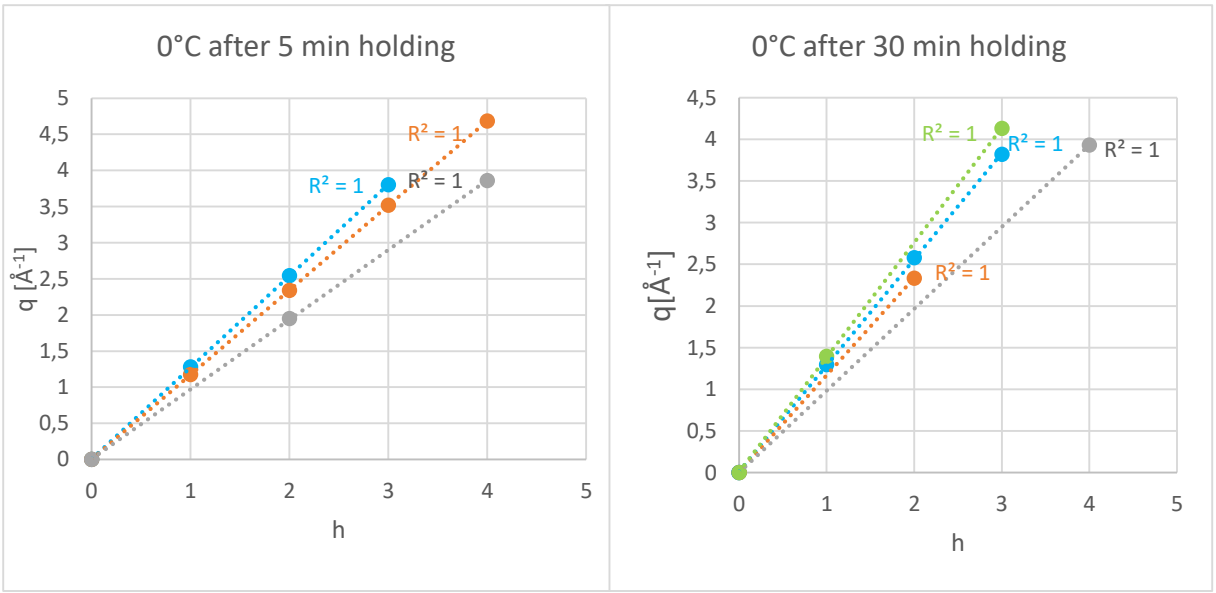

Fig. 4.41 Peaks of crystal phases from SAXS diffractogram of MF2 sample in relation to Miller indexes after fast cooling. Blue phase represents peaks of first formed α polymorph, orange those of the second α polymorph, green those of β' polymorph and grey those of γ-3L polymorph.

Tab. 4.18 Crystal phases from SAXS fast cooling analysis of MF2.

a)

α				
Q	**h**	**d-spacing [Å]**	**Crystallization temperature [°C]**	**Melting temperature [°C]**
1.27294	1	49.4	~20	>20
2.53542	2	24.8		
3.80487	3	16.5		

b)

α				
q	**h**	**d-spacing [Å]**	**Crystallization temperature [°C]**	**Melting temperature [°C]**
1.17529	1	53.5	~10	0 (after 30 min)
2.33314	2	26.9		
4.68372	4	13.4		

c)

β' (2L)				
q	**h**	**d-spacing [Å]**	**Crystallization temperature [°C]**	**Melting temperature [°C]**
1.35615	1	46.3	0 (after 10 min)	>20
4.11148	3	15.3		

d)

γ (3L)				
q	**h**	**d-spacing [Å]**	**Crystallization temperature [°C]**	**Melting temperature [°C]**
3.90949	4	16.1	~0	~18

A further comparison of the crystallization patterns after slower and faster cooling rate was made evaluating differences between diffractograms at the lowest temperature. When the sample has just reached the end of the cooling ramp (Fig. 4.42) diffractograms show the same α polymorphs, while more stable ones are not formed yet in the more rapid process because of the insufficient time for molecules to align in crystalline forms. However, after temperature holding period (Fig. 4.43) diffractograms represented the same peaks even though those related to the more stable polymorphs were more developed.

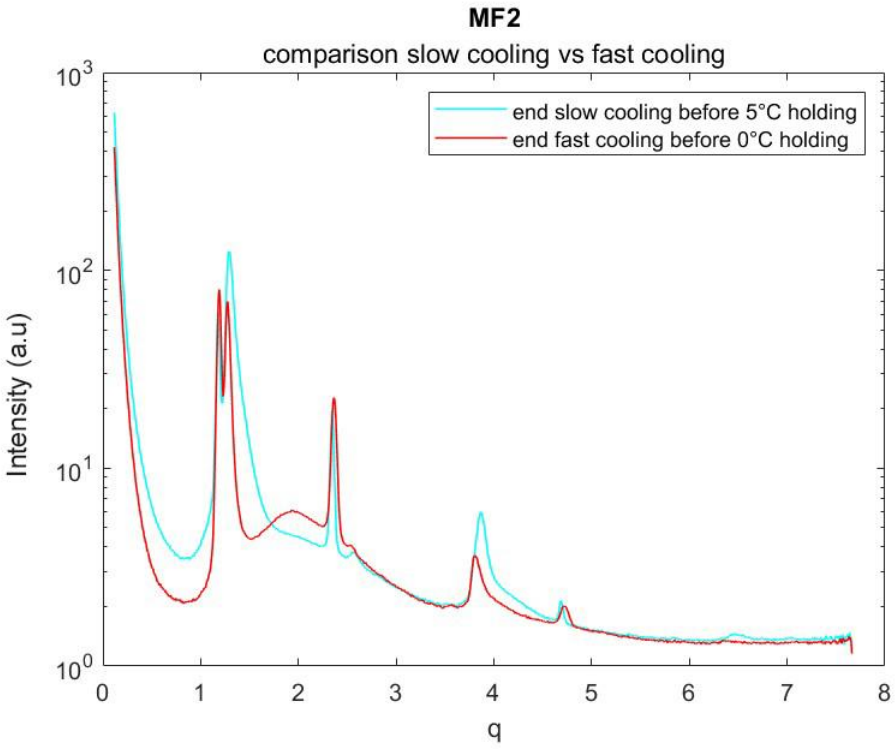

Fig. 4.42 Comparison of SAXS diffractograms of MF2 sample after slow cooling and fast cooling.

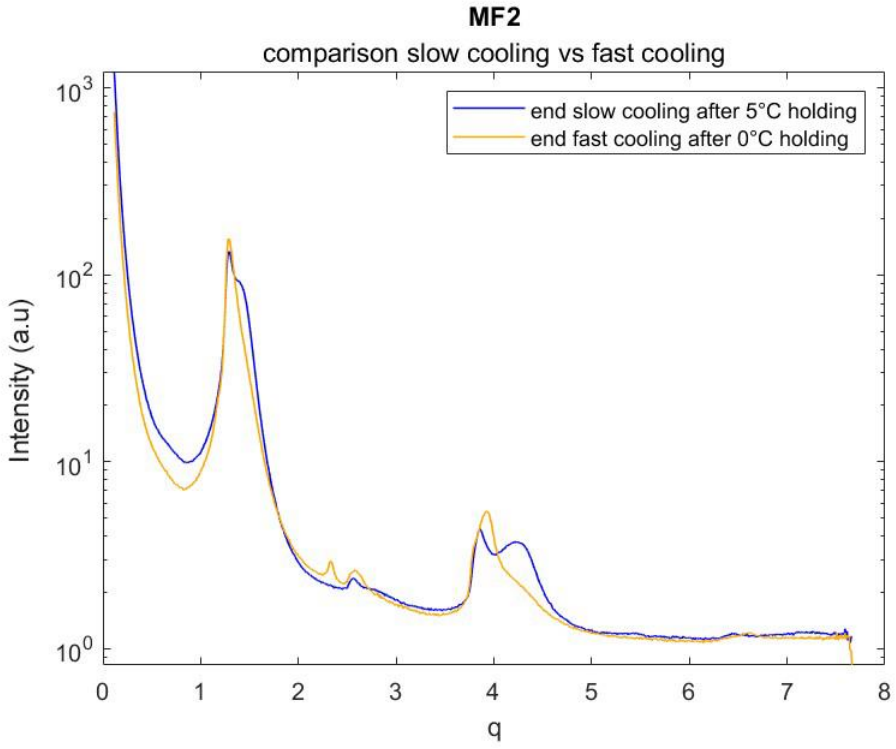

Fig. 4.43 Comparison of SAXS diffractograms after temperature holding following slow cooling and following fast cooling of MF2 sample.

4.6.2 MF4

MF4 sample was firstly studied at room temperature as well. It is already acknowledged that this compound is only partly crystallized around 20°C. However, static diffractogram (Fig. 4.44) acquired before any thermal protocol application shows some peaks, meaning some fractions are organized in regular structures. As displayed in Tab. 4.19 peaks in Fig. 4.44 can be linked to two different crystal phases. It is important to highlight that these two polymorphs show very similar d-spacing values compatible with a bilayered structure even though their melting points are different. It is then deduced that one is a β' polymorph that is less stable and melts at lower temperatures while the most stable one is a β form, as it is demonstrated by the fact that it is still solid above 40°C. Fig. 4.46 shows the melting process of the sample and the decreasing of intensity of the peaks; however, due to the very subtle distance among the q values, peaks are overlapped and fitting was necessary. Moreover, applying a heating rate of +10°C/min it is difficult to perceive melting points in details, but some relevant considerations are useful to understand sample behaviour. At 27°C the diffractogram is completely superimposable to the static one, meaning there is no fraction whose melting point is under this temperature. At 37°C peaks are beginning to decrease but at 47.1°C it is only seen a single crystal phase.

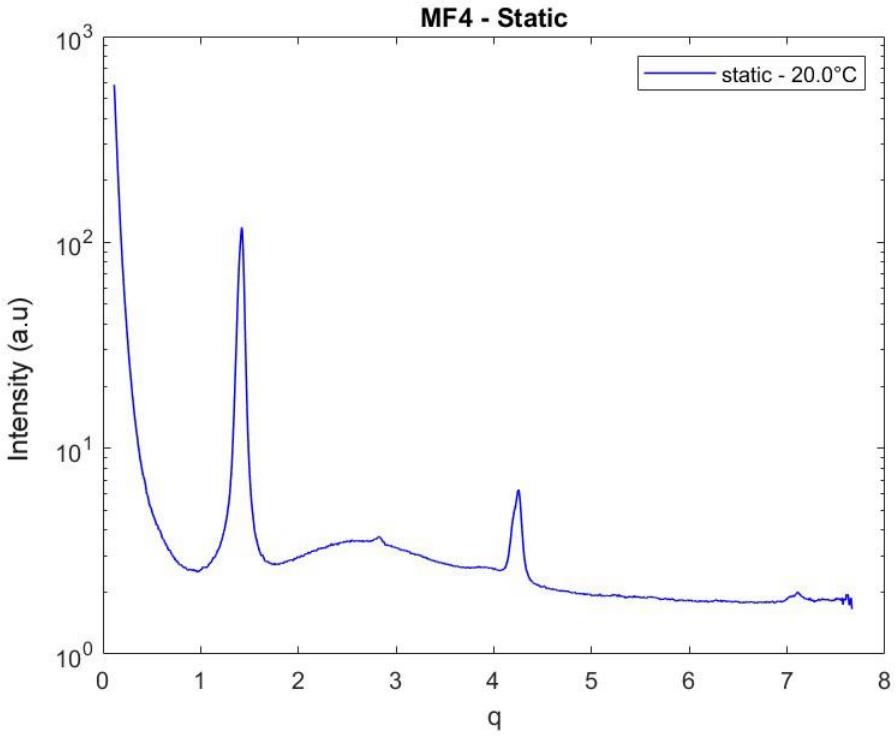

Fig. 4.44 SAXS diffractogram of the melting phase of MF2 sample.

Tab. 4.19 Crystal phases from SAXS static analysis of MF4.

a)

β' (2L)			
Q	**h**	**d-spacing [Å]**	**Melting temperature [°C]**
1.40302	1	44.8	~35
4.19201	3	15.0	

b)

β (2L)			
q	**h**	**d-spacing [Å]**	**Melting temperature [°C]**
1.41942	1	44.3	>47
2.82837	2	22.2	
4.25127	3	14.8	
7.10405	5	8.8	

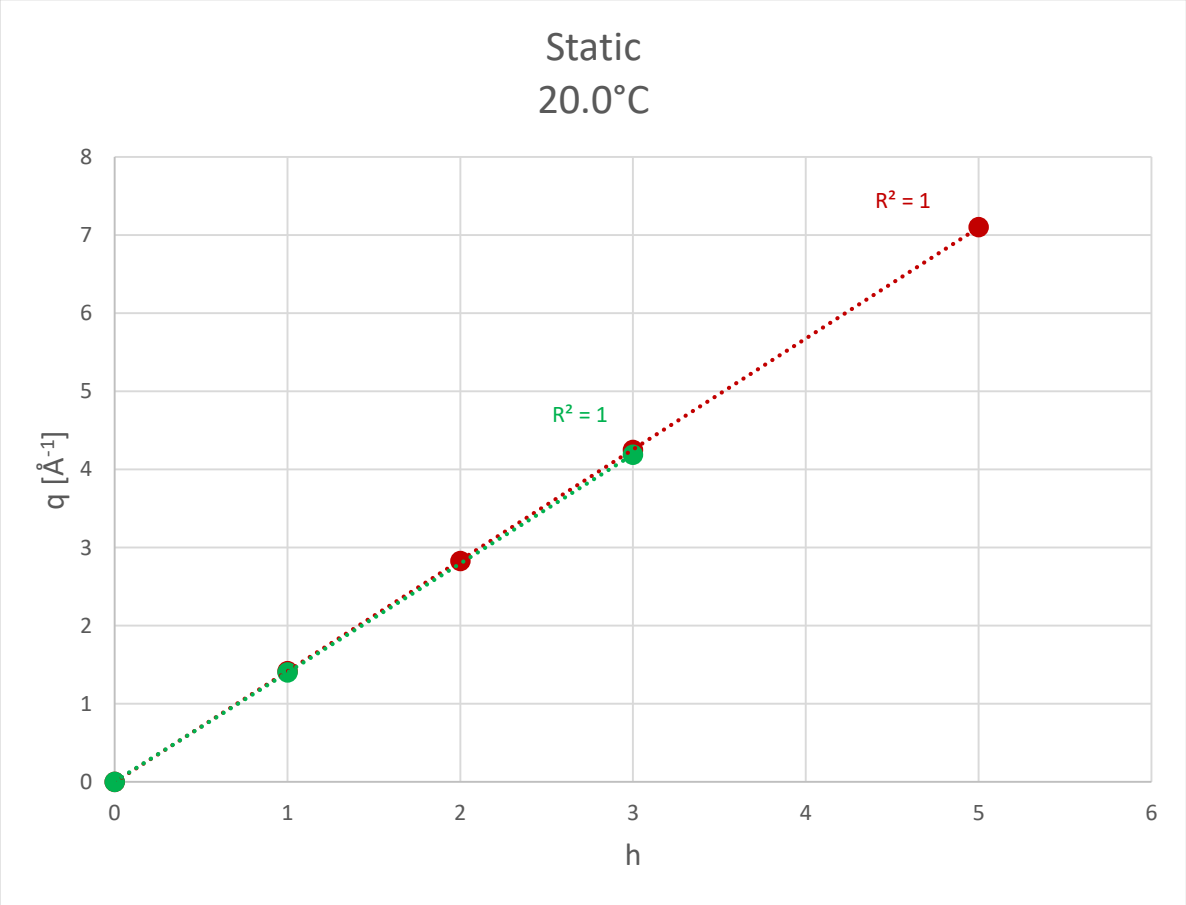

Fig. 4.45 Peaks of crystal phases from SAXS static diffractogram of MF4 sample in relation to Miller indexes at room temperature. Green line represents peaks of β polymorph and red those of β′ polymorph.

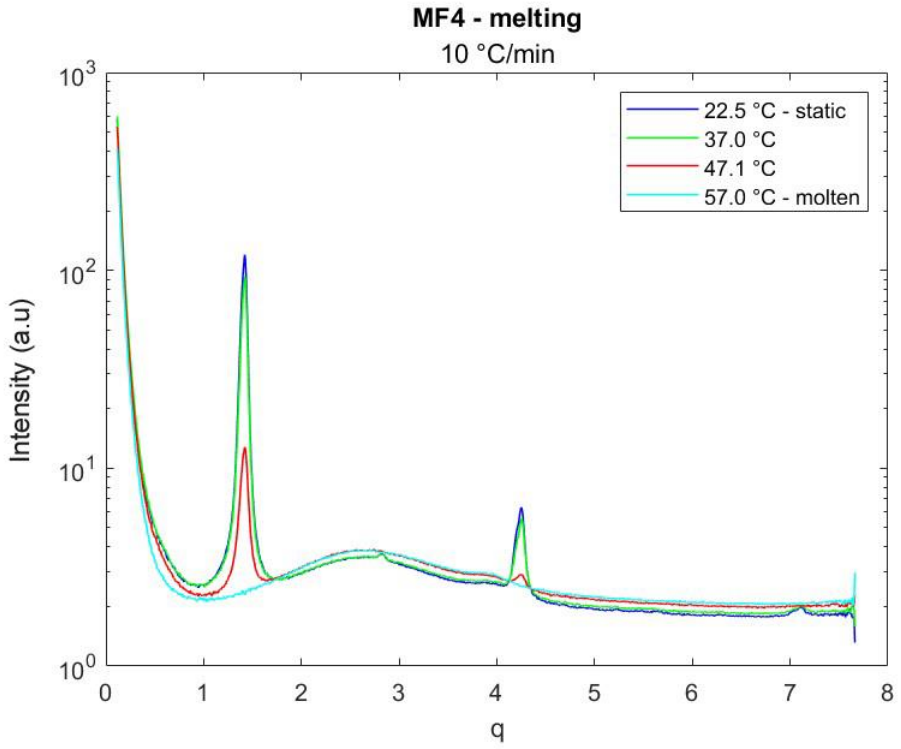

Fig. 4.46 SAXS diffractogram of the melting phase at +10°C/min of MF4 sample.

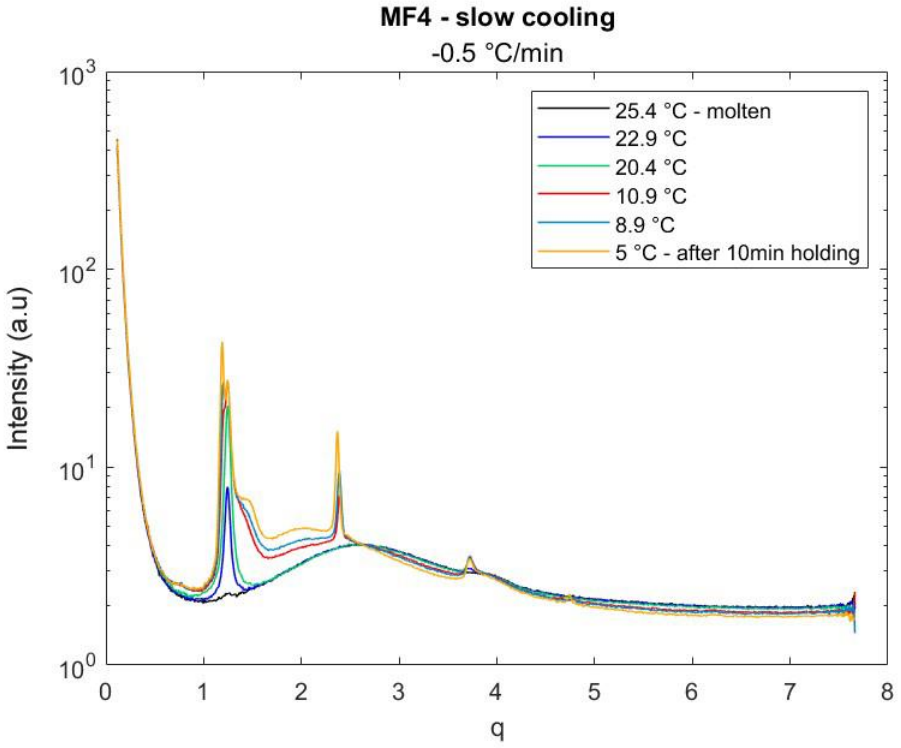

Fig. 4.47 SAXS diffractogram of the slow cooling phase at -0.5°C/min of MF4 sample.

The first cooling ramp at lower rate led to the formation of numerous peaks (Fig. 4.47). The first one began to show at around 24°C as it is already quite intense at 22.9°C, as well as the 3rd order peak of the same α polymorph (Tab. 4.20 (a)). This phase kept growing and another α form appeared at 10.9°C (Tab. 4.20 (b)) with two sharp peaks corresponding to 1st and 2nd orders together with the 4th order peak that showed as the cooling process proceeded. At the same time at 10.9°C a shoulder begins to grow on the right of the first peak as well as around q value of 0.7 $Å^{-1}$. However, those shoulders do not fully develop during the cooling ramp and the following 10 minutes holding, thus the definition of peaks is quite complex.

Tab. 4.20 Crystal phases from SAXS slow cooling crystallization analysis of MF4.

a)

α			
q	**h**	**d-spacing [Å]**	**Crystallization temperature [°C]**
1.24504	1	50.5	~24
3.72117	3	16.9	

b)

α			
q	**h**	**d-spacing [Å]**	**Crystallization temperature [°C]**
1.18924	1	52.8	~11
2.36802	2	26.5	
4.73952	4	13.3	

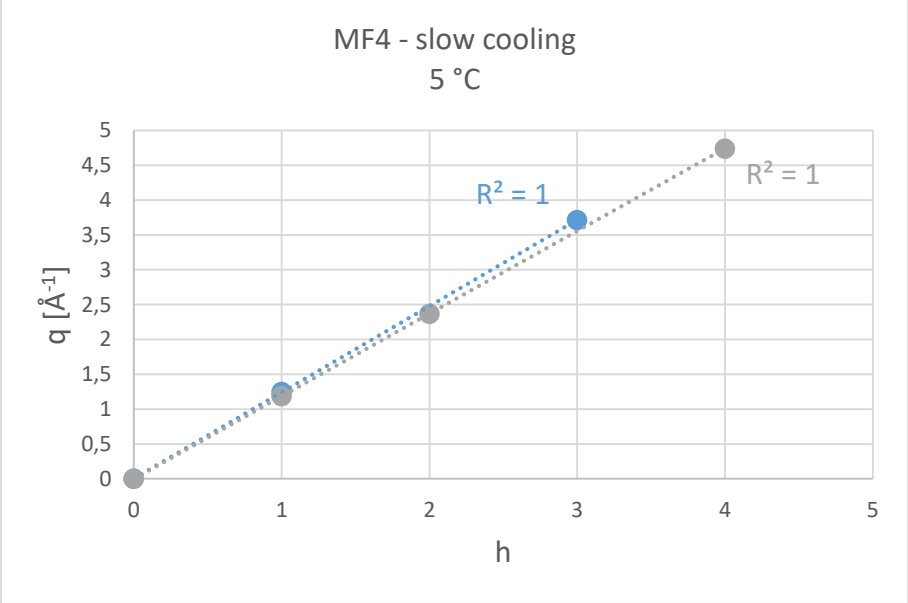

Fig. 4.48 Peaks of crystal phases from SAXS diffractograms of MF4 sample in relation to Miller indexes after slow cooling crystallization. Both blue and grey lines represent α polymorphs, first and second to form respectively.

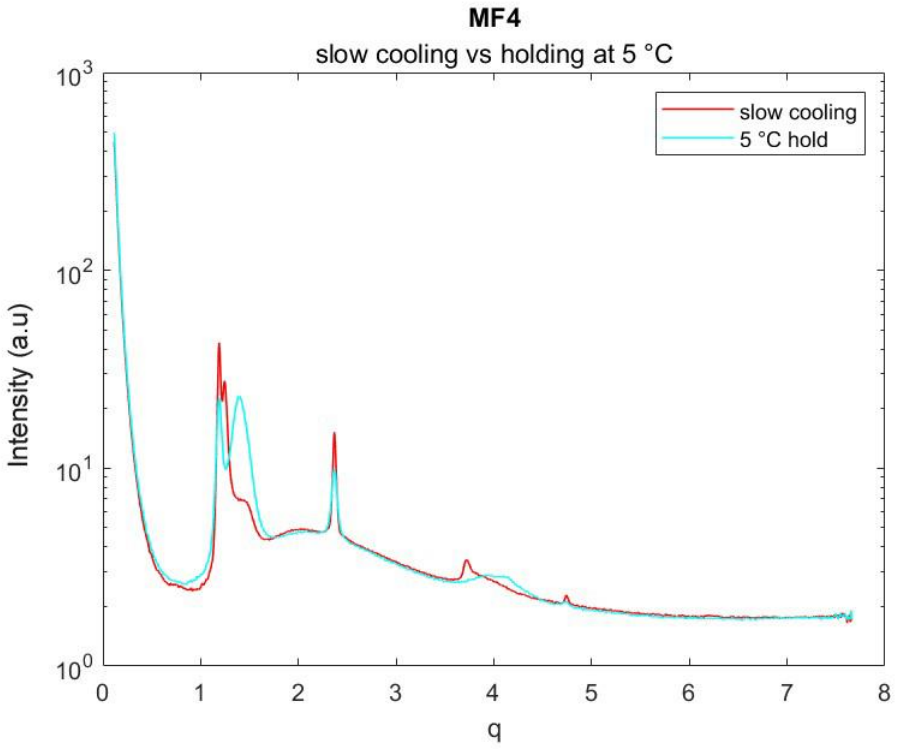

Fig. 4.49 Comparison of SAXS diffractograms at the end of the slow cooling crystallization and after 5°C storage of MF4 sample.

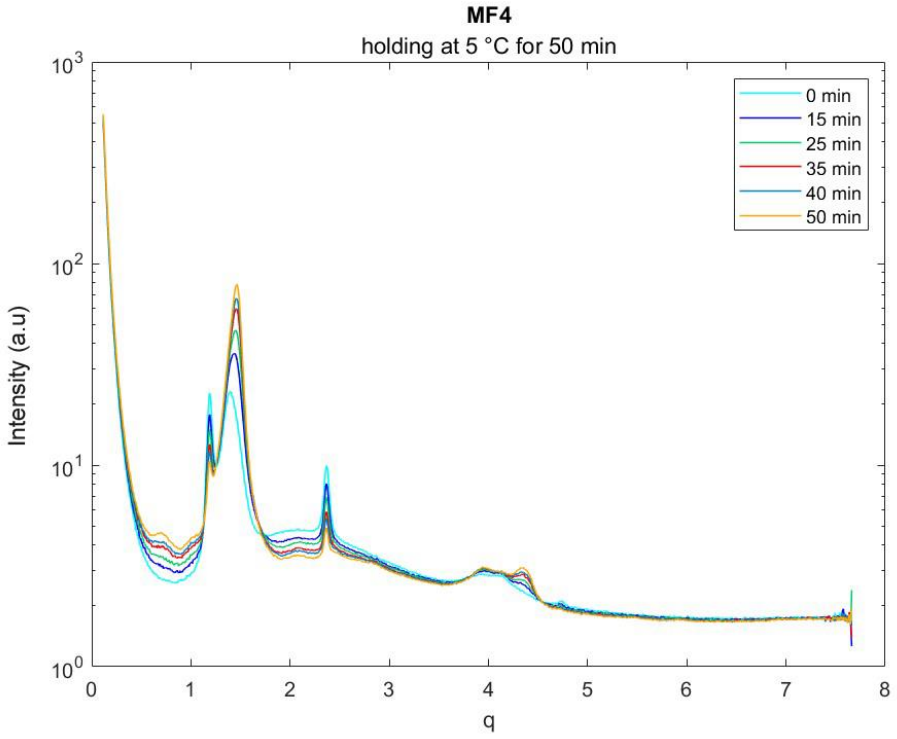

Fig. 4.50 SAXS diffractogram of the temperature holding phase at 5°C after slow cooling ramp of MF4 sample.

The sample is then stored at 5°C then the analysis is resumed and a further temperature holding period of 50 minutes at 5°C was examined. Fig. 4.49 shows the differences between diffractograms before and after the unstudied period of storage. The first α form peaks crystallized at higher temperature are not seen anymore, hence this phase is likely quite unstable and only exists for a reduced range of temperatures. The second α form is decreasing as well, even though its peaks can still be seen after 50 minutes from the restart of the analyses (Fig. 4.50). On the other hand, shoulders that showed at the end of the slow cooling ramp have grown into two phases that are overlapped, creating a broad peak around 1.42 $Å^{-1}$. For this reason, Origin fitting tool was again used to find q values of the center of those. It is found that during the 50 minutes where temperature is kept at 5°C four different polymorphs appear. First one is the α form originated during cooling, while the most intense peak is the sum of peaks from an unstable 3L-γ form and a more stable β that developed from 15 minutes on. Finally weaker shoulders from another polymorph are observed after ~25 minutes. This lately phase was associated to a β'-3L form because of the long time required for it to crystallize. This form is likely formed by pluriunsaturated and short chain TAGs as testified by the low melting point (K. Sato et al., 2005). Fig. 4.50 represents the evolution of the diffractograms during the temperature holding and developing of peaks. In Fig. 4.51 peaks of each polymorph are collected in the same graph even if they reached their maximum intensity at different times.

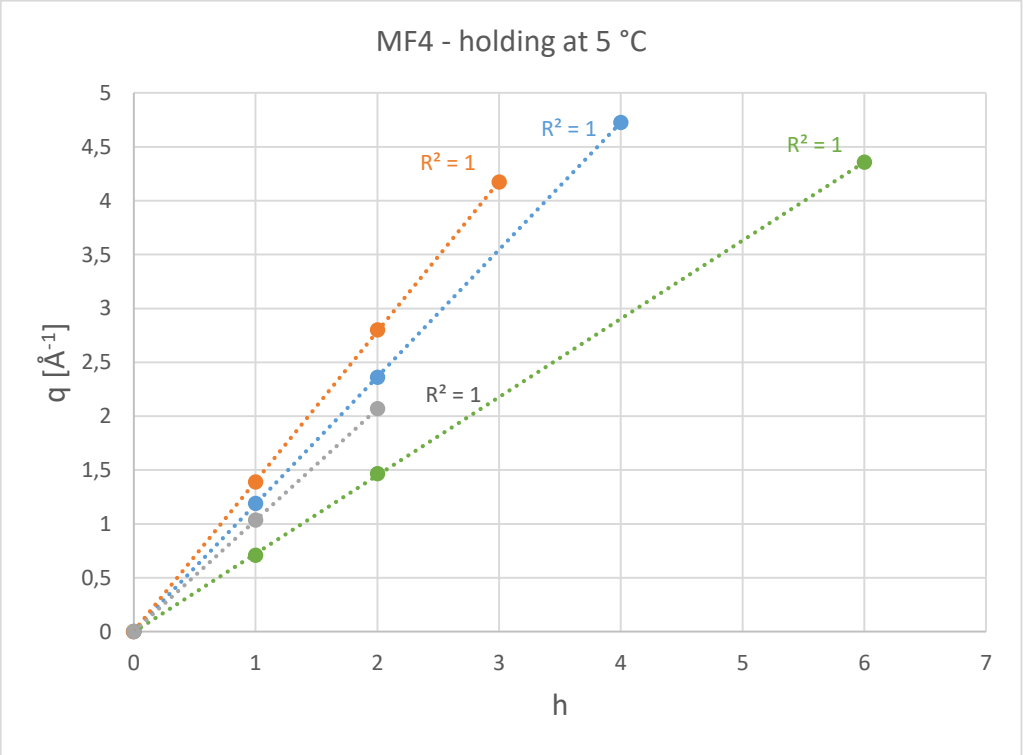

Fig. 4.51 Peaks of crystal phases from SAXS diffractograms of MF4 sample in relation to Miller indexes during 5°C temperature holding. Blue line represents α polymorph, grey line represents β'-3L polymorph, green line 3L-γ polymorph and orange line β polymorph.

Tab. 4.21 Crystal phases from SAXS analysis during temperature holding at 5°C of MF4.

a)

α				
q	**h**	**d-spacing [Å]**	**Crystallization temperature [°C]**	**Melting temperature [°C]**
1.18924	1	52.8	~11	<13
2.36104	2	26.6		
4.72557	4	13.3		

b)

β' (3L)				
q	**h**	**d-spacing [Å]**	**Crystallization temperature [°C]**	**Melting temperature [°C]**
1.03579	1	60.7	5 (after ~25 min of holding)	~13
2.06809	2	30.4		
3.96581	4	15.8		

c)

γ (3L)				
q	**h**	**d-spacing [Å]**	**Crystallization temperature [°C]**	**Melting temperature [°C]**
0.707964	1	88.8	5 (during storage)	~20
1.46464	2	42.9		
4.35671	6	14.4		

d)

β (2L)				
q	**h**	**d-spacing [Å]**	**Crystallization temperature [°C]**	**Melting temperature [°C]**
1.38931	1	45.2	5 (after ~25 min)	~48
2.80047	2	22.4		
4.17149	3	15.1		

The following heating process (Fig. 4.52) consents to have a full vision of peaks relation thanks to their melting temperatures. The weak shoulders from β'-3L polymorph are already decreased at 13°C and completely disappeared before 22°C. Peaks from α form are totally gone before 13°C, coherently with the instability typical of this polymorph. Trilayered γ-form is completely molten before 22°C too, as at this temperature only three peaks linked to the most stable β form are still present and they are even growing. At 35°C peaks of the most stable form are still clear but reduced and at 48°C the last trace of 1st order β peak is the only one that is still visible. D-spacing values of this last described polymorph are consistent with 2L-β form observed in the static diffractogram of the room temperature stored sample and melting temperatures do correspond as well. It is then understood that this polymorph, despite its high stability has a rapid crystallization process as it is already formed after a couple hours.

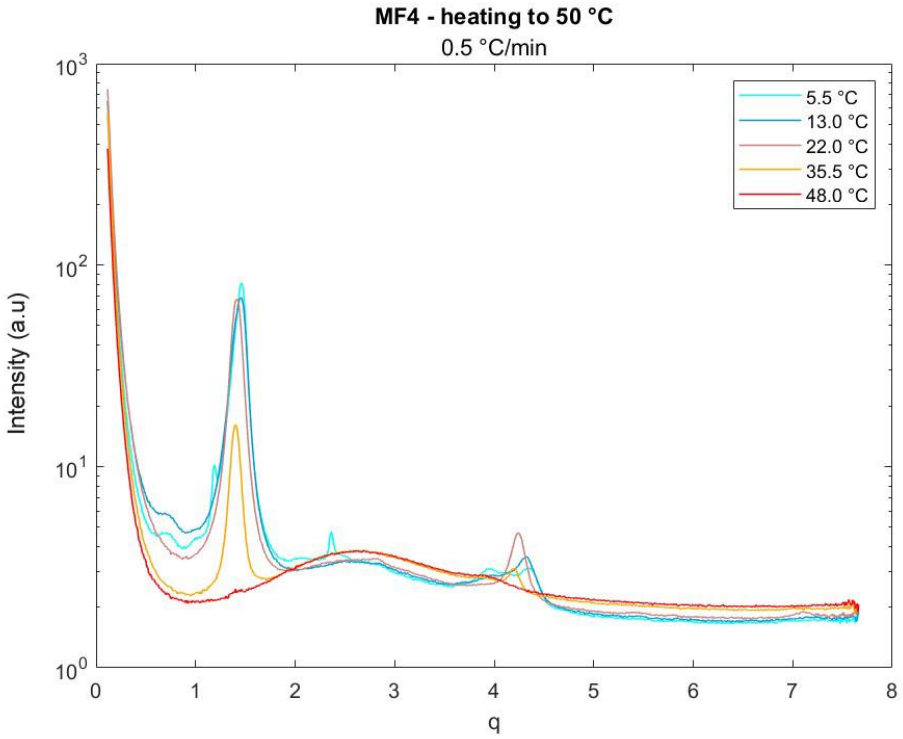

Fig. 4.52 SAXS diffractogram of the heating phase at +0.5°C/min after 5°C holding of MF4 sample.

The dynamic study of crystallization was again repeated applying a faster cooling rate as showed in Fig. 4.53 and Fig. 4.54 illustrating fast cooling and the following heating process respectively. Even in this case those two phases were interrupted by a temperature holding at 5°C but it lasted only 24 minutes (Fig. 4.54). As seen in the diffractograms, the same crystallization scheme of slow cooling process is replicated but the formation of peaks was incomplete due to the less time available for molecules to align.

At the reaching of 5°C the crystallization was less further along than before, indeed only the two α forms developed. Crystallization temperatures are lowered of a several degrees as the first peak is seen at 20°C instead of 24°C and second phase peaks appear at 10°C. The reduced amount of time given to TAGs to form regular structures avoids the formation of the most stable polymorphs. For this reason even after the temperature holding no change is seen in peaks pattern (Fig. 4.54).

As the sample was heated up again until fully molten (Fig. 4.55), more stable polymorphs were still developing. At 18.2°C the more unstable α form was already molten replicating the behaviour of the slow cooling process. However, even though temperature was raising peaks from the 3L-γ polymorph and those from the stable β form appeared at 18.2 and 25.2°C, just to melt again around 25 and 45°C respectively. Melting points were lowered because of the reduced formation of stable crystals and for this reason the energy required to bring molecules back to the liquid form was lower as well.

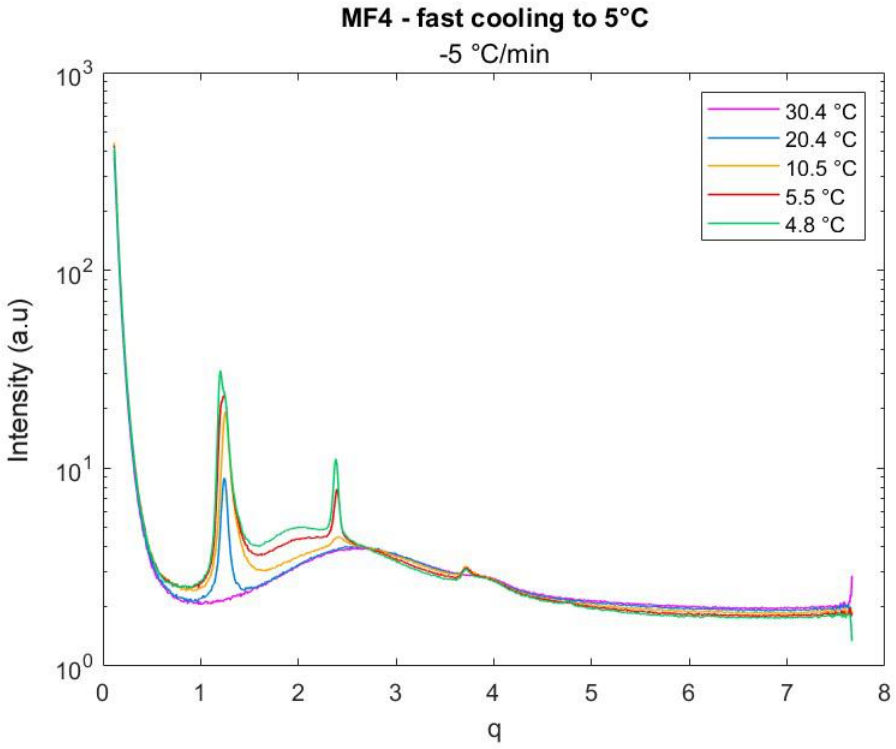

Fig. 4.53 SAXS diffractogram of the fast cooling phase at -5°C/min of MF4 sample.

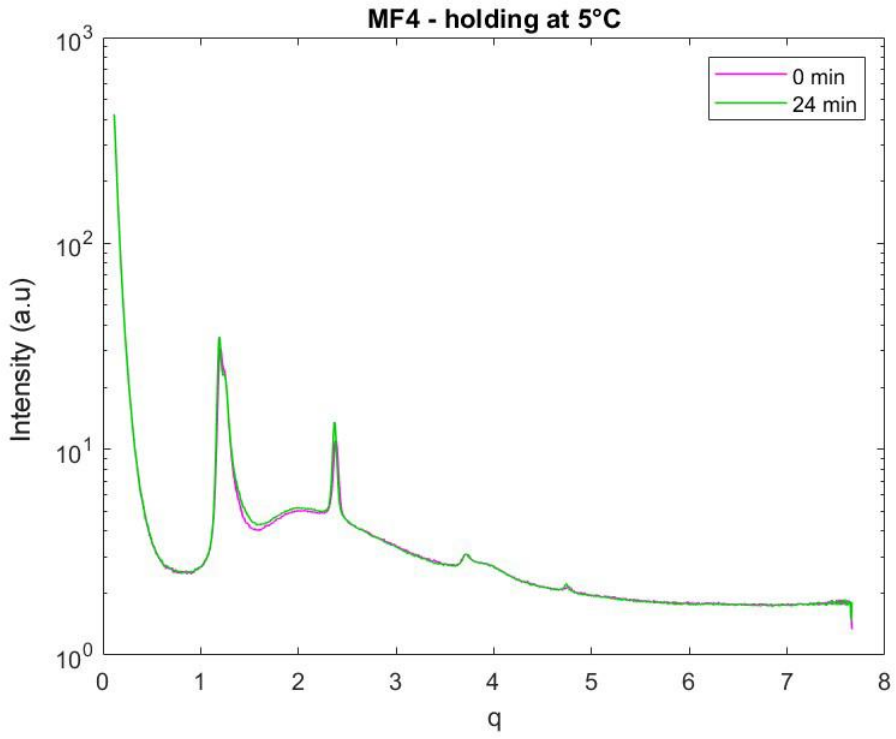

Fig. 4.54 SAXS diffractogram of the temperature holding at 5°C after fast cooling ramp of MF4 sample.

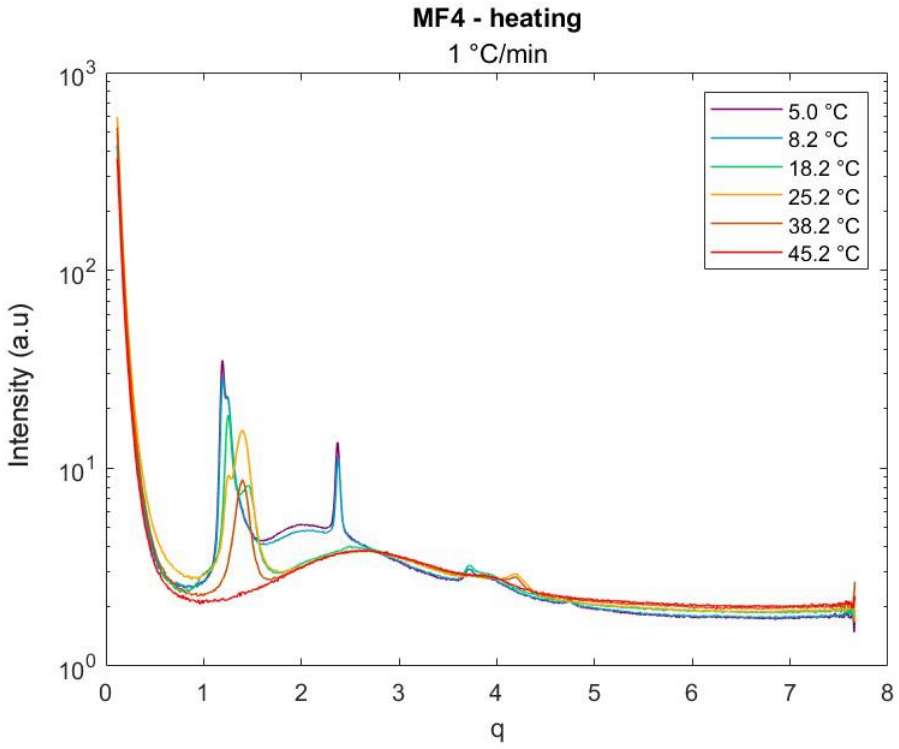

Fig. 4.55 SAXS diffractogram of the heating phase at +1°C/min after fast cooling ramp of MF4 sample.

4.6.3 Cocoa Butter

SAXS analysis of CB sample were performed with a reduced thermal protocol compared to the plant based fat samples study because of the huge amount of information about this subject coming from literature. For the same reason, the identification of peaks was clear and consistent with known cocoa butter polymorphs and their physical properties.

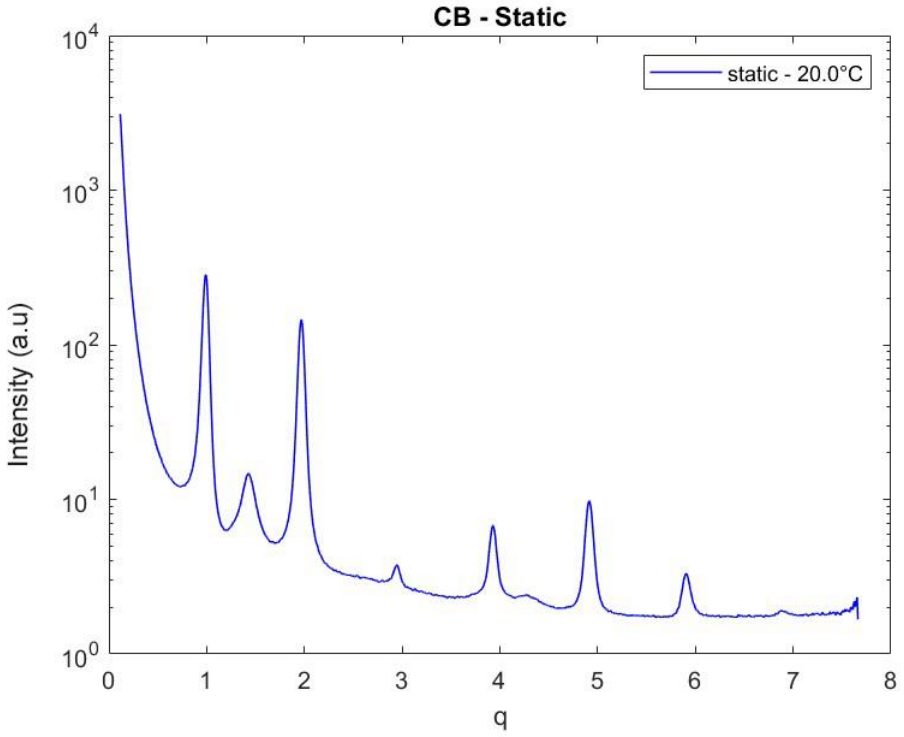

Fig. 4.56 Static SAXS diffractogram of CB sample at 20°C.

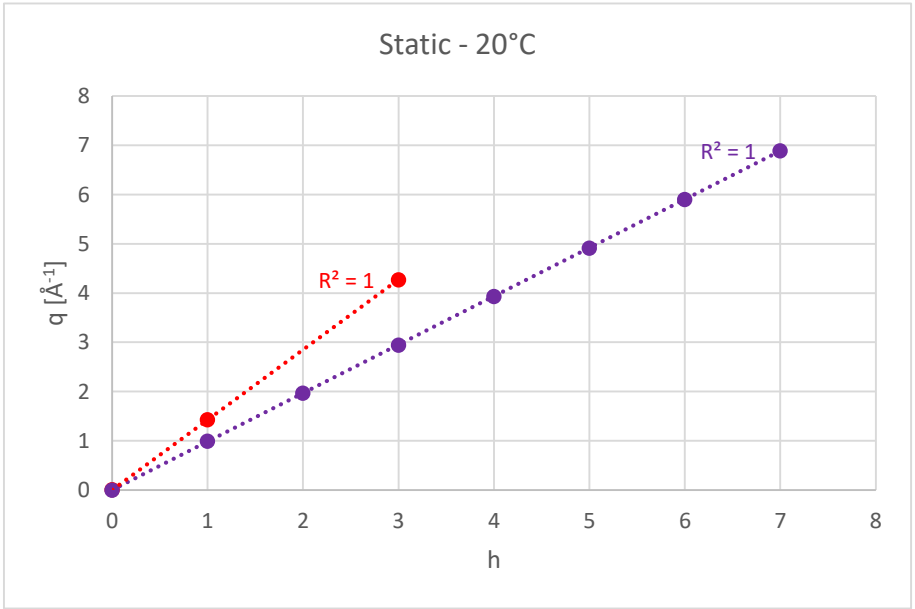

Fig. 4.57 Peaks of crystal phases from SAXS static diffractograms of CB sample in relation to Miller indexes. Red line represents form IV polymorph and purple line form V polymorph.

Static diffractogram peaks pattern in Fig. 4.56 is the typical profile of CB in its form V (β-3L) and form IV (β'-2L) as demonstrated by long spacing values that reflect literature data as well as by their melting temperature range.

Tab. 4.22 Polymorphs from static SAXS diffractogram of CB.

a)

β' (2L)			
q	**H**	**d-spacing [Å]**	**Melting temperature [°C]**
1.4264	1	44.0	~30
4.2722	3	14.7	

b)

β (3L)			
q	**h**	**d-spacing [Å]**	**Melting temperature [°C]**
0.9939	1	63.2	~35
1.9704	2	31.9	
2.9469	3	21.3	
3.9304	4	16.0	
4.9139	5	12.8	
5.90435	6	10.6	
6.88783	7	9.1	

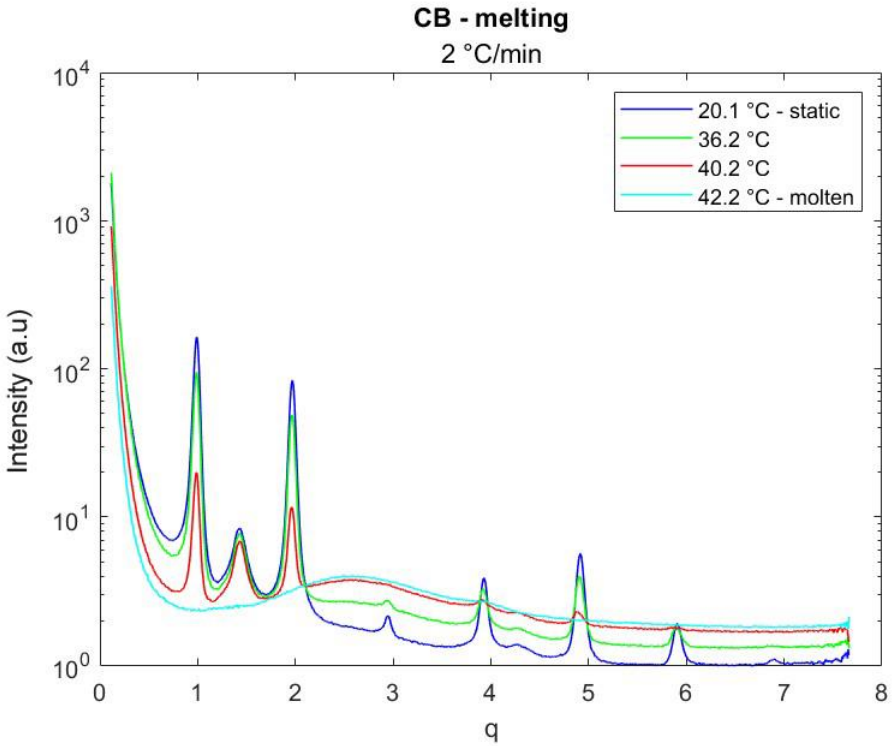

Fig. 4.58 SAXS diffractogram of melting phase of CB sample at +2°C/min.

During the melting process, first slight changes began to show at around 28°C and complete melting was reached at 42.2°C (Fig. 4.58). The two phases melting points are quite close so it was difficult to determine which peaks were generated from each polymorph. However, peaks originated from the same crystal phase when plotted against their Miller indexes aligned, so it was possible to differentiate crystal phases.

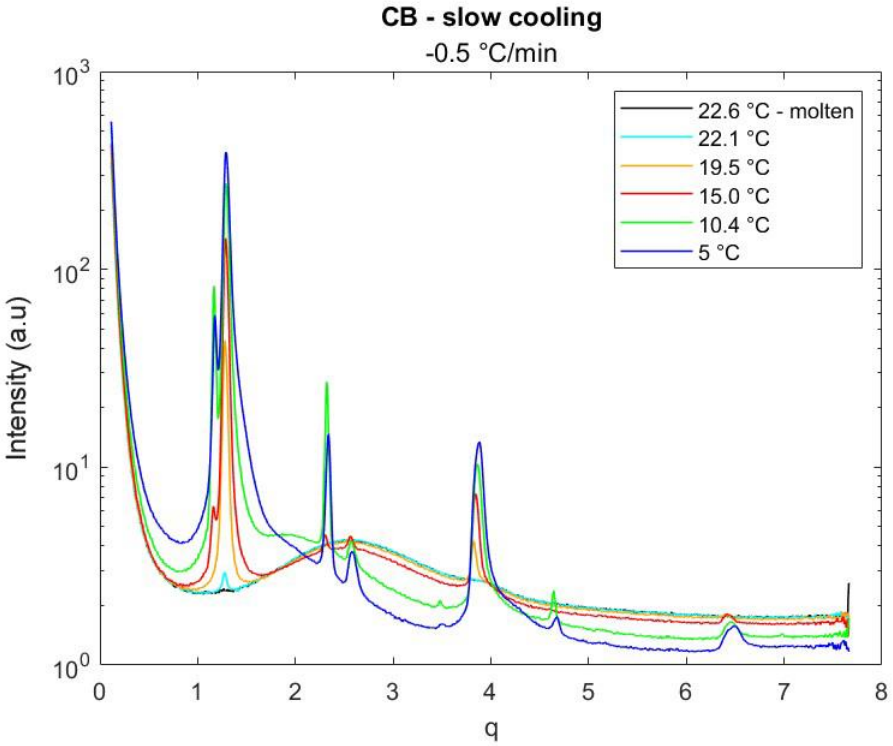

Fig. 4.59 SAXS diffractogram of the slow cooling phase at -0.5°C/min of CB sample.

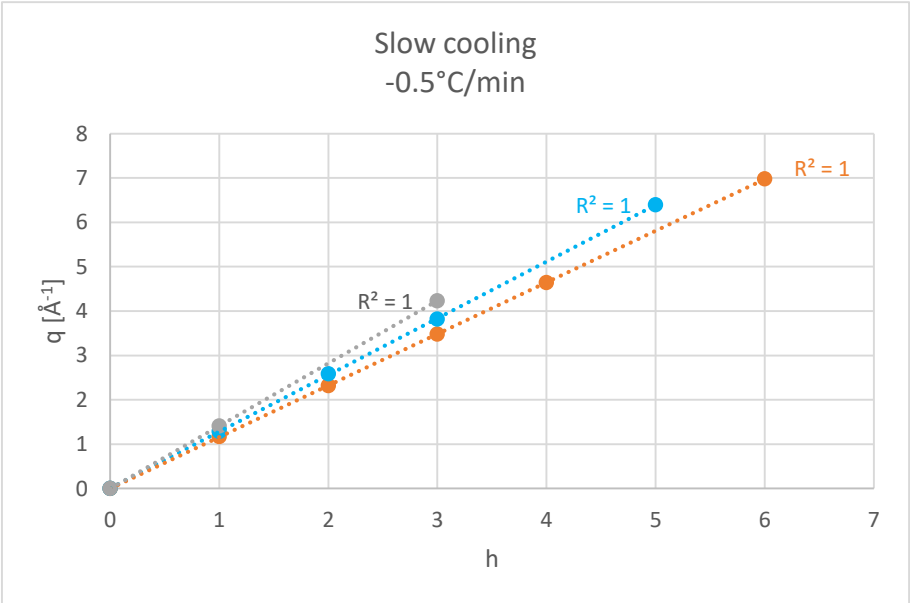

Fig. 4.60 Peaks of crystal phases from SAXS diffractograms of CB sample formed during slow cooling (-0.5°C/min) and the following holding in relation to Miller indexes. Blue line represents α polymorph, orange line the less stable α polymorph and grey one the β' one.

The sample was then cooled to 5°C with a slow cooling rate and other peaks appeared (Fig. 4.59). The first peak appeared at around 22°C, representing the 1st order of the α polymorph, followed by the 2nd, 3rd and 5th order peaks of the same phase. A second α form began to show at 15°C, but disappeared quickly as it was already decreasing before reaching the end of the cooling ramp. In this case it was possible to observe up to the 6th order reflection. Given the rapid formation and the melting temperatures those peaks can be associated to form I and form II of CB.

Tab. 4.23 Polymorphs from SAXS diffractogram formed during slow cooling of CB.

a)

α				
Q	**h**	**d-spacing [Å]**	**Crystallization temperature [°C]**	**Melting temperature [°C]**
1.28689	1	48.8	~22	~25
2.58424	2	24.3		
3.81882	3	16.5		
6.39260	5	9.8		

b)

α				
q	**h**	**d-spacing [Å]**	**Crystallization temperature [°C]**	**Melting temperature [°C]**
1.17529	1	53.5	~15	5 (during holding)
2.33314	2	26.9		
4.68372	4	13.4		

c)

β' (2L)				
q	**h**	**d-spacing [Å]**	**Crystallization temperature [°C]**	**Melting temperature [°C]**
1.41244	1	44.5	5 (during holding)	~30
4.23035	3	14.9		

Fig. 4.61 shows that by the end of the 20 minutes long temperature holding at 5°C, peaks related to the first formed phase remain almost constant while the less stable one is nearly disappeared in the last acquired diffractogram. At the same time, a more stable polymorph starts to form as proved by shoulders forming on the right of the α-phase peaks, especially on the 1st and 3rd order ones. The sample was then heated to 45°C and it was totally molten when reaching 31.6°C (Fig. 4.62). The last formed phase can be associated to form IV as melting point is consistent to literature (S. Bresson et al., 2011), as well as its long spacing. While the two unstable forms are decreasing along the increase in temperature, the β' related peaks followed a different path. Indeed, they were still undergoing a growing period up to 24.6°C and then the melting process of this polymorphs began too. This late formation is caused by the higher complexity of this form and the longer time required for molecules to arrange in the correct structure. The crystallization process was then repeated increasing the cooling rate and the peak scheme appeared equal to the previous ramp, unless for the unseen peaks linked

to form IV. This result is predictable because the sample is given shorter time, hence only formation of metastable polymorphs is possible.

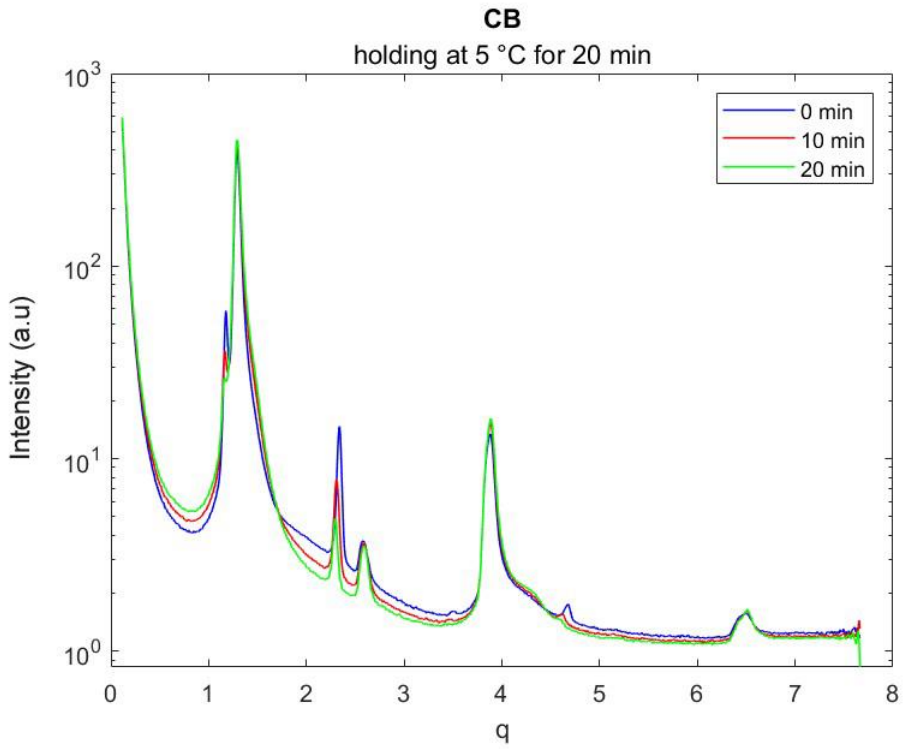

Fig. 4.61 SAXS diffractogram of the temperature holding phase after slow cooling crystallization of CB sample.

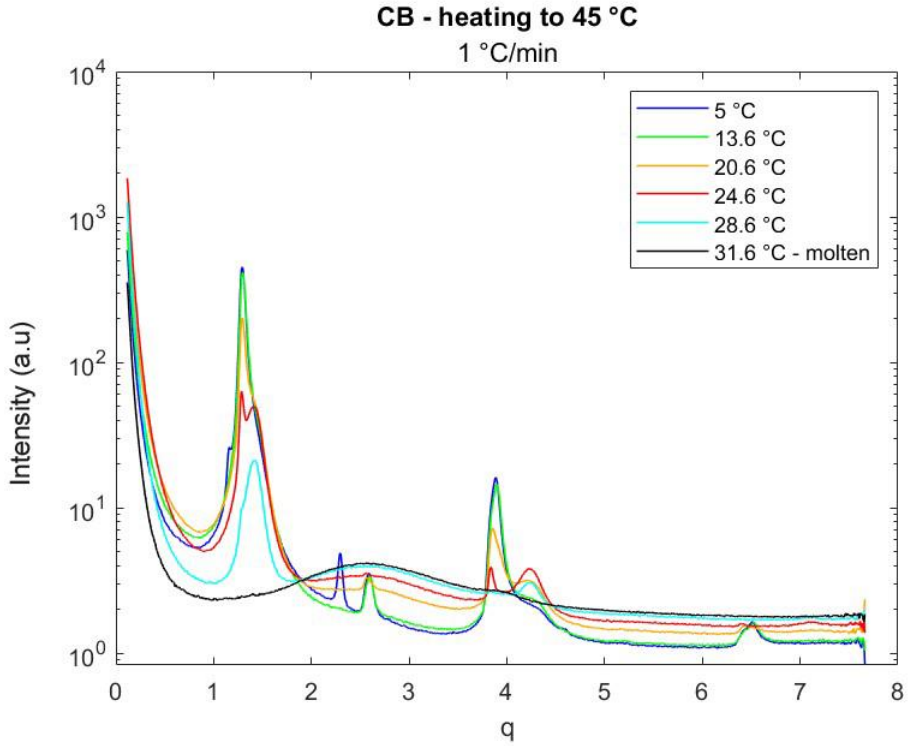

Fig. 4.62 SAXS diffractogram of the heating phase at +1°C/min of CB sample.

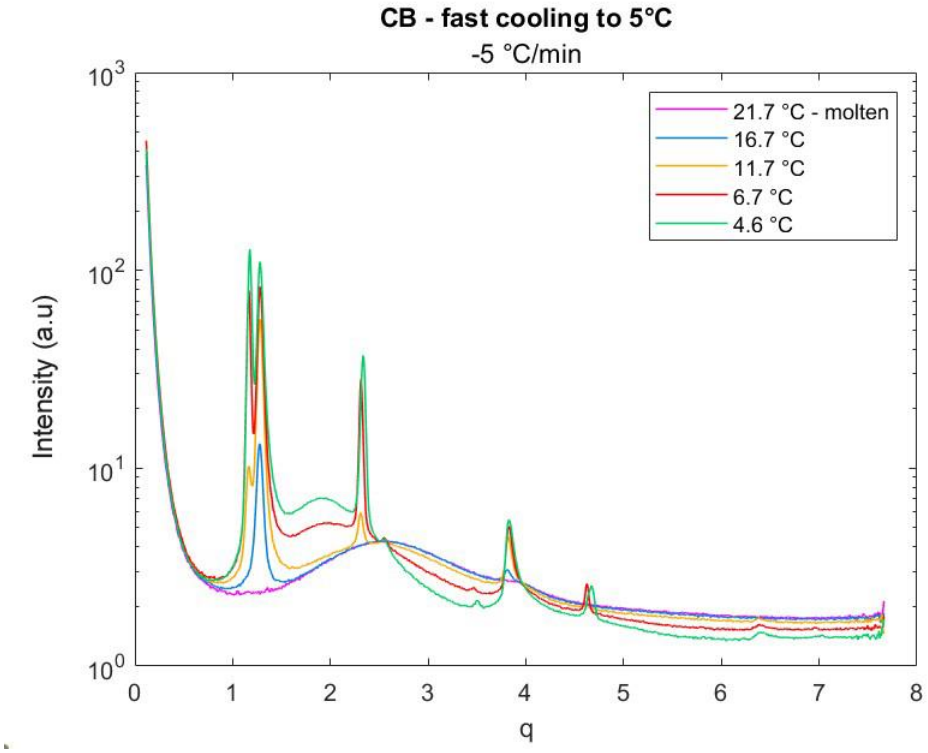

Fig. 4.63 SAXS diffractogram of the fast cooling phase at -5°C/min of CB sample.

4.6.4 Mixtures in CB

Following the analysis of pure compounds, the study of crystallization behaviour of mixtures in CB can be studied in detail, focusing particularly on the differences between milk fat and plant based fat mixtures.

In Fig. 4.64 the comparison among static diffractograms is shown. The general peak pattern is maintained constant in all the samples, meaning that none of them alters the CB crystallization process in its entirety. However, some smaller differences can be noticed, starting from the shape of the major peaks. Firstly, peaks associated to form IV in the CB static diffractogram are poorly defined and not very intense. This is not the case of the mixtures, meaning that a higher fraction has crystallized in the metastable form instead of the more stable β' polymorph.

When MF is mixed with CB, milk fat presence in the sample reduces the stability. Peaks representing the form V are less sharp, indicating that a minor fraction of the compound has reached a stable β-3L structure. A similar situation appears when CB is mixed with MF4 while in MF2 mixture peaks are sharper and more intense.

Melting profiles (Fig. 4.65) are almost totally equivalent to pure CB, but it is important to highlight differences in the temperature of complete melting. While pure CB is molten at 42.2°C, MF 20% mixtures reaches liquid phase faster even if the gap is very limited. Regarding plant based fats, they have the opposite effect as they increase this temperature above 44°C. Hence, plant based fats move the melting point of the mixtures to 2.5/3°C higher compared to Milk Fat mixture. This subject may need further studies in order to better understand if finished products characteristics could be impacted by such changes in physical properties.

The slow cooling process of the three mixtures (Fig. 4.66) followed the same path but the formation of shoulders associated to form IV was not simultaneous. While MF seems to postpone the happening of this transition, MF2 mixture showed more developed shoulders by the end of temperature holding period.

The following heating process (Fig. 4.67) highlights some differences in the melting points. Because less β' polymorph developed, the total melting is reached earlier in MF 20 mixture when compared to MF4 20. In MF2 20 sample the transition to the most stable form was further along, as the most unstable form developed at low temperature is fully molten before the heating process starts. However, MF2 20 sample reaches the point of total melting at 32.8°C while MF 20 needs to increase temperature up to 37.1°C. Melting point variations are a fundamental part of the study of physical properties because they influence chocolate organoleptic properties. However, it is more important to focus on the first heating process that started from samples in form V because this is the required crystal form in chocolate industry, since it has the right melting point in order to match body temperature.

Finally, MF2 20 and MF4 20 mixtures where cooled again at a faster rate to analyse changes in polymorph formation (Fig. 4.68). The crystallization proceeded in the same way of how it did during the previous slow cooling process but the metastable form IV did not form at all. This is expected because this form requires longer time to arrange and unlike the slow cooling process this ramp was not followed by a temperature holding. If the experiment was continued with enough time at 5°C this polymorph would have formed as well lately.

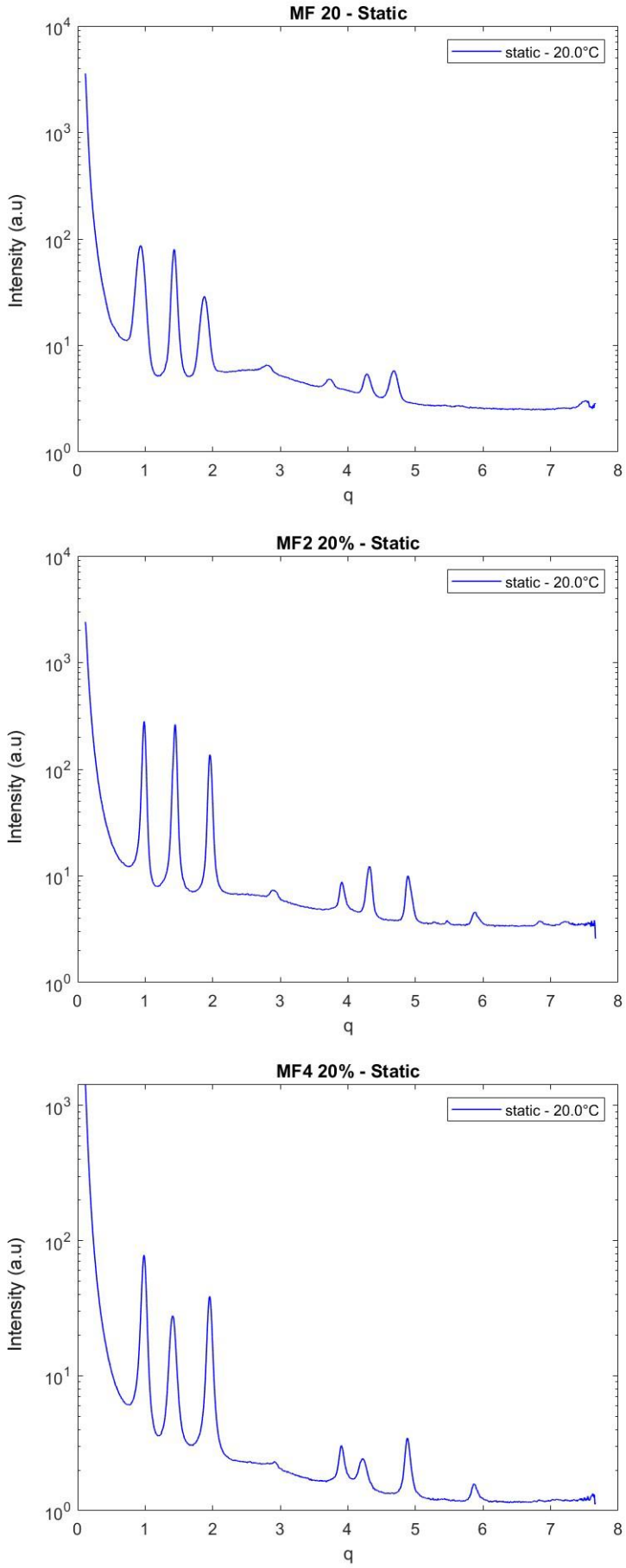

Fig. 4.64 Static SAXS diffractograms of CB mixture samples at 20°C.

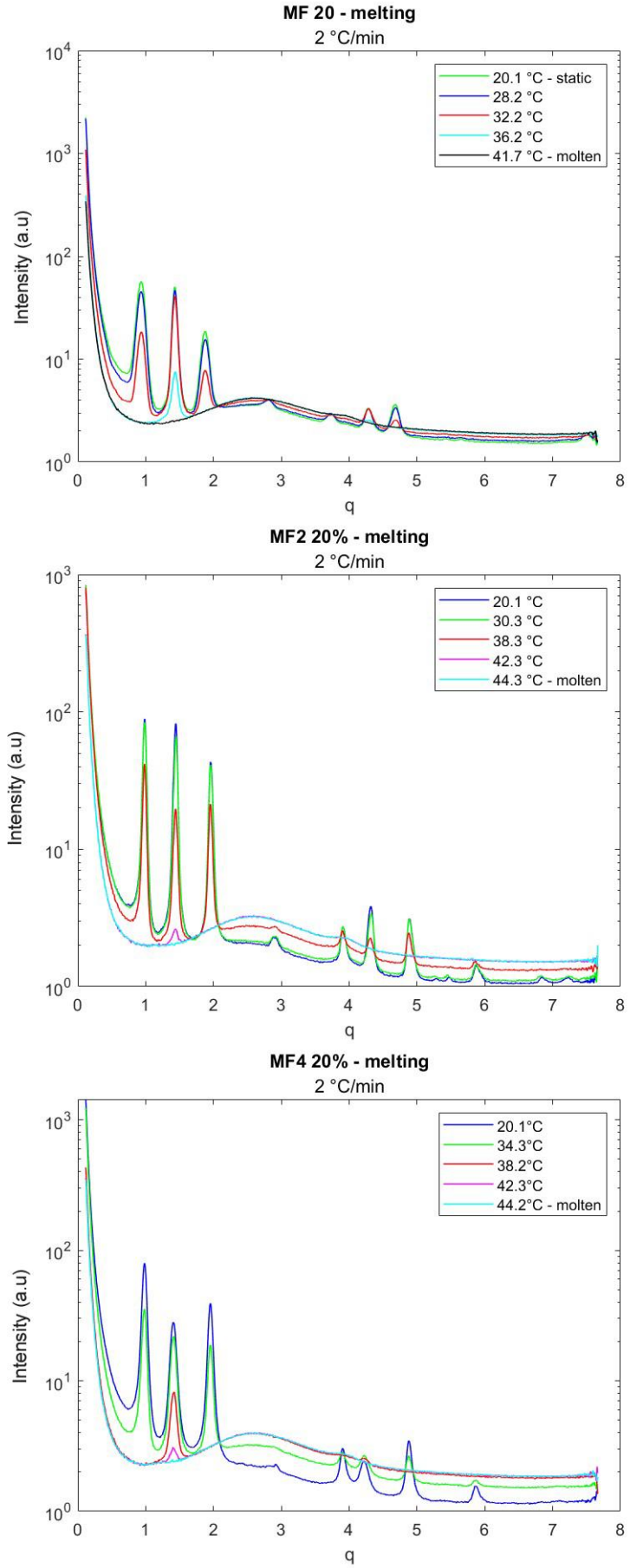

Fig. 4.65 SAXS diffractograms of melting phase of CB mixture samples at 2°C/min.

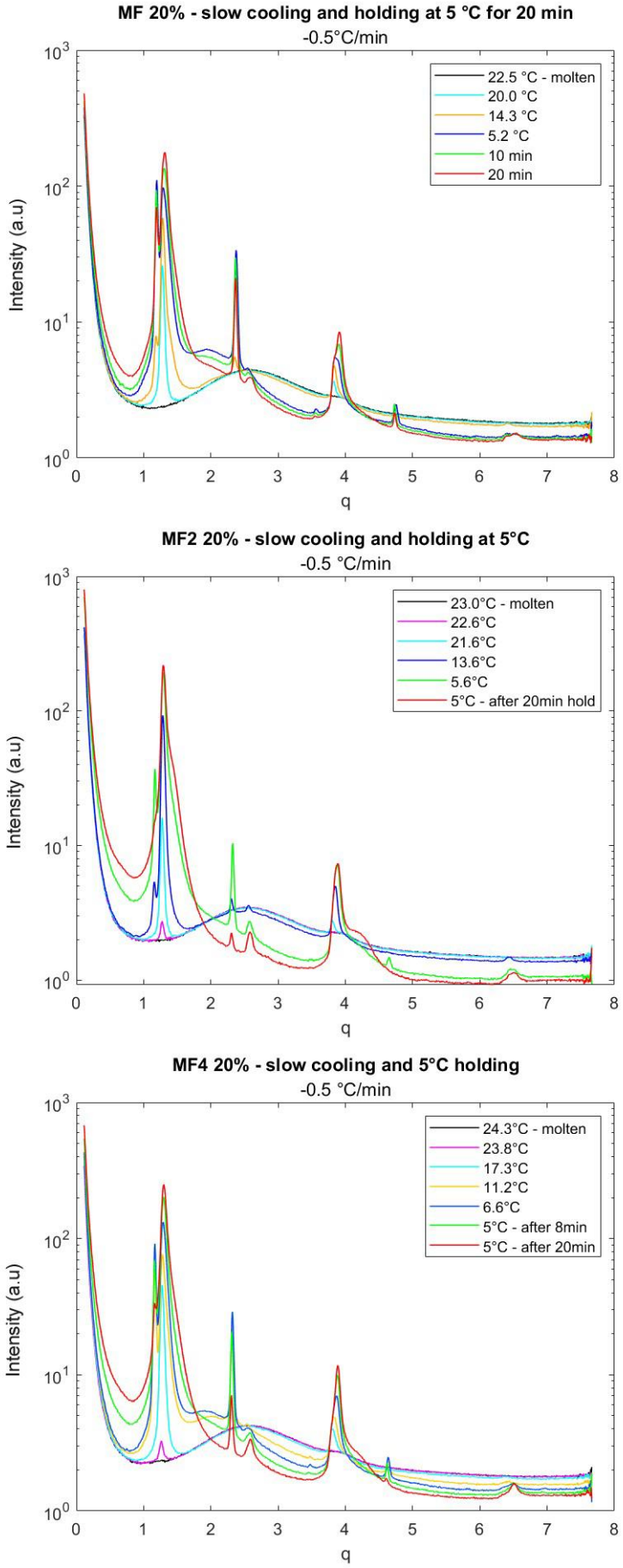

Fig. 4.66 SAXS diffractograms of slow cooling crystallization of CB mixture samples at -0.5°C/min.

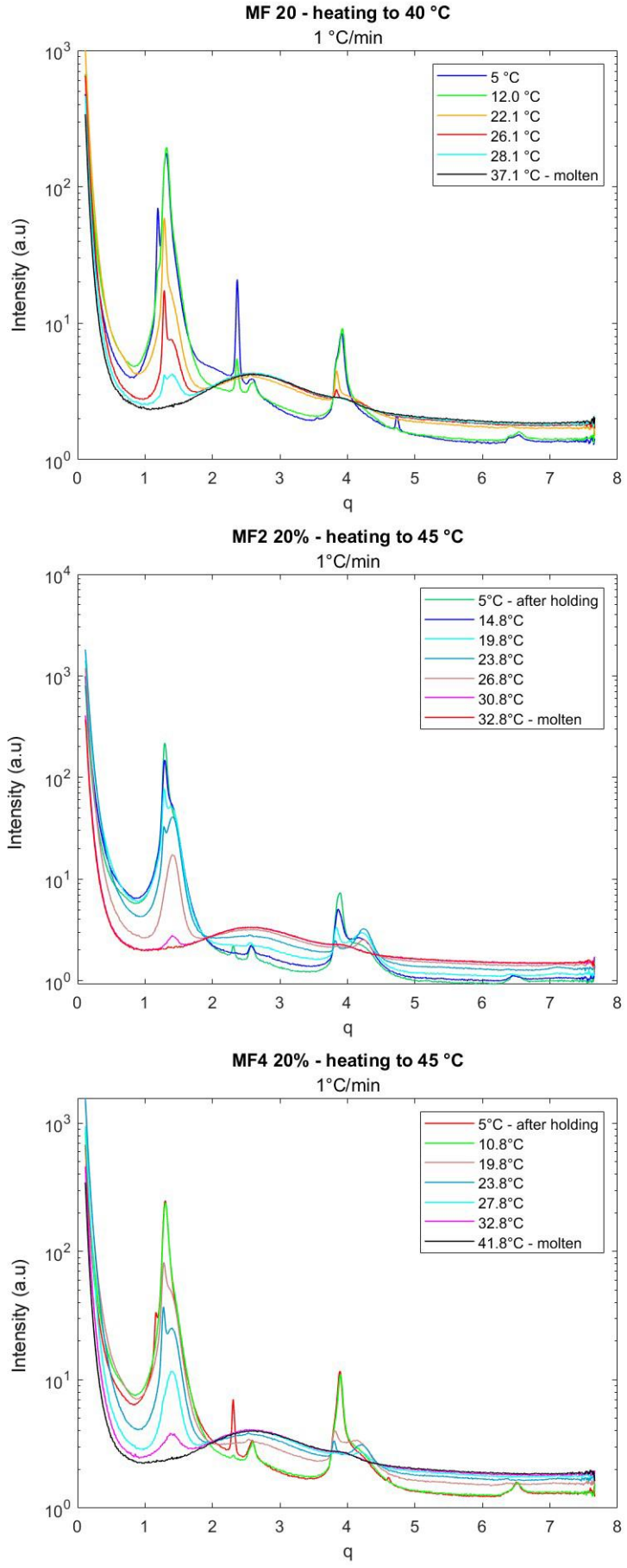

Fig. 4.67 SAXS diffractograms of heating process of CB mixture samples at +1°C/min.

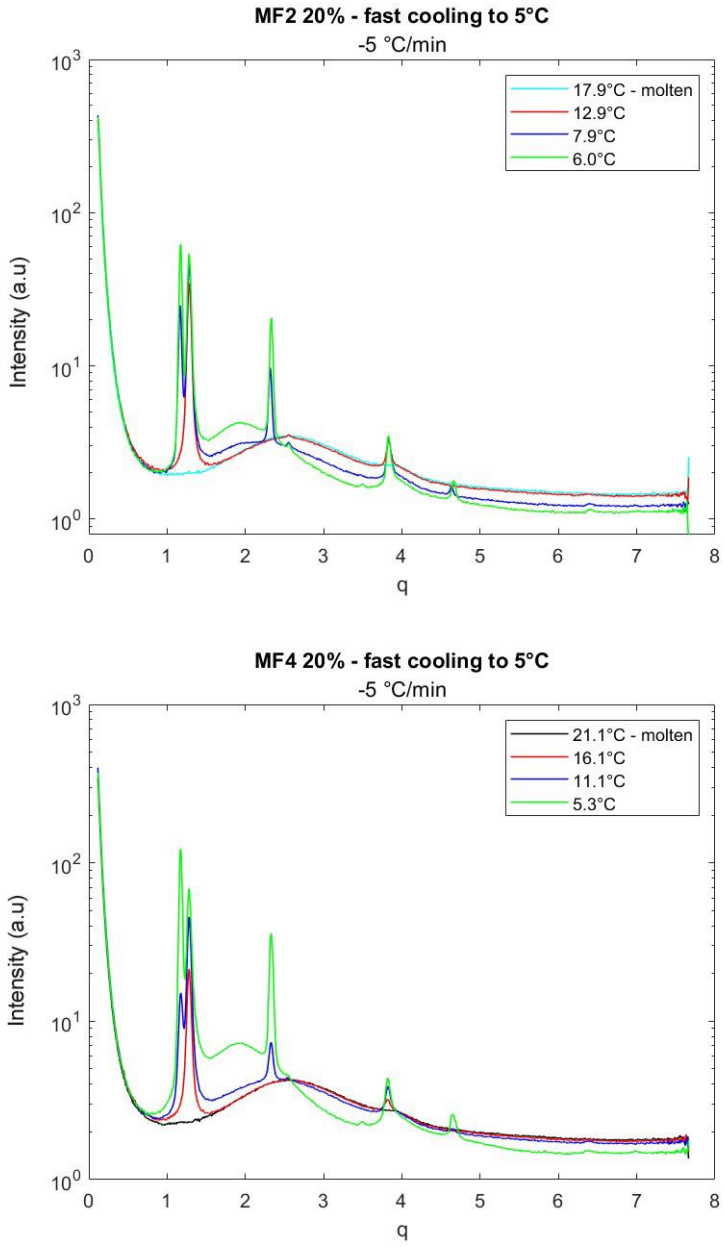

Fig. 4.68 SAXS diffractograms of fast cooling crystallization of CB mixture samples at -5°C/min.

Chapter 5: Conclusions

Plant based fats are the new frontier of chocolate industry thanks to many beneficial factors they can bring to finished products. Many consumers face lactose intolerance problems that do not allow the consumption of products containing milk derivatives, while another main category of today's customers choose to adopt a vegan lifestyle that does not apply to the classic chocolate formulation. This thesis showed how their applications can cover multiple aspects. First of all, it is possible to replace animal fats with fats coming from a more sustainable and consumer friendly fat type leading to a wider capacity to satisfy food market requests. In addition to this the ability to formulate specific fat mixtures in order to meet certain goals in terms of physical and organoleptic properties is a huge milestone in chocolate manufacturing.

The analysis of pure samples of MF2 and MF4 helped to understand their composition main traits and how they influenced their crystallization behaviour. MF2 was found to be mainly composed by the same TAGs that constitute the largest fraction of natural cocoa butter, making it a sort of artificial reproduction of the natural compound. However, the complexity of its formulation brought to the formation of different crystal forms that do not replicate CB polymorphic structure. It is also important to notice that its melting point is higher than that of CB and that of MF as well. This caused an increasing in melting temperature of its mixture in CB when compared to pure CB sample. Linkam images allowed to focus on its particular morphology, indeed it crystallizes in two different phases, the first one as spherical agglomerates while the second one shows smaller homogeneous crystals.

MF4 sample composition was drastically different from MF2 because of the high percentage of unsaturated fatty acids. This translates in OOO being the major TAG and a wide range of polyunsaturated TAGs. The presence of olein has a relevant impact on MF4 analysis because of its inability to form crystalline structures. This molecule melting point is lower than typical CB triglycerides one, moreover the high unsaturation percentage brings the solid fat content of this sample down to 17% at 25°C. This has an important impact on the characteristics of this sample, because it occurs in a creamy consistency when at room temperature. This trait is shared by MF as well, even if in that case the lower melting point of some fractions was caused by short chain fatty acids presence.

However, even if MF2 and MF4 specific properties were very different, they acted on CB crystallization in a similar way. Mixtures containing 20% of the studied plant based fats showed the same crystal forms of the CB-MF mixture. However, the developing of form IV polymorph was faster when mixed with MF4 or even more when mixed with MF2 while it was slowed by MF addition.

References

Bayard, M.; Cancell, M.; Leal-Calderon, F. “Crystallization of emulsified anhydrous milk fat: The role of confinement and of minor compounds. A DSC study”. *Food Chemistry*. 2022, 373, 131606.
DOI: 10.1016/j.foodchem.2021.131605

Bresson, S.; Lecuelle, A.; Bougrioua, F.; El Hadri, M.; Baeten, V.; Courty, M.; Pilard, S.; Rigaud, S.; Faivre, V. “Comparative structural and vibrational investigations between cocoa butter (CB) and cocoa butter equivalent (CBE) by ESI/MALDI-HMRS, XRD, DSC, MIR and Raman spectroscopy”. *Food Chemistry*. 2021, 363, 130319.
DOI: 10.1016/j.foodchem.2021.130319

Bresson, S.; Rousseau, D.; Ghosh, S.; El Marssi, M.; Faivre, V. “Raman spectroscopy of the polymorphic forms and liquid state of cocoa butter”. *European Journal of Lipid Science and Technology*. 2011, 113, 992–1004.
DOI: 10.1002/ejlt.201100088

Campos, R.; Ollivon, M.; Marangoni, A.G. “Molecular Composition Dynamics and Structure of Cocoa Butter”. *Crystal Growth and Design*. 2010, vol.10, 205-217.
DOI: 10.1021/cg900853e

Ewens. H.; Metilli, I.; Simone, E. “Analysis of the effect of recent reformulation strategies on the crystallization behaviour of cocoa butter and the structural properties of chocolate”. *Current Research in Food Science*. 2021, 4, 105-114.
DOI: 10.1016/j.crfs.2021.02.009

Ghazani, S.M.; Marangoni, A.G. “The Ternary Solid State Phase Behavior of Triclinic POP, POS, and SOS and Its Relationship to CB and CBE Properties”. *Cryst. Growth Des*. 2019, 19, 704-713.
DOI: 10.1021/acs.cgd.8b01273

Ghazani, S. M.; Marangoni, A. G. “Molecular Origins of Polymorphism in Cocoa Butter”. *Annual Review of Food Science and Technology*. 2021, 12, 567–590
DOI: 10.1146/annurev-food-070620-022551

Hadri, M.E.; Bresson, S.; Lecuelle, A.; Bougrioua, F.; Baeten, V.; Nguyen, V.H.; Faivre, V.; Courty, M. “Structural and Vibrational Investigations of Mixtures of Cocoa Butter (CB), Cocoa Butter Equivalent (CBE) and Anhydrous Milk Fat (AMF) to Understand Fat Bloom Process”. *Applied Sciences*. 2022, 12, 6594
DOI: 10.3390/app12136594

Herman-Lara, E.; Tejeda-Paz, M.; Martìnez-Sànchez, C.E.; Rodrìguez-Miranda, J.; Ramìrez-Rivera, E.J.; Hernàndez-Santos, B.; Juàrez-Barrientos, J.M. “Differential scanning calorimetry coupled with chemometric tools for determining adulteration with vegetable fat in fresh cheeses”. LWT-Food Science and Technology. 2017, vol.85, 269-274.
DOI: 10.1016/j.lwt.2017.07036

Himawan, C.; Starov, V.M.; Stapley, A.G.F. “Thermodynamic and kinetic aspects of fat crystallization”. *Advances in Colloid and Interface Science*. 2006, 122, 3-33.
DOI: 10.1016/j.cis.2006.06.016

Jahurul, M.H.A.; Zaidul, I.S.M.; Norulaini, N.A.N.; Sahena, F.; Jinap, S.; Azmir, J.; Sharif, K.M.; Mohd Omar, A.K. “Cocoa butter fats and possibilities of substitution in food products concerning cocoa varieties, alternative sources, extraction methods, composition, and characteristics”. *Journal of Food Engineering*. 2013, 117, 467-476.
DOI: 10.1016/j.jfoodeng.2012.09.024

Ladd Parada, M.; Sadeghpour, A.; Vieira, J.; Povey, M.; Rappolt, M. “Global Small-Angle X-ray Scattering Data Analysis of Triacylglycerols in the α-Phase (Part II)”. *The Journal of Physical Chemistry*. 2018, 122, 10330-10336.
DOI: 10.1021/acs.jpcb.8b06708

Lambert, A.; Bougrioua, F.; Abbas, O.; Courty, M.; El Marssi, M.; Faivre, V.; Bresson, S. “Temperature dependent Raman and X-ray diffraction studies of anhydrous milk fat”. *Food Chemistry*. 2018, 267, 187-195
DOI: 10.1016/j.foodchem.2017.09.006

Le Révérend, B.J.D.; Fryer, P.J.; Coles, S.; Bakalis, S. “A Method to Qualify and Quantify the Crystalline State of Cocoa Butter in Industrial Chocolate”. *Journal of the American Oil Chemists' Society*. 2009
DOI: 10.1007/s11746-009-1498-9

Lipp, M.; Simoneau, C.; Ulberth, F.; Anklam, E.; Crews, C.; Brereton, P.; de Greyt, W.; Schwack, W.; Wiedmaier, C. “Composition of Genuine Cocoa Butter and Cocoa Butter Equivalents”. *Journal of Food Composition and Analysis*. 2001, 14, 399-408.
DOI: 10.006/jfca.2000.0984

Lopez, C.; Briard-Bion, V.; Camier, B.; Gassi, J.Y. “Milk Fat Thermal Properties and Solid Fat Content in Emmental Cheese: A Differential Scanning Calorimetry Study”. Journal of Dairy Science. 2006, vol.89, no.8, 2894-2910
DOI: 10.3168/jds.S0022-0302(06)72562-0

MacMillan, S.D.; Roberts, K.J.; Rossi, A.; Wells, M.A.; Polgreen, M.C.; Smith, I.H. “In Situ Small Angle X-ray Scattering (SAXS) Studies of Polymorphism with the Associated Crystallization of Cocoa Butter Fat Using Shearing Conditions”. *Crystal Growth and Design*. 2002, vol.2, no.3, 221-226.
DOI: 10.1021/cg0155649

Maikhaylyk, O.O.; Hamley, I.W. “The Packing of Triacylglycerols from SAXS Measurements: Application to the Structure of 1,3-Distearoyl-2-oleoyl-*sn*-glycerol Crystal Phases”. *Journal of Physical Chemistry B*. 2004, 108, 8069-8083.
DOI: 10.1021/jp0379704

Marty-Terrade, S.; Marangoni, A.G. “Impact of Cocoa Butter Origin on Crystal Behaviour”. *Cocoa Butter and Related Compounds.* 2012, 245-274.
DOI: 10.1016/B978-0-9830791-2-5.50014-1

Metin, S.; Hartel, R.W. “Milk Fat and Cocoa Butter”. *Cocoa Butter and Related Compounds*. 2012, 365-392.
DOI: 10.1016/B978-0-9830791-2-5.50018-9

Nosratpour, M.; Kochan, K.; Ma, J.; Wang, Y.; Wood, B.R.; Haritos, V.S.; Selomulya, C. “Fatty acid distribution and polymorphism in solid lipid particles of milkfat and long chain omega-3 fatty acids”. *Food Chemistry*. 2022, 381, 132245.
DOI: 10.1016/j.foochem.2022.132245

Pirouzian, H.R.; Konar, N.; Palabiyik, I.; Oba, S.; Toker, O.S. “Pre-crystallization process in chocolate: Mechanism, importance and novel aspects”. *Food Chemistry*. 2020, 321, 126718
DOI: 10.1016/j.foodchem.2020.126718

Podchong, P.; Aumpai, K.; Sonwai, S.; Rousseau, D. “Rice bran wax effects on cocoa butter crystallisation and tempering”. *Food Chemistry*. 2022, 397
DOI: 10.1016/j.foodchem.2022.133635

Ramel, P. R.; Marangoni, A. G. “Characterization of the polymorphism of milk fat within processed cheese products”. *Food Structure*. 2017, 12, 15-25
DOI: 10.1016/j.foostr.2017.03.001

Sasaki, M.; Ueno, S.; Sato, K. “Polymorphism and Mixing Phase Behavior of Major Triacylglycerols of Cocoa Butter”. *Cocoa Butter and Related Compounds.* 2012, 151-172
DOI: 10.1016/B978-0-9830791-2-5.50009-8

Sato, K.; Ueno, S. “Polymorphism in Fats and Oils”. *Bailey’s Industrial Oil and Fat Products*. 2005, 77-120.
DOI: 10.1002/047167849x.bio020

ten Grotenhuis, E.; van Aken, G.A.; van Malssen, K.F.; Schenk, H. “Polymorphism of Milk Fat Studied by Differential Scanning Calorimetry and Real-Time X-ray Powder Diffraction”. *Journal of the American Oil Chemists’ Society*. 1999, vol.76, no.9, 1031-1039
DOI: 10.1007/s11746-999-0201-5

Toro-Vasquez, J.F.; Charò-Alonso, M.A.; Morales-Rueda, J.A.; Pérez-Martinez, J.D. “Molecular Interactions of Triacylgrlycerides in Blends of Cocoa Butter with *trans*-free Vegetable Oils”. *Cocoa Butter and Related Compounds.* 2012, 393-416.
DOI: 10.1016/B978-0-9830791-2-5.50019-0

Tzompa-Sosa, D.A.; Ramel, P.R.; van Valenberg, H.J.F.; van Aken, G.A. “Formation of β Polymorphs in Milk Fats with Large Differences in Triacylglycerols Profiles”. *Journal of Agricultural and Food Chemistry*. 2016, 64, 4152-4157.
DOI: 10.1021/acs.jafc.5b05737

Verstringe, S.; De Clercq, N.; Nguyen, T.M.; Kadivar, S.; Dewettinck, K. “Enzymatic and Other Modification Techniques to Produce Cocoa Butter Alternatives”. *Cocoa Butter and Related Compounds.* 2012, 443-474.
DOI: 10.1016/B978-0-9830791-2-5.50021-9

Yao, Y; Liu, W.; Zhang, D.; Li, R.; Zhou, H.; Li, C.; Wang, S. “Dynamic changes in the triacylglycerol composition and crystallization behavior of cocoa butter”. LWT – Food Science and Technology. 2020, 129, 109490.
DOI: 10.1016/j.lwt.2020.109490

Yao, Y.; Zhao, G.; Yan, Y.; Mu, H.; Jin, Q.; Zou, X.; Wang, X. “Milk fat globules by confocal Raman microscopy: Differences in human, bovine and caprine milk”. *Food Research International*. 2016, 80, 61-69
DOI: 10.1016/j.foodres.2015.12.017

List of figures

List of tables

List of abbreviations

CB Cocoa Butter

CBA Cocoa Butter Alternative

CBE Cocoa Butter Equivalent

CBS Cocoa Butter Substituent

DSC Differential Scanning Calorimetry

FA Fatty Acid

MF Milk Fat

O Oleic Acid

OOP 1,2-Dioleoyl-3-Palmitoyl Glycerol

OOS 1,2-Dioleoyl-3-Stearoyl Glycerol

OPO 1,3-Dioleoyl-2-Palmitoyl Glycerol

OSO 1,3-Dioleoyl-2-Stearoyl Glycerol

P Palmitic Acid

PLM Polarized Light Microscopy

POP 1,3-Dipalmitoyl-2-Oleoyl Glycerol

POS -Palmitoyl-2-Oleoyl-3-Stearoyl Glycerol

PPO 1,2-Dipalmitoyl-3-Oleoyl Glycerol

PPP 1,2,3-Tripalmitoyl Glycerol

RT Room Temperature

S Stearic Acid

SAXS Small Angle X-ray Scattering

SFC Solid Fat Content

SOS 1,3-Distearoyl-2-Oleoyl Glycerol

SSO 1,2-Distearoyl -3-Oleoyl Glycerol

SSS 1,2,3-Tristearoyl Glycerol

TAG Triglyceride

Tm Melting Temperature

XRPD X-Ray Powder Diffraction

XRD X-Ray Diffraction